COMPUTATIONAL FORAYS INTO THE ELECTRONIC STRUCTURE OF RADICALS

by

Marissa Lyn Estep

(Under the Direction of Henry F. Schaefer III)

ABSTRACT

Quantum chemical studies are presented on several gas-phase radicals. The first project details computations of the properties of the methylsulfinyl radical, which is central to remote marine atmospheric sulfur chemistry. The second explores the mechanism of the reaction between ozone and the methylsulfinyl radical, showing that a previous theoretical study vastly overestimated the reaction barrier, likely as a result of improper method choice. The focus then shifts to radicals found in the combustion of butanol; computations of infrared frequencies resulted in suggested reassignments of several experimental modes. Finally, the interactions of uracil with neutral alkali metal atoms appear to involve substantial transfer of the unpaired electron to the nucleobase, despite the low electron affinity of the latter.

INDEX WORDS: sulfur chemistry, atmospheric chemistry, combustion chemistry, radicals, quantum chemistry, electronic structure theory

COMPUTATIONAL FORAYS INTO THE ELECTRONIC STRUCTURE OF RADICALS

by

Marissa Lyn Estep

B.S. Liberty University, 2014

A Dissertation Submitted to the Graduate Faculty
of the University of Georgia in Partial Fulfillment
of the Requirements for the Degree

Doctor of Philosophy

Athens, Georgia

2019

COMPUTATIONAL FORAYS INTO THE ELECTRONIC STRUCTURE OF RADICALS

by

Marissa Lyn Estep

Major Professor: Henry F. Schaefer III

Committee: Gary E. Douberly

Jeffrey Urbauer

Electronic version approved:

Suzanne Barbour

Dean of the Graduate School

University of Georgia

May 2019

ACKNOWLEDGEMENTS

Many people made this dissertation possible. Prior to starting this degree, I knew it would be academically demanding, but I had no idea how personally challenging it would be. The support of my friends and family was absolutely essentially to navigating these years. Even your names would be hard to fit on this page, but you deserve far more than a cursory mention.

Dr. Nancy Richardson has been an amazing friend and mentor. I owe her an enormous debt of gratitude for her kindness and generosity. Without her, I would not be where I am today without her. She always encouraged me to pay it forward rather than repaying her. In the next phase of my career I hope to follow her example by using my scientific education to bless the next generation of students and society.

Dr. Schaefer has been a fantastic research advisor who values each of his students both as a scientist and as a person. I'm grateful to have worked these years with and for him. The success of the Schaefer group is grounded in the excellent group of people Dr. Schaefer has recruited over the years. I have learned something from each of you; thank you: Adam, Andreas, Andrew, Avery, Boyi, Bryan, Chenyang, James, Jared, Jonathon, Jonathon, Kevin, Kevin, Matt, Mark, Megha, Michael, Mitchell, Sarah, Dr. Turney, Walter, Xiao, Zhi, many summer students and visiting scholars, and especially Preston, who started the same week I did and consistently exhibited grace and patience as we each experienced the growing pains of a young scientist. Along with these excellent scientists, the CCQC continues to run due to fantastic administrative staff. Kathryn and Sybil have gone way beyond the call of duty in their roles. Thank you!

I absolutely wouldn't have reached this point without my friends and church family here in Athens. Thank you, thank you, thank you for standing by me in support as I studied a subject that probably seems overly esoteric. You went beyond surface relationships, helping me grow as a scientist and as a person.

My parents deserve undying gratitude for the sacrifices they made to provide a solid homeschool education, for the endless curiosity they modeled for me, and for their endless encouragement and tough love.

To my dear siblings: I have missed many years of birthdays and debate tournaments and promotions. I hope to make up for some of that lost time now. But I also plan to cheer for you the way you have for me as you do the hard things in life. < 3

Finally, this dissertation would not have reached completion without the work of the Holy Spirit in my life thanks to the sacrifice of Jesus Christ applied to my life. Thank You, Lord.

TABLE OF CONTENTS

CHAPTER 1

INTRODUCTION AND LITERATURE REVIEW

Dissertation Structure

This dissertation begins with a necessarily cursory overview of methods commonly employed in *ab initio* electronic structure computations, including quantum chemical methods involved in the treatment of systems with unpaired electrons. In the following chapters, I present four research projects on radical species. The first two concern the methylsulfinyl radical, starting with a published quantum chemical characterization of the radical and ending with an investigation of the possible mechanism of its reaction with ozone. In the third project chapter, I present a study of radicals related to acetaldehyde and vinyl alcohol through removal of a single hydrogen or hydroxyl radical. The fourth project outlines the nature of the interaction between neutral alkali metal atoms and the nucleobase uracil. I conclude this work with a summary of my findings.

Quantum Chemistry for Radical Systems

Open-shell chemical species are defined as those with one or more unpaired electrons. Although quantum chemical computations on radicals can be quite challenging,[1] computational quantum chemistry offers quite a bit of value to studies of these radical species, particularly those in the gas phase. Quantum chemical *ab initio* predictions can be used to both guide and interpret experimental work, including spectroscopy and investigations of reaction mechanisms and the resulting kinetics. Because theoretical methods are not limited to predictions of observables, they also serve as a basis for conceptual reasoning about the nature of chemical bonding, providing mental models that can improve chemists' intuition and predictive power. Many other areas of chemistry also benefit from quantum chemical calculations, but the work in this dissertation will focus on computational applications in gas-phase radical chemistry.

Following an overview of quantum chemical methods important for treatment of radicals in this chapter, the subsequent chapters detail specific investigations of gas-phase radicals using these methods. The work

concludes with conclusions and a few thoughts on the future of quantum chemistry.

> The underlying physical laws necessary for the mathematical theory of a large part of physics and the whole of chemistry are thus completely known, and the difficulty is only that the exact application of these laws leads to equations much too complicated to be soluble. It therefore becomes desirable that approximate practical methods of applying quantum mechanics should be developed, which can lead to an explanation of the main features of complex atomic systems without too much computation. (Paul M. Dirac)

As Dirac pointed out,[2] we are in possession of the physical equations needed to predict and describe all of chemistry, but without appropriate approximations, cannot reasonably solve these equations. In this dissertation, I describe application of such approximate methods to several chemical applications. First, however, I provide an overview of quantum chemistry as a field and of the methods employed in this work.

The Schrödinger Equation

The time-dependent Schrödinger equation[3–5] is the exact nonrelativistic equation governing the motion of the electrons and protons that constitute molecules. Although exact solution of chemical problems requires use of the Dirac equation,[6] which accounts for relativity, the inaccuracies associated with a nonrelativistic treatment may frequently be neglected without dire consequence. In the remaining cases, relativistic corrections or effective core potentials may often be used instead of a full relativistic treatment.

Quantum chemists often restrict their consideration to the time-independent Schrödinger equation, which we solve to find stationary states.

Since electrons move several orders of magnitude faster than protons, most theoretical chemistry employs the Born-Oppenheimer approximation, wherein the nuclear and electronic degrees of freedom are treated separately. This leads to the fundamental concept of the potential energy surface, a map of the energy as a function of the nuclear coordinates. This approximation breaks down when multiple electronic potential energy surfaces are close together, as in a conical intersection. Potential energy surfaces provide a conceptual starting point for geometry optimization, which will be discussed later.

Self-Consistent Field Theory

Self-consistent field theory is a method to approximately solve the Born-Oppenheimer Schrödinger equation for multi-electron atoms. Employs the variational method, which makes use of the variational principle.

The variational principle states that for any normalized, well-behaved function Ψ that satisfies the boundary conditions of the problem, the energy obtained by using Ψ as a wavefunction will be greater than or equal to the exact energy according to

$$\int \Psi^* \Psi d\tau \geq E_{exact}$$

Restricted,[7,8] unrestricted,[9] and restricted open-shell[10,11] Hartree–Fock theory. Unrestricted Hartree-Fock (UHF) is the simpler of the two open-shell reference methods, but always suffers from some degree of spin contamination. Spin contamination is observed in spin expectation values higher than those of the state under consideration, and is caused by mixing of higher-spin states with the desired state. Severe spin contamination can indicate that the UHF wave function is a poor approximation to the desired state of the system at the geometry of interest. In some cases the reference may provide a better description of the system at a slightly different geometry; in others, severe spin contamination may be diagnostic of multireference character in the system. If the system is not significantly multireference, a different single-reference wavefunction may be a reasonable first approximation to the system. Restricted open-shell Hartree-Fock (ROHF) is one possible option in this case. ROHF forces the spin operator to assume the desired expectation value, avoiding spin contamination completely. However, this results in more complicated equations that make analytic gradients and Hessians nontrivial. Additionally, an ROHF reference is not guaranteed to be a better descriptor of the system, and can suffer from similar shortcomings in a less obvious way (as spin contamination cannot be used as a diagnostic).

Another choice of reference employs Brueckner orbitals, which are obtained during a coupled-cluster computation.[12,13] Brueckner orbitals have been used to avoid the symmetry-breaking issues common in ROHF treatments, but unfortunately can be subject to similar difficulties.[14]

The Hartree-Fock solutions for a molecular problem represent electronic states. The lowest of these, the ground state, tends to be the easiest to find, but in many cases one or more excited states are needed. This is true for any sort of electronic spectroscopy, but is also important in some macromolecular computations where statistical mechanics must be applied.

Correlated Methods

Although Hartree–Fock is a good first approximation for many chemical systems, it is a mean-field approach. As such, it neglects the instantaneous interactions between electrons. Although this correlation is responsible for only a tiny percentage of the energy of the system, the resulting effect on energy differences is quite

important to chemistry, and an extensive family of methods has been built on this foundtation.

The goal of computational quantum chemistry is to exactly solve the Born–Oppenheimer Schrödinger equation. Another way of phrasing this is to say we are trying to solve full configuration interaction (FCI). Starting with a single HF reference wavefunction, FCI incorporates terms corresponding to all possible excitations of electrons from occupied to unoccupied orbitals. FCI is exact within the given basis set. However, its cost scales factorially, making it intractable for all but the very smallest systems. Other methods have been found more practical for regular use.

The correlation energy of a system is the difference between the FCI energy and the SCF energy. This correlation energy can be further divided into static and dynamic correlation. Static correlation, which will be discussed further below, is present in systems that require more than one Slater determinant to properly model the zeroth-order wavefunction, and will be mentioned again in the section on multireference systems. Dynamic correlation, which is treated using the correlated methods discussed in this section, accounts for the instantaneous interactions of electrons; in contrast to the picture presented by HF and other mean-field methods, electrons do not merely interact with the electrostatic average of the other electrons.

A common approach to solving the Schrödinger equation employs perturbation theory. This line of attack entails exact solution of a zeroth-order problem that is close to the problem of interest followed by a perturbation that can be added to the zeroth-order solution to give the problem of interest.

$$\hat{H} = \hat{H}_0 + \hat{H}'$$

One approach to adding correlation to HF is to treat the correlation as a perturbation and use the equations of RSPT. The second-order energy correction results in the widely used second-order Møller–Plesset perturbation theory (MP2) method.[15] Although higher-order corrections have been used in quantum chemistry, these have mainly fallen out of favor; although the relevant perturbation series should converge in the limit of an infinite number of terms, many times they exhibit wild oscillations for smaller numbers.[16] In such cases, higher orders of perturbation theory may perform worse than lower orders.[17] Since each order of perturbation theory adds computational complexity and cost, this is a sad state of affairs. Additionally, better methods with the same scaling as these higher-order MPn methods have been developed in the interim. Second-order Møller-Plesset perturbation theory (MP2) is the most widely-used and reliable of the MPn methods.

One of the most celebrated methods for treating dynamic correlation, coupled cluster theory, affords many desirable qualities at a cost comparable to the woefully oscillatory higher-order perturbation theory methods. Since its chemical debut in Čížek's 1966 paper,[18] coupled cluster theory has developed a reputation

as one of the most accurate methods of computational quantum chemistry. Crawford and Schaefer published an accessible introduction to coupled cluster theory in 2000.[19] Unlike truncated configuration interaction methods, coupled cluster methods are size-consistent and size-extensive; as expected for a phsycial system, energies scale with the size of the system under these methods.[20] Coupled cluster theory with singles, doubles, and perturbative triple excitations, abbreviated CCSD(T),[21] is one of the most successful quantum chemistry methods in terms of accuracy obtained for cost. When used with a basis set of cc-pVTZ quality, CCSD(T) is considered the "gold standard" of quantum chemistry. More affordable implementations of coupled cluster theory, particularly DLPNO methods,[22] can be applied to larger molecular systems. Coupled cluster theory is most straightforwardly used to treat the ground electronic state of a system, but can also be used to model excited states of a different symmetry than the ground state through occupation number constraints.

To approximate the full CI limit of relative electronic energies with high accuracy, the focal point approach (FPA) of Allen and coworkers[23–26] employs high-level coupled cluster theory. Two of the projects detailed in this work employ coupled cluster theory with single, double, triple, and perturbative quadruple excitations [CCSDT(Q)].[27–29] The focal point approach also extrapolates to the complete basis set limit using the Dunning correlation-consistent basis sets. The focal point approach typically reaches the goal of chemical accuracy, with error well under 1 kcal mol^{-1}.

As an added bonus, coupled cluster theory wavefunctions for open-shell systems tend to suffer from a reduced degree of spin contamination than their UHF references, as long as the reference is only moderately spin-contaminated.[30]

Basis Sets

Exact representation of molecular wavefunctions in theory requires an infinite set of basis functions. In practice, quantum chemical computations are restricted to finite basis sets. The majority of molecular quantum chemical computations are performed with basis sets composed of Gaussian functions Ae^{ar^2}. Although Slater functions Ae^{ar} are a more accurate representation of the behavior of electrons near the atomic nuclei, they are much more difficult to integrate. A good compromise between computational cost and accuracy is to add Gaussian functions in a way that approximates a Slater orbital, A variety of basis sets have been constructed with different numbers of these Gaussian-type orbitals for each atom in the system and different numbers of Gaussians constituting each orbital.

Pople basis sets[31] are some of the oldest extant basis sets and are well-suited to Hartree-Fock computations, offering fortuitous cancellation of errors in some cases. Although the smallest of these basis sets are not suited to modern publication-quality results, they can still be used advantageously for troubleshooting

computations and for educational purposes. The larger Pople basis sets still see extensive use.

The Dunning cc-pVnZ (n=D,T,Q,5) correlation-consistent basis sets,[32] so named because they converge smoothly to the complete basis-set limit for correlated methods, are named according to n, the number of Slater-type functions composing each orbital.The second-row atoms Al-Ar are insufficiently treated by the original Dunning basis sets, as detailed by Wilson and Yockel.[33] The cc-pV($n+d$)Z basis sets include tight d functions to alleviate this.[34] Almlöf and Taylor[35] constructed the NASA Ames atomic natural orbital (ANO) basis sets. Like the Dunning basis sets, these basis sets are frequently used with wavefunction-based methods, resulting in fundamental frequencies comparable or in some cases slightly better to those obtained with Dunning basis sets.[36] The standard Dunning basis sets cannot properly model anions and electron affinities; to do so, basis sets must be augmented with diffuse functions.[37,38] The Ahlrichs Def2 basis sets[39,40] are commonly used in density functional theory computations, but may require added augmentation to properly treat electron affinities.[41] The seasonal basis sets are available with intermediate degrees of augmentation.[42]

Many basis sets for heavier elements on the periodic table must be used with effective core potentials (ECPs). The Schrödinger equation, which is nonrelativstic, is sufficient for many chemical problems, but in other problems the effect of relativity cannot be neglected. Explicit treatment of relativistic effects can be computationally unaffordable; for many systems treatment with ECPs is preferred. In this work, we mainly consider those designed for use with Ahlrichs basis sets and those used in conjunction with the Dunning basis sets for alkali and alkaline earth metals.

To a point, the bigger the basis set, the better. Since nonrelativistic computational quantum chemical methods are in various ways approximating the full configuration interaction result at the complete basis set limit, it may seem that using the largest basis set possible is always the best option. However, very large basis sets can create numerical instabilities. The best basis set for a given situation contains enough of the appropriate types of functions to model the chemistry. If benchmark experimental data are unavailable on similar system, several basis sets may need to be tested to determine how sensitive the system is to basis set size and composition.

For heavy elements with $Z \approx 25$, relativistic effects may be too computationally expensive to treat explicitly, but too important to ignore. Effective core potentials (ECPs) suffice for many of these systems. ECPs replace core electrons with a potential that accounts for relativistic effects.

Density Functional Theory

Kohn-Sham density functional theory, the type of DFT used for molecular quantum chemistry, was presented by the eponymous authors in 1965.[43] Kohn and Sham built off of the 1964 work of Hohenberg and Kohn.[44]

One of the Hohenberg-Kohn theorems posits the existence of an exact functional mapping the electron density to the electronic energy of the system. Although this universal functional is not known, approximate functionals abound. These approximations differ in complexity, computational cost, and accuracy, and different functionals tend to perform better in different situations. Since DFT includes correlation but carries the same formal scaling as Hartree–Fock theory, it is a much more affordable way to attempt an exact solution of the electronic energy. For this reason, it is the *de facto* standard in numerous quantum chemical applications involving more than a handful of heavy atoms. Several categories of functionals are commonly used; although they do not systematically approach the exact answer as coupled cluster methods do, functionals in successive categories can be imagined ascending a ladder to chemical accuracy.[45] For open-shell systems, a spin-unrestricted formalism is recommended, as it better reflects the way Kohn-Sham orbitals are constructed than does a spin-restricted formalism; related to this, the idea of spin contamination conveys little meaning for density functional theory.[46]

Geometry Optimizations and Frequencies

The methods discussed above can be used to compute energies and properties of molecular systems. To correctly model a real system, these computations must be performed using optimized geometries. Geometry optimization is the process of finding stationary points on a potential energy surface. A stationary point is one at which the gradient is zero; the gradient is a matrix of first derivatives of the energy with respect to coordinates. Minimizing a function with respect to $3N$ coordinates, where N is the number of atoms in the system, is by no means a trivial task, but modern quantum chemistry packages contain algorithms that can quite often find the desired geometry. The gradient (and in some cases, the hessian, or second derivative matrix) can be obtained analytically for some methods, but in others can only be computed numerically.

Although geometry optimization algorithms may be able to optimize elusive structures, generally a good starting geometry is required for successful geometry optimization. Once an optimized stucture is obtained, a frequency job must be run at the same level of theory. The harmonic frequencies of a molecular system are proportional to the square roots of the diagonalized hessian. Therefore, a minimum energy geometry will have only real vibrational frequencies, corresponding to upward curvature along all dimensions. A single imaginary mode identifies a saddle point structure, which we label a transition state. Following the imaginary mode in either direction along the associated coordinate will lead to the minima connected by the transition state. More than one imaginary mode identifies a higher-order saddle point, which generally indicates a need for further optimization of the structure.

The harmonic frequencies computed to verify location of minimum-energy geometries may qualitatively

reflect the vibrational frequencies available for probing with vibrational spectroscopy, but are not expected to give qualitative values for these frequencies. The harmonic oscillator may be considered a first approximation to molecular vibration, the quartic terms in a series expansion for which cubic and quartic terms are likely needed. Computation of these further terms is frequently accomplished using second-order vibrational perturbation theory.

As seen above, perturbation theory can be used to solve electronic structure theory problems, but it can also be used in modeling molecular vibrations. Here the harmonic oscillator is treated as the zeroth-order approximation, and the remaining terms in the series are treated as a perturbation.

Multireference Methods

A single Slater determinant serves as an excellent first approximation to the wavefunction for the ground states of many molecular systems, but many excited states, reactions, and even ground states exhibit static correlation, requiring contributions from multiple determinants. Such multiconfigurational systems [1] must be treated using multiple configuration state functions. The methods used to do so are known as multireference methods. In contrast to popular single reference methods, multireference methods are rarely black-box, often requiring the user to choose a space of configurations that will appropriately model the orbitals needed for the necessary chemistry.

Many multireference methods employ complete active space self-consistent field theory (CASSCF) as a first approximation to which dynamic correlation can be added. CASSCF requires the user to select an active space; the CASSCF algorithm will then perform full configuration within that space. Generally, the active space should include orbitals relevant to the chemistry, such as those needed to model the breaking of a bond. [47] CASSCF is a variational method in the chosen active space, but an active space that yields a lower energy than another will not necessarily provide an improved treatment of the underlying chemistry. Additionally, while a large active space may include orbitals that are necessary for the chemistry of interest, it could also contain orbitals that are extraneous to that focus. In some cases, CASSCF fails to even give a qualitatively correct potential energy surface; the shape of the PES may change upon adding static correlation. Therefore, the optimum active space may be the one on which dynamic correlation may be most advantageously added rather than one one which yields the lowest overall CASSCF energy.

Dynamic correlation in multireference systems is often treated using perturbation theory, as in second-order complete active space perturbation theory (CASPT2). [48,49] If perturbative approaches fail, multireference configuration interaction (MRCI) can be tried for small systems. [50] The high cost and lack of size consistency of MRCI make it unsuitable for larger systems.

The T_1 diagnostic[51] measures how well single-reference coupled cluster theory performs for closed-shell systems. Open-shell systems require additional consideration,[52] and may be described quite well by coupled cluster theory even in cases with a large T_1 diagnostic. Many talented theoreticians have devoted decades to multireference coupled cluster, which is intended to satisfy a number of criteria.[53] However, the set of methods that fall under this label for the most part remain a computationally demanding curiosity.

Equation of motion coupled cluster (EOM-CC)[54,55] is a single reference method that is also effective at treating some multireference systems. Other applications of EOM-CC include computations of transition properties such as oscillator strengths and investigations of excited states.

CHAPTER 2

THE METHYLSULFINYL RADICAL CH_3SO EXAMINED[1]

[1]Accepted by *Physical Chemistry Chemical Physics*. Reprinted here with permission of publisher. M. Estep and H. F. Schaefer, *Phys. Chem. Chem. Phys.*, 2016, **18**, 22293

Abstract

Methylsulfinyl radical, a key intermediate in marine atmospheric chemistry, plays a central role in the oxidation of dimethyl sulfide. CH_3SO has been extensively studied here with *ab initio* quantum mechanical methods, with methods as complete as CCSDT(Q) in conjunction with basis sets as large as cc-pV(5+d)Z. In this research, we report high-level predictions for the ground and first excited electronic states of the methylsulfinyl radical. The structures of the $\tilde{X}\ ^2A''$ and $\tilde{A}\ ^2A'$ states are quite different with S–O distances of 1.499 and 1.652 Å, respectively. The $\tilde{X}$ to $\tilde{A}$ energy difference is predicted to be 45.1 kcal mol^{-1}, compared to 21.1 kcal mol^{-1} for the analogous well-characterized methylperoxy radical CH_3OO. The CH_3SO barrier to internal rotation is 0.92 kcal mol^{-1}. The unknown $\tilde{X}\ ^2A''$ torsional vibrational frequency τ is predicted to be 142 cm^{-1} (harmonic) and 128 cm^{-1} (anharmonic). Our predictions of the $\tilde{A}\ ^2A'$ excited state vibrational frequencies are the first to be reported.

Introduction

Volatile sulfur-containing species impact global temperatures through modulation of cloud cover by serving as the primary cloud condensation nuclei (CCN) in the remote marine atmosphere.[56] However, the impact of the atmospheric sulfur cycle (Figure 2.1) on global

climate is not limited to temperature effects. Atmospheric sulfur-containing species can be oxidized to sulfuric acid, an important component of acid rain.[57] Human activities perturb this influential cycle, but biogenic contributions to the cycle still rival anthropogenic input.[58] Dimethyl sulfide (DMS, CH_3SCH_3), the primary biogenic contribution, is produced by cleavage[58,59] of the S–C bond in dimethylsulfoniopropionate [DMSP, $(CH_3)_2S^+CH_2CH_2COO^-$], a zwitterion copiously excreted by marine algae.[57–64] In 1987, Charlson, Lovelock, Andreae, and Warren (CLAW) proposed that sulfates derived from dimethylsulfide are the primary cloud condensation nuclei (CCN) in the remote marine atmosphere, creating a negative feedback loop for global temperature.[56] This CLAW hypothesis suggests that warmer or sunnier conditions augment algal growth, in turn elevating dimethylsulfide production, extending cloud cover, and reducing global temperatures. Despite the complexity of DMS oxidation in the marine boundary layer,[65] a substantial portion proceeds through the methylsulfinyl radical (CH_3SO).[66,67] In this research, we examine the methylsulfinyl radical, an important intermediate in oxidation pathways to sulfates and sulfuric acid.

Several atmospheric reactions yield methylsulfinyl radical: i) release of molecular oxygen from $CH_3S(O)OO$; ii) reactions of CH_3S with ozone, NO_2, or molecular oxygen; iii) hydroxyl radical attack on CH_3SOH; or iv) oxygen abstraction from CH_3SOO by NO.[68–70] Under typical marine atmospheric conditions, methylsulfinyl

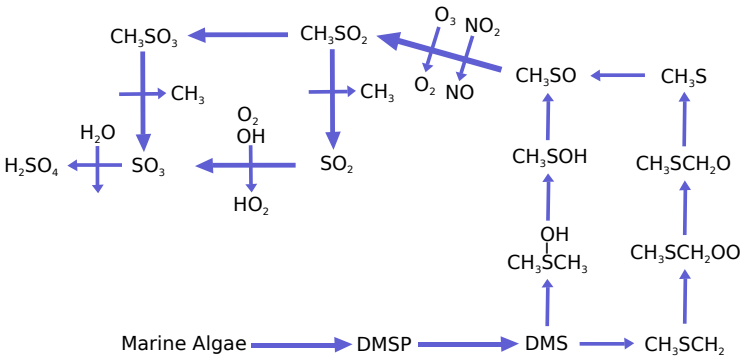

Figure 2.1: Partial atmospheric sulfur cycle. Dimethlysulfoniopropionate (DMSP) is produced by marine algae and is cleaved to dimethyl sulfide (DMS), which is subsequently oxidized to a host of atmospheric sulfur species.

---

radical is primarily consumed via reaction with ozone to produce SO_2.[67] With 72±22% of DMS converted to SO_2,[71] the reactions of the methylsulfinyl radical have garnered some attention,[69,72] and the radical itself demands further study.

Comparison with experimental and computational work on methylperoxy radical (CH_3OO), a far more thoroughly studied isovalent congener of the methylsulfinyl radical,[73–79] promises chemical intuiton for studies of the methylsulfinyl radical. Like the methylperoxy radical, the C_s methylsulfinyl radical has a $^2A''$ electronic ground state, with a $^2A'$ first excited state.[73,74] The recently predicted CH_3OO CCSDTQ/CBS excitation energy between these two electronic states is 21.1 kcal mol^{-1} with inclusion of zero-point vibrational energy and focal point analysis corrections.[74]

The methylsulfinyl radical has seen many fewer *ab initio* studies than its peroxy congener. Of the publications reporting computed vibrational frequencies for CH_3SO,[73,76–79] only one has reported anharmonic computational frequencies, computed using B3LYP/ 6-311++G(2df,2pd), a popular density functional theory method.[76] Density functional theory methods frequently give satisfactory results, but often with less reliable error analysis than that available for convergent quantum mechanical methods.

The 1972 electron spin resonance (ESR) study by Kochi and coworkers predicted a methylsulfinyl radical structure resembling that of the methylperoxy radical, also concluding that the upaired electron will primarily occupy an S–O bonding π orbital.[80] Kochi discussed the effects of hyperconjugation on the geometric structure, and noted that the temperature dependence of the ESR spectrum could correspond to a hydrogen atom eclipsing the π orbital.

The ESR spectrum of methylsulfinyl radical was reconsidered in 1974.[81] The results of the 1974 study suggest that the structure possesses a plane of symmetry, with one hydrogen either trans to the oxygen or

eclipsing it. The experiments did not provide sufficient evidence to distinguish between the two structures, instead leaving determination of the geometric structure to theory.

A 1982 self-consistent field theory study postulated restricted rotation of the methyl group about the C–S bond at low temperatures, with free rotation at high temperatures.[82] While the barrier to rotation has not been reported at a high level of theory, this prediction is consistent with intuition for the size of a methyl rotational barrier.

A 1989 ESR and computational study by Sevilla and coworkers reported spin densities of 0.41 on oxygen and 0.59 on sulfur, obtained using computational charges and nuclear screening constants with an experimentally determined hyperfine coupling value.[83] The ESR data indicate that the methyl group in the methylsulfinyl radical rotates freely at 100K.

To date, only two experimental studies have measured the infrared frequencies of the methylsulfinyl radical. In 2010, Chu and Lee characterized the S–O stretch mode around 1071 cm^{-1} using a step-scan Fourier spectrometer.[79] In a beautiful 2013 study, Schreiner and coworkers IR frequencies for eleven of the twelve modes, missing only the lowest-frequency mode corresponding to torsion of the methyl group around the C–S bond.[73] No IR spectral data are yet available for this torsional mode, making it an important data point for computational analysis. Furthermore, no experimental IR spectra are available for any of the excited electronic states of the methylsulfinyl radical.

To address the dearth of vibrational frequency studies on methylsulfinyl radical, we seek to compute the fundamental modes of the ground and first excited states of methylsulfinyl radical using coupled-cluster theory. In addition, we compute the first excitation energy and methyl rotational barrier for this radical using focal point analysis. Finally, we investigate the fluorescence lifetime of the first excited electronic state ($\tilde{A}\ ^2A'$) of the methylsulfinyl radical.

Methods

Geometries

Geometries for the ground and first excited electronic states of the methylsulfinyl radical were optimized using coupled cluster theory with all single & double, and perturbative triple excitations [CCSD(T)][21,84–87] as implemented in CFOUR.[88] The excited state was obtained by constraining occupation numbers for the Hartree-Fock molecular orbitals. The geometry of the transition state for rotation about the C–S bond was similarly optimized using the CCSD(T)/ANO2 method. Optimizations used the full NASA Ames atomic natural orbital (ANO) basis set, ANO2 (H:(8s6p4d3f), Li-Ne:(13s8p6d4f2g), S:(18s13p6d4f2g), contracted to

H:[4s3p2d1f], Li-Ne:[5s4p3d2f1g], S:[6s5p3d2f1g]). In parallel computations the truncated NASA Ames basis set, ANO1 (H:(8s6p4d), C:(13s8p6d4f), S:(18s13p6d4f) was contracted to (H:[4s2p1d], Li-Ne:[4s3p2d1f], S:[5s4p2d1f]).[35] For second-order vibrational perturbation theory (VPT2) fundamental vibrational modes obtained using coupled-cluster theory, the truncated NASA Ames ANO basis sets ANO0 and ANO1 sometimes match experiment more closely than do the Dunning correlation-consistent basis sets of comparable size.[36] Unrestricted Hartree-Fock (UHF) reference wavefunctions were used for all studies. In the absence of substantial spin contamination, UHF references are typically preferable to restricted open-shell reference wavefunctions.[89]

Vibrational Frequencies

Harmonic vibrational frequencies for each geometry were computed at the above described levels of theory. Fundamental vibrational modes were predicted by adding anharmonic corrections and orbital relaxation corrections to the harmonic frequencies. VPT2 anharmonic frequency corrections[90] were predicted with the CCSD(T)/ANO1 method using PyVPT2[91]. To correct for orbital relaxation, geometries and frequencies were further investigated using Brueckner coupled cluster with doubles and perturbative triples, employing the ANO1 basis set [BCCD(T)/ANO1].[12,13,92] Orbital relaxation corrections to the vibrational frequencies were computed as the differences between the BCCD(T)/ANO1 freqencies and the CCSD(T)/ANO1 frequencies.

Excitation Energy

The CCSDT(Q) first excitation energy was extrapolated to the complete basis set (CBS) limit using focal point analysis.[23,24,26,93] The Dunning correlation-consistent cc-pVnZ basis sets with n =D,T,Q,5 were used, with tight d functions employed for sulfur using the cc-pV(n+d)Z basis sets; in this paper, we will refer to this combination of basis sets as simply cc-pV(n+d)Z for the appropriate value of n.[33] Single-point energies for the FPA scheme were computed at the CCSD(T)/ANO2 geometries computed above.

ZPVE predictions for the ground state and first excited state were begun by summing the CCSD(T)/ANO2 harmonic frequencies. This was followed by CCSD(T)/ANO1 anharmonic ZPVE corrections and orbital relaxation corrections. The latter were computed by taking the difference between ZPVEs for the BCCD(T)/ANO1 and CCSD(T)/ANO1 harmonic frequencies. The ZPVE correction for focal point analysis consisted of the final difference between the ground state and excited state ZPVE values.

Mass-velocity relativistic corrections with 1- and 2-electron Darwin contributions were computed with the CCSD(T)/cc-pVTZ method. Relativistic, non-diagonal Born-Oppenheimer (DBOC), zero-point vibrational energy (ZPVE), and core corrections were added to the focal point results to finalize the evaluation of the

transition origin for the first excited state.

Rotational Transition State

Similarly, the barrier to rotation about the C–S bond was computed using a focal point extrapolation approach. However, the ZPVE correction added to the final result included only the difference between CCSD(T)/ANO2 harmonic contributions for the two states.

Transition Properties

Transition properties such as oscillator strength were computed using the EOM-CCSD coupled cluster method with single and double excitations with the large ANO2 basis set. EOM computations were performed at both the ground state ($\tilde{X}\ ^2A''$) and the excited state ($\tilde{A}\ ^2A'$) CCSD(T)/ANO2 equilibrium geometries. In both cases the vertical transition from the ground state to the excited state is considered. EOM computations at the ground state geometry are relevant to absorption processes, while those at the excited state equilibrium geometry may be used to determine fluorescence properties.

With the exception of the Bruekner doubles coupled-cluster corrections and the EOM-CCSD/ANO2 computations, which were computed using the Psi4 electronic structure theory package,[94] computations were performed using the CFOUR electronic structure theory package,[88] which includes analytic gradients for CCSD and CCSD(T).[95]

Results and Discussion

Stationary points

The $\langle S^2 \rangle$ values for open-shell species fell within 0.05 of the 0.75 value expected for doublet systems. This allows the responsible use of an unrestricted Hartree-Fock (UHF) reference for the ground electronic state [Figure (2.2)], first excited electronic state [Figure (2.3)], and rotational barrier transition state [Figure (2.4)]. Cartesian coordinates for all stationary point geometries are available in the Supporting Information. Relevant geometrical parameters computed in the current study are given in Table (2.1).

In the present geometry optimizations, the excited state C–S bond length is slightly (0.011 Å) longer, the S–O bond is substantially (0.153 Å) longer, and the CSO angle is significantly (12°) smaller compared to the results for the ground state.

Table 2.1: Methylsulfinyl radical CCSD(T)/ANO2 equilibrium geometrical parameters. Bond distances are in angstroms, angles in degrees

	Ground State ($\tilde{X}\ ^2A''$)	Excited State ($\tilde{A}\ ^2A'$)
C–S (Å)	1.802	1.813
S–O (Å)	1.499	1.652
∠CSO	106.1	94.0

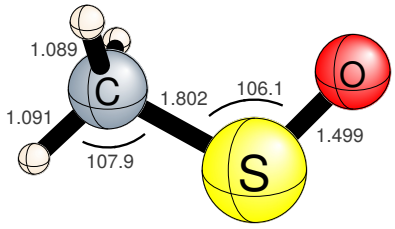

Figure 2.2: Ground state methylsulfinyl radical geometry optimized with the CCSD(T)/ANO2 method.

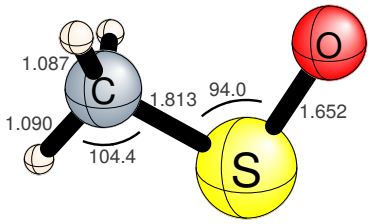

Figure 2.3: Excited state methylsulfinyl radical geometry optimized with the CCSD(T)/ANO2 method.

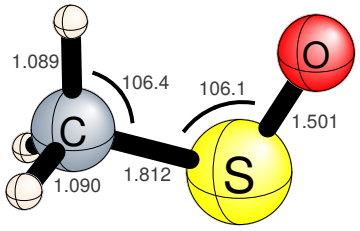

Figure 2.4: $\tilde{X}\ ^2A''$ rotational transition state geometry optimized with the CCSD(T)/ANO1 method.

Table (2.2) compares the S–O bond length in sulfur monoxide to that in methylsulfinyl radical. Due to the electronegativity difference between oxygen and sulfur, the orbitals localized to sulfur and oxygen in methylsulfinyl radical have an asymmetric character that distinguishes them from the orbitals localized to the two oxygens in methylperoxy radical. This can be understood in terms of perturbing SO with an alkyl group or hydrogen, which is similar in effect to adding an electron to SO to form the SO^- radical.

Table 2.2: Several S–O bond lengths in Å. Methylsulfinyl radical bond lengths were computed in this work, while the isolated diatomic S–O distances are from the experimental and computational literature

$SO(^1\Delta)$[96]	1.492			CH_3SO ($^2A'$)	1.652
		SO^- $^2\Pi$	1.570[97]		
$SO(^3\Sigma^-)$[98]	1.482			CH_3SO ($^2A''$)	1.499

The 1974 ESR study of Nishikida and Williams concluded that the radical is localized to a sulfur π^* orbital in the ground electronic state.[81] Our results confirm those of Nishikida and Willams, indicating that the singly-occupied orbital is indeed an orbital of π^* character, with contributions from both the sulfur and the oxygen (Figure 2.5). The 1989 ESR study by Swarts et al.[83] concluded that a greater spin density resides on the sulfur atom than that on the oxygen atom. In line with these findings, Mulliken population analysis on our CCSD(T)/ANO2 results indicates that the sulfur atom has a spin density of 0.58 and the oxygen atom has a spin density of 0.41, with the remaining atoms contributing 0.01 to the total spin density. Intuitively, excitation into an antibonding orbital should result in a weaker, longer bond, as computed theoretically here.

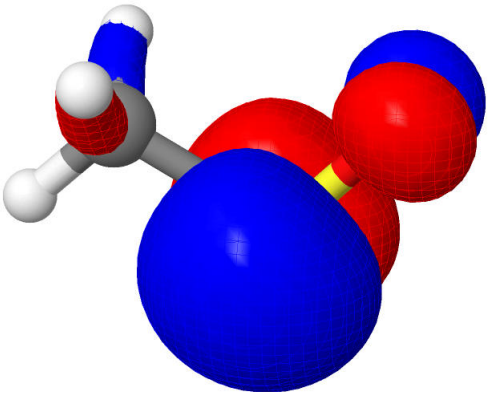

Figure 2.5: Methylsulfinyl radical ground electronic state singly-occupied molecular orbital.

Transition origin

Using focal point analysis, we predict a transition origin of $T_0 = 45.08$ kcal mol^{-1} for the excitation from the ground electronic state ($\tilde{X}$ $^2A''$)to the lowest excited state ($\tilde{A}$ $^2A'$) of methylsulfinyl radical (Table 2.3). The corrections due to MP2 (+21.6 kcal mol^{-1}), CCSD (7.6 kcal mol^{-1}), and CCSD(T) (1.6 kcal mol^{-1}) all significantly affect our final predictions. The CCSD(T) result is more reliable than expected, due to a fortuitous cancellation of the CCSDT and CCSDT(Q) contributions.

Table 2.3: Focal point analysis of energy difference between ground ($\tilde{X}\ ^2A''$) electronic state and first excited ($\tilde{A}\ ^2A'$) electronic state, kcal mol^{-1}

Basis set	UHF	+δMP2	+δCCSD	+δCCSD(T)	+δCCSDT	+δCCSDT(Q)	NET
(D+d)Z	+24.30	+17.76	−5.10	+1.18	−0.07	+0.27	[+38.35]
(T+d)Z	+29.07	+19.99	−7.04	+1.52	−0.29	+0.23	[+43.49]
(Q+d)Z	+29.58	+20.82	−7.41	+1.59	[−0.29]	[+0.23]	[+44.52]
(5+d)Z	+29.74	+21.19	−7.48	+1.61	[−0.29]	[+0.23]	[+45.01]
CBS	[+29.81]	[+21.59]	[−7.56]	[+1.64]	[−0.29]	[+0.23]	[+45.42]

Final $\Delta H_{0K} = \Delta E_e$[CCSDT/CBS] + Δ_{ZPVE}[CCSD(T)/cc-pV(T+d)Z] + Δ_{core}[CCSD(T)/cc-pV(T+d)Z] + Δ_{rel}[CCSD(T)/cc-pV(T+d)Z] + Δ_{DBOC}[UHF/cc-pV(T+d)Z] = + 45.420 − 0.300 + 0.103 − 0.139 − 0.009 = **+45.08 kcal mol^{-1}**

Table 2.4: Methylsulfinyl radical ground state vibrational frequencies in cm^{-1}. Anharmonic frequencies were computed by applying CCSD(T)/ANO1 anharmonic corrections to the CCSD(T)/ANO2 harmonic frequencies. CCSD(T)/ANO2 harmonic intensities are reported in km mol^{-1} in parentheses. The descriptions used here and in all tables in the present paper follow the published notation for the methylperoxy radical vibrational frequencies.[74] The notation used here is v: stretch, δ: bend, τ: torsion, d: deformation, u: umbrella, ρ: rock, w: wag, s: symmetric, a: asymmetric

Mode	Sym	Description	ANO2 Harmonic	+Anharm	+Brueckner	Final	Experiment[73]
ν_1	a′	v_s(CH$_3$)	3147	-148.0	-0.9	2998 (2.7)	2995
ν_2	a′	v_s(CH$_3$)	3042	-118.2	-1.0	2923 (3.6)	2919
ν_3	a′	d(CH$_3$)	1466	-40.5	-0.3	1425 (6.7)	1417
ν_4	a′	u(CH$_3$)	1327	-33.7	-0.4	1293 (0.7)	1289
ν_5	a′	v(SO)	1095	-15.8	-15.2	1064 (39.2)	1068
ν_6	a′	ρ(CH$_3$)	950	-22.2	-0.2	928 (9.8)	927
ν_7	a′	v(CS)	695	-16.1	-0.6	658 (12.1)	670
ν_8	a′	δ(CSO)	334	1.1	-0.7	334 (7.0)	341
ν_9	a″	v_a(CH$_3$)	3149	-150.6	-0.8	2998 (1.9)	2995
ν_{10}	a″	d_a(CH$_3$)	1452	-41.6	-0.3	1410 (8.4)	1405
ν_{11}	a″	w(CH$_3$)	890	-17.0	0.3	873 (1.3)	868
ν_{12}	a″	τ(HCSO)	142	-13.7	-0.3	128 (0.4)	–

Anharmonic vibrational frequencies

Besides the work of Chu and Lee,[79] the comprehensive research of Schreiner and coworkers[73] represents the only experimental report of methylsulfinyl IR frequencies. The Schreiner experiments are more complete, with all but one of the modes observed. Table 2.10 reports both experimental and theoretical ground state vibrational frequencies from the literature for the methylsulfinyl radical.

Our predicted fundamental frequencies for the ground state and first excited state are reported in Tables 2.4 and 2.5. Frequencies for the rotational transition state may be found in Table 2.6. Harmonic frequencies were predicted for the ground state, first excited state, and the rotational transition state at both the CCSD(T)/ANO1 and CCSD(T)/ANO2 levels. Anharmonic corrections for the ground state and first excited state were computed at the CCSD(T)/ANO1 level. While the O–O stretch in methylperoxy radical is coupled to the methyl rock motion, in methylsulfinyl radical these motions are largely uncoupled.

Table 2.5: Vibrational frequencies in cm^{-1} for the $\tilde{A}\ ^2A'$ first excited electronic state of CH_3SO. Anharmonic frequencies were computed by applying CCSD(T)/ANO1 anharmonic corrections to the CCSD(T)/ANO2 harmonic frequencies. CCSD(T)/ANO2 harmonic intensities are reported in km mol^{-1} in parentheses. No experimental or published computational frequencies are available for the excited electronic states of methylsulfinyl radical.

Mode	Sym	Description	ANO2 Harmonic	+Anharm	+Brueckner	Final
ν_1	a′	$v_a(CH_3)$	3158	-148.1	-0.2	3009 (3.9)
ν_2	a′	$v_s(CH_3)$	3053	-116.3	-0.6	2936 (11.0)
ν_3	a′	$d(CH_3)$	1489	-42.2	-0.4	1446 (9.8)
ν_4	a′	$u(CH_3)$	1330	-35.7	-1.1	1293 (6.6)
ν_5	a′	v(SO)	958	-16.7	-0.9	940 (7.0)
ν_6	a′	$\rho(CH_3)$	734	-10.2	0.8	725 (1.1)
ν_7	a′	v(CS)	683	-19.2	-1.6	662 (4.0)
ν_8	a′	δ(CSO)	253	-0.8	-0.9	251 (5.4)
ν_9	a″	$v_a(CH_3)$	3164	-151.3	-0.2	3013 (2.5)
ν_{10}	a″	$d_a(CH_3)$	1447	-37.5	-0.7	1409 (7.0)
ν_{11}	a″	$w(CH_3)$	980	-17.5	-0.4	962 (5.1)
ν_{12}	a″	τ(HCSO)	209	-7.7	0.0	201 (0.0)

Table 2.6: Harmonic vibrational frequencies in cm^{-1} computed using CCSD(T)/ANO2 for the rotational transition state on the $\tilde{A}\ ^2A'$ ground electronic state of CH_3SO. CCSD(T)/ANO2 harmonic intensities are reported in km mol^{-1} in parentheses.

Mode	Sym	Description	ANO2 Harmonic	
ν_1	a′	v_a(CH)	3150	0.4
ν_2	a′	v(CH)	3043	3.6
ν_3	a′	δ(HCH)	1467	10.9
ν_4	a′	$u(CH_3)$	1320	2.1
ν_5	a′	v(SO)	1090	46.1
ν_6	a′	$d(CH_3)$	930	4.4
ν_7	a′	v(CS)	695	14.6
ν_8	a′	δ(CSO)	357	7.6
ν_9	a″	v_a(CH)	3142	2.6
ν_{10}	a″	ρCH_3	1456	8.2
ν_{11}	a″	w(CH)	889	0.3
ν_{12}	a″	$\tau(CH_3)$	$145i$	0.6

Table 2.7: Transition properties for electronic transitions $\tilde{X}\ ^2A'' \leftarrow \tilde{A}\ ^2A'$ and $\tilde{A}\ ^2A' \leftarrow \tilde{X}\ ^2A''$. The former transition is relevant to fluorescence, while the latter can be used to study absorption processes. Notation follows that of Ref. 19

	$\tilde{X}\ ^2A''$	$\tilde{A}\ ^2A'$
	Equilibrium	Equilibrium
Vertical excitation energy	54.0 kcal mol^{-1}	32.3 kcal mol^{-1}
Transition dipole moment	0.098 Debye	0.058 Debye
Oscillator strength	5.5×10^{-4}	1.1×10^{-4}

Table 2.8: Comparison of the transition properties in the present research to experimental and computational results from the literature[73]

	λ_{max}	ΔE	Einstein A Coefficient	Fluorescence Lifetime
EOM-CCSD/ANO2 (Current work)	529.9 nm	54 kcal mol^{-1}	1.312 $\times 10^5$ Hz	0.103 ms
TD-UB3LYP/6-311+G(3df,3pd)[73]	540 nm	53 kcal mol^{-1}	–	–
Experiment[73]	530 nm	54 kcal mol^{-1}	–	–

The orbital relaxation Brueckner correction for the S–O stretch is significant (-15.2 cm^{-1}) for the ground state, as expected since the radical is largely localized on the S–O moiety. This 15.2 cm^{-1} Brueckner correction also brings the theory into closer agreement with the matrix isolation experiments of Schreiner.[73] The Brueckner correction is unexceptional (-0.9 cm^{-1}) in the excited state; this stands in contrast to the analogous situation in methylperoxy radical, for which the orbital relaxation corrections for the two modes contributing to the O–O stretches are of the same order in the ground (-1.4 cm^{-1} and -6.9 cm^{-1}) and first excited (-2.5 cm^{-1}and -7.1 cm^{-1}) states.

Transition Properties

TD-UB3LYP/6-311+G(3df,3pd) electronic transitions to the three lowest excited electronic states have been previously reported in the literature.[73] Both the earlier theoretical results and, more importantly, the experimental UV-vis measurements, of the vertical transition to the lowest excited state compare favorably to the currently computed EOM-CC values (Table 2.19).

We report a fluorescence lifetime of 0.1 ms, significantly shorter than the equivalent methylperoxy radical fluorescence lifetime of 4.7 ms.[92] Our λ_{max} of 529.9 nm corresponding to the excitation energy computed by EOM-CC compares very agreeably to the λ_{max} of 530 nm available from the experimental UV-vis results (Table 2.8). However, this excellent concurrence must be tempered with the possibility that the matrix used in the experiment may shift the observed wavelength.

Table 2.9: Focal point analysis of energy difference between ground ($\tilde{X}\ ^2A''$) electronic state energy minimum and rotational transition state, kcal mol^{-1}

	UHF	+δMP2	+δSD	+δSD(T)	+δSDT	+δSDT(Q)	NET
(D+d)Z	+0.98	+0.05	−0.14	−0.03	−0.00	−0.00	[+0.86]
(T+d)Z	+1.22	+0.14	−0.19	−0.03	−0.00	[−0.01]	[+1.13]
(Q+d)Z	+1.26	+0.12	−0.20	−0.04	[−0.00]	[−0.01]	[+1.14]
(5+d)Z	+1.27	+0.12	−0.20	−0.04	[−0.00]	[−0.01]	[+1.13]
CBS	[+1.26]	[+0.12]	[−0.20]	[−0.05]	[−0.00]	[−0.01]	[+1.12]

ΔH_{0K} = ΔE_e[CCSDT/CBS] + Δ_{ZPVE}[CCSD(T)/cc-pV(T+d)Z] + Δ_{core}[CCSD(T)/cc-pV(T+d)Z] + Δ_{rel}[CCSD(T)/cc-pV(T+d)Z] + Δ_{DBOC}[UHF/cc-pV(T+d)Z] = +1.1168 – 0.1422 + 0.0068 – 0.0050 – 0.0022 = **+0.98 kcal mol^{-1}**

Rotational Transition State

Focal point analysis (Table 2.9) indicates that the barrier for rotation about the C–S bond is 0.98 kcal mol^{-1}, significantly higher than the 0.72 kcal mol^{-1} barrier to C–O rotation in the methylperoxy radical.[75] This may be understood qualitatively in terms of the decreased hybridization between s and p orbitals in sulfur, in light of electronegativity differences, and possibly in consideration of the hyperconjugation mentioned in Kochi's study[80] of the methylsulfinyl radical. The difference between this rotational barrier and that of the methylperoxy radical is less substantial than the difference between the first excitation energy of methylsulfinyl radical and that of methylperoxy radical.

Conclusions

We have here described the high-level characterization of the ground and first excited electronic states of the methylsulfinyl radical, including an accurate transition origin for the excitation between these two electronic states. Excitation of this radical from the ground electronic state ($\tilde{X}\ ^2A''$) to the first excited state ($\tilde{A}\ ^2A'$) increases the S–O bond length by 0.153 Å and decreases ∠CSO by 12°. Our population analysis indicates that the unpaired electron is primarily shared between the oxygen and sulfur atoms, with a spin density of 0.58 residing on the sulfur and a spin density of 0.41 residing on the oxygen. The remaining atoms contribute a total of only 0.01 to the spin density. Our prediction of 45.1 kcal mol^{-1} for the transition origin precedes experimental determination of this energy difference, as it is a prediction of the adiabatic transition, rather than the vertical transition at 530 nm observed experimentally. This transition origin is significantly larger than the corresponding value of 21.1 kcal mol^{-1} for methylperoxy radical. The computed λ_{max} of 529.9 nm (54 kcal mol^{-1}) matches Schreiner's experimental result very favorably.[73] We have determined the barrier to rotation about the C–S bond to be 0.9 kcal mol^{-1}, small but somewhat larger than the 0.7 kcal mol^{-1} barrier in methylperoxy radical[75]. In the absence of an experimental determination of the ground state

torsional vibrational frequency τ, our prediction (128 cm^{-1}) is the most reliable available. In addition, future experimental investigations of the $\tilde{A}\ ^2A'$ state should benefit from our predictions of the vibrational frequencies, the first available in the literature.

Acknowledgements

This research was supported by the U. S. Department of Energy, Chemical Sciences Division, Fundamental Interactions, Computational and Theoretical Chemistry Program. M.E. thanks Justin Turney, Jay Agarwal, Kevin Moore, Andreas Copan, and Andrew Launder for helpful discussions.

Supplementary Information

All states considered in the present work were doublet states optimized in C_s symmetry.

CH_3SO Ground Electronic State ($\tilde{X}\ ^2A''$)

Occupation numbers:

	A''	A'
α	13	4
β	13	3

Table 2.10: Ground state ($\tilde{X}\ ^2A'$) methylsulfinyl radical frequency values found in the literature, reported in cm^{-1}.

		Harmonic					Anharmonic		Expt	
Mode	Sym	B3LYP[76]	B3LYP[77]	AE-CCSD(T)[73]	Gaussian-4[73]	B3LYP[79]	B3P86[79]	B3LYP[76]	expt[73]	expt[79]
ν_1	a″	3131	3129	3151	3144	3128	3148	2981	2995	–
ν_2	a′	3037	3035	3065	3042	3035	3047	2917	2919	–
ν_3	a′	1460	1459	1477	1460	1460	1450	1419	1417	–
ν_4	a′	1323	1326	1324	1319	1322	1313	1299	1288	–
ν_5	a′	1061	1072	1077	1057	1051	1081	1047	1068	1071 ± 1
ν_6	a′	947	948	944	941	948	944	921	926	–
ν_7	a′	662	665	690	663	660	683	646	669	–
ν_8	a′	332	336	328	322	331	333	333	340	–
ν_9	a′	3130	3129	3149	3141	3127	3147	2979	2995	–
ν_{10}	a″	1446	1445	1464	1445	1446	1436	1404	1405	–
ν_{11}	a″	887	887	888	883	889	882	869	868	–
ν_{12}	a″	137	141	134	127	137	138	93	–	–

Minimum-Energy Structure CCSD(T)/ANO1

Software:	CFour 1.0
Theory:	CCSD(T)/ANO1
Charge:	0
Multiplicity:	2
Frozen Core:	ON
Geometry Convergence:	1.0E-9

Equilibrium Geometry (Å):

H	-2.2591906630	0.3561031197	-0.0000000000
C	-1.4602099596	-0.3875247704	-0.0000000000
S	0.1231740905	0.4885941747	-0.0000000000
O	1.1835752818	-0.5811629339	0.0000000000
H	-1.5230460854	-1.0092567076	0.8931384867
H	-1.5230460854	-1.0092567076	-0.8931384867

Frequencies (cm^{-1}):

139.2032
331.0387
685.8069
890.2235
946.6529
1083.8226
1324.6757
1449.1373
1463.4529
3041.1660
3145.7567
3148.8905

ZPVE:	26.2317 kcal mol^{-1}
SCF Convergence:	1.0E-10
CC Convergence:	1.0E-10
UHF Reference energy	-512.043458240531 E_h
Final energy	-512.679538426120 E_h
$\langle S^2 \rangle$	0.776
T1	0.033
T2	0.02
Gradient	Analytic

Minimum-Energy Structure CCSD(T)/ANO2

Software:	CFour 1.0
Theory:	CCSD(T)/ANO2
Charge:	0
Multiplicity:	2
Frozen Core:	ON
Geometry Convergence:	1.0E-9

Equilibrium Geometry (Å):

H	-2.2509697198	0.3613035509	-0.0000000000
C	-1.4559420392	-0.3851022499	-0.0000000000
S	0.1223153099	0.4847998944	-0.0000000000
O	1.1811859407	-0.5761743588	0.0000000000
H	-1.5199830223	-1.0056807712	0.8927955110
H	-1.5199830223	-1.0056807712	-0.8927955110

Frequencies (cm^{-1}):

142.4783
334.1565
695.0646
889.7511
949.8553
1095.3919
1327.1385
1451.5482
1466.0564
3041.9176
3146.9911
3148.9728

ZPVE:	25.2881 kcal mol^{-1}
SCF Convergence:	1.0E-10
CC Convergence:	1.0E-10
UHF Reference energy	-512.048095598701 E_h
Final energy	-512.719438774341 E_h
$\langle S^2 \rangle$	0.787
T1	0.032
T2	0.02
Gradient	Analytic

Minimum-Energy Structure BCCD(T)/ANO1

Software:	Psi4
Theory:	BCCD(T)/ANO1
Charge:	0
Multiplicity:	2
Geometry Convergence:	RMS Force 1.0E-6
Equilibrium Geometry (Å):	

H	-2.2594566935	0.3558335612	0.0000000000
C	-1.4603694998	-0.3878107179	0.0000000000
S	0.1228335457	0.4891309447	0.0000000000
O	1.1844319104	-0.5819680454	0.0000000000
H	-1.5233592211	-1.0095450019	0.8932064012
H	-1.5233592211	-1.0095450019	-0.8932064012

Frequencies (cm^{-1}):

138.943
330.339
685.228
890.537
946.447
1068.615
1324.281
1448.792
1463.173
3040.193
3144.860
3148.136

ZPVE:	25.2027 kcal mol^{-1}
Final energy	-512.6800499 E_h
Gradient	Numeric

Rotational transition state CCSD(T)/ANO1

Software:	CFour 1.0
Theory:	CCSD(T)/ANO1
Charge:	0
Multiplicity:	2
Frozen Core:	ON
Geometry Convergence:	1.0E-9
Equilibrium Geometry (Å):	

C	-1.4693671390	0.3853395912	0.0000000000
S	0.1258648563	-0.4898561090	0.0000000000
O	1.1853767123	0.5835494121	0.0000000000
H	-1.2343313229	1.4494445999	0.0000000000
H	-2.0379349717	0.1205712899	-0.8920704853
H	-2.0379349717	0.1205712899	0.8920704853

Frequencies (cm^{-1}):

142.7966i
354.6870
685.5770
886.6665
925.9689
1078.4911
1316.6356
1452.5510
1464.0369
3042.6275
3141.5675
3159.7328

ZPVE:	25.0310 kcal mol^{-1}
SCF Convergence:	1.0E-10
CC Convergence:	1.0E-10
UHF Reference energy	-512.618840637054 E_h
Final energy	-512.677886444682 E_h
$\langle S^2 \rangle$	0.785
T1	0.033
T2	0.03
Gradient	Analytic

Rotational Transition State CCSD(T)/ANO2

Software:	CFour 1.0
Theory:	CCSD(T)/ANO2
Charge:	0
Multiplicity:	2
Frozen Core:	ON
Geometry Convergence:	1.0E-9
Equilibrium Geometry (Å):	

C	-1.4647912058	0.3828937921	0.0000000000
S	0.1251703058	-0.4862751136	0.0000000000
O	1.1824656024	0.5789596144	0.0000000000
H	-1.2334134703	1.4468259345	0.0000000000
H	-2.0315186500	0.1160617102	-0.8914816009
H	-2.0315186500	0.1160617102	0.8914816009

Frequencies:

144.7431i
357.0137
695.3994
889.1443
929.6082
1089.8934
1320.2352
1455.9998
1466.7974
3043.4856
3142.3001
3160.4886

ZPVE:	25.0895 kcal mol^{-1}
SCF Convergence:	1.0E-10
CC Convergence:	1.0E-10
UHF Reference energy	-512.046146830428 E_h
Final energy	-512.717729459839 E_h
$\langle S^2 \rangle$	0.787
T1	0.032
T2	0.02
Gradient	Analytic

CH_3SO ($\tilde{A}\ ^2A'$)

Occupation numbers:

	A''	A'
α	13	4
β	12	4

Minimum-energy structure CCSD(T)/ANO1

Software:	CFour 1.0
Theory:	CCSD(T)/ANO1
Charge:	0
Multiplicity:	2
Frozen Core:	ON
Geometry Convergence:	1.0E-9
Equilibrium Geometry (Å):	

H	-2.2221601568	0.1737208367	-0.0000000000
C	-1.3676909325	-0.5039113213	-0.0000000000
S	0.0841391191	0.5896686273	-0.0000000000
O	1.1711325837	-0.6707228759	0.0000000000
H	-1.3744586861	-1.1177119764	0.8987375735
H	-1.3744586861	-1.1177119764	-0.8987375735

Frequencies (cm^{-1}):

205.2934
253.0606
682.4609
725.0451
957.2973
978.9611
1330.3587
1445.0348
1485.8584
3052.8142
3156.1938
3161.4989

ZPVE:	24.9215 kcal mol^{-1}
SCF Convergence:	1.0E-10
CC Convergence:	1.0E-10
UHF Reference energy	-511.998265754416 E_h
Final energy	-512.611374451606 E_h
$\langle S^2 \rangle$	0.763
T1	0.031
T2	0.02
Gradient	Analytic

Minimum-energy structure CCSD(T)/ANO2

Software:	CFour 1.0			
Theory:	CCSD(T)/ANO2			
Charge:	0			
Multiplicity:	2			
Frozen Core:	ON			
Geometry Convergence:	1.0E-9			
Equilibrium Geometry (Å):				
	H	-2.2144127479	0.1895280279	-0.0000000000
	C	-1.3678704294	-0.4965783375	-0.0000000000
	S	0.0878554674	0.5849046086	-0.0000000000
	O	1.1638318427	-0.6688467415	0.0000000000
	H	-1.3782781817	-1.1085931940	0.8986136032
	H	-1.3782781817	-1.1085931940	-0.8986136032
Frequencies (cm^{-1}):				
	208.7370			
	252.9643			
	683.1387			
	734.1697			
	957.8931			
	980.0153			
	1330.1197			
	1447.4180			
	1488.7834			
	3052.9625			
	3157.4615			
	3164.1043			
ZPVE:	24.9571 kcal mol^{-1}			
SCF Convergence:	1.0E-10			
CC Convergence:	1.0E-10			
UHF Reference energy	-512.001816668576 E_h			
Final energy	-512.649312382801 E_h			
$\langle S^2 \rangle$	0.763			
T1	0.033			
T2	0.03			
Gradient	Analytic			

Minimum-energy structure BCCD(T)/ANO1

Software:	Psi4
Theory:	BCCD(T)/ANO1
Charge:	0
Multiplicity:	2
Frozen Core:	ON
Geometry Convergence:	RMS Force 1.0E-6
Equilibrium Geometry (Å):	

H	-2.222342124016	0.174313836993	0.000000000000
C	-1.368422526616	-0.504079381007	0.000000000000
S	0.084378490184	0.589254071593	0.000000000000
O	1.171279318284	-0.669795298707	0.000000000000
H	-1.374973502616	-1.117793070507	0.898833577500
H	-1.374973502616	-1.117793070507	-0.898833577500

Frequencies (cm^{-1}):

205.3281
252.1836
680.8362
725.8256
956.3662
978.5290
1329.2747
1444.3636
1485.4765
3051.1885
3155.9744
3161.3445

ZPVE:	24.9127 kcal mol^{-1}
Final energy	-512.719438774341 E_h
Gradient	Numeric

Table 2.11: Energy values (Hartree) used for focal point analysis corrections

State	GS	XS	TS
Frozen Core	−512.666892057105	−512.597077904741	−512.665097275290
All-Electron	−513.106058947981	−513.036081301753	−513.104253347319
MVD1	−1.14331055382883	−1.14353012096674	−1.14331840488828
MVD2	−0.03879361835091	−0.03879607869464	−0.03879371581377
DBOC	+0.0103944588	+0.0103798740	+0.0103910206

Table 2.12: ZPVE values (kcal mol^{-1}) used for focal point analysis corrections

State	GS	XS	TS
Harmonic ZPVE	25.2317	24.9216	25.0895
Anharmonic ZPVE	-0.3451	-0.3451	–
Brueckner ZPVE	-0.0290	-0.0088	–
Total ZPVE	24.8576	24.5677	25.0895

Table 2.13: Corrections for GS-XS focal point analysis, kcal mol^{-1}

Core:	0.1026
Relativistic:	−0.1393
ZPVE:	−0.2999
DBOC:	−0.0092

Table 2.14: Corrections for GS-TS focal point analysis, kcal mol^{-1}

Core:	0.0068
Relativistic:	−0.0050
ZPVE:	−0.1422
DBOC:	−0.0022

Energy Values for FPA

Table 2.15: Electronic ground state energy values for focal point approach (Hartree)

	Basis			
Theory	cc-pV(D+d)Z	cc-pV(T+d)Z	cc-pV(Q+d)Z	cc-pV(5+d)Z
UHF	-511.9687350	-512.0340500	-512.0478183	-512.0512207
MP2	-512.4128803	-512.6030323	-512.6620159	-512.6842617
CCSD	-512.4495456	-512.6337504	-512.6864678	-512.7036359
CCSD(T)	-512.4640947	-512.6597788	-512.7159919	-512.7344252
CCSDT	-512.4651670	-512.6607039		
CCSDT(Q)	-512.4667102	-512.6624277		

Table 2.16: Rotational transition state on electronic ground state energy values for focal point approach (Hartree)

	Basis			
Theory	cc-pV(D+d)Z	cc-pV(T+d)Z	cc-pV(Q+d)Z	cc-pV(5+d)Z
UHF	-511.9671655	-512.0321108	-512.0458040	-512.0492043
MP2	-512.4112259	-512.6008681	-512.6598030	-512.6820525
CCSD	-512.4481154	-512.6318921	-512.6845768	-512.7017501
CCSD(T)	-512.4627131	-512.6579651	-512.7141621	-512.7326064
CCSDT	-512.4637905	-512.6588974		
CCSDT(Q)	-512.4653406			

Table 2.17: Electronic excited state energy values for focal point approach (Hartree)

	Basis			
Theory	cc-pV(D+d)Z	cc-pV(T+d)Z	cc-pV(Q+d)Z	cc-pV(5+d)Z
UHF	-511.9300131	-511.9877195	-512.0006739	-512.0038235
MP2	-512.3458547	-512.5248398	-512.5816924	-512.6030895
CCSD	-512.3906399	-512.5667778	-512.6179486	-512.6343849
CCSD(T)	-512.4033016	-512.5903783	-512.6449429	-512.6626007
CCSDT	-512.4044801	-512.5917619		
CCSDT(Q)	-512.4055911	-512.5931238		

Table 2.18: methylsulfinyl radical $\mathcal{T}_1$ and $\mathcal{T}_2$ amplitudes for states under study.

	Basis	Ground State	Excited State	Transition State
$\mathcal{T}_1$	ANO1	0.033	0.031	0.033
	ANO2	0.032	0.033	0.032
maxt_{ij}	ANO1	0.02	0.03	0.03
	ANO2	0.02	0.03	0.02

Table 2.19: Transition properties for electronic transitions $\tilde{X}\ ^2A'' \leftarrow \tilde{A}\ ^2A'$ and $\tilde{A}\ ^2A' \leftarrow \tilde{X}\ ^2A''$. The former transition is relevant to fluorescence, while the latter can be used to study absorption processes. Notation follows that of Ref.[74]:

	$\tilde{X}\ ^2A''$	$\tilde{A}\ ^2A'$
	Equilibrium	Equilibrium
$\tilde{\nu}_{\tilde{A}}$	18872 cm^{-1}	11299 cm^{-1}
$\lvert\langle\tilde{X}\rvert\hat{\mu}_z\lvert\tilde{A}\rangle\rvert$	0.098 Debye	0.058 Debye
$f_{\tilde{A}}$	5.5×10^{-4}	1.1×10^{-4}

Vertical excitation energy: $\tilde{\nu}_{\tilde{A}} = \frac{\omega_{\tilde{A}}}{2\pi c}$

Transition dipole moment: $|\langle\tilde{X}|\hat{\mu}_z|\tilde{A}\rangle| \equiv \sqrt{\langle\tilde{X}|\hat{\mu}_z|\tilde{A}\rangle\langle\tilde{A}|\hat{\mu}_z|\tilde{X}\rangle}$

Oscillator strength: $f_{\tilde{A}} = \frac{2}{3}\frac{m_e}{e^2\hbar}\omega_{\tilde{A}}|\langle\tilde{X}|\hat{\mu}|\tilde{A}\rangle|^2$

Table 2.20: Ground electronic state spin densities calculated using Mulliken population analysis for the CCSD(T)/ANO2 method with a UHF reference. The final two atoms listed are the equivalent hydrogens. A spin density of 0.58099757 resides on the sulfur, with a spin density of 0.40894725 on the oxygen. The remaining atoms contribute only 0.01005518 to the spin density.

Z-matrix center	Population
H	-0.00030509
C	-0.01374331
S	0.58099757
O	0.40894725
H	0.01205179
H	0.01205179

CHAPTER 3

VIABILITY OF THE METHYLSULFINYL RADICAL-OZONE REACTION[2]

[2]To be submitted to *ChemPhysChem, A European Journal of Chemical Physics and Physical Chemistry.*

Abstract

Although integral to remote marine atmospheric sulfur chemistry, the reaction between methylsulfinyl radical (CH_3SO) and ozone poses challenges to theoretical treatments. The lone theoretical study on this reaction reported an unphysically large barrier of 66 kcal mol^{-1} for the addition of CH_3SO and O_3. Using several computational methods, including density-fitted MP2 computations, we demonstrate here that this result stems from improper use of MP2 with a single-reference, unrestricted Hartree–Fock (UHF) wavefunction. We then characterized the potential energy surface using density functional theory (DFT). We then in very preliminary work searched for stationary points with CASSCF and complete active space second-order perturbation theory (CASPT2). The DFT computations revealed an adduct and a transition state with a low energetic barrier of around 1 kcal mol^{-1}. CASSCF and CASPT2 scans instead indicate that the reaction is barrierless. These results concur with the literature that the reaction proceeds completely to SO_2.

Introduction

The biogenic release of dimethylsulfide to the remote marine atmosphere is a major source of global sulfur emissions, on par with human contributions to total sulfur emissions.[58–66,68] Because the sulfur-containing products of dimethylsulfide oxidation may play an important role in climate regulation,[56,57] it is important to correctly model the reactions involved in this oxidation. Most of the biogenic sulfur that is oxidized to SO_2 in the remote marine atmosphere proceeds through the addition of the methylsulfinyl radical (CH_3SO) and ozone; the SO_2 formed can in turn be converted to sulfuric acid.[99] A qualitatively incorrect description of the CH_3SO and O_3 reaction could lead to discrepancies in predictions of SO_2 concentration in the atmosphere. Along with ozone, O_2 may be considered a likely oxidant for CH_3SO, as it is the most abundant oxidant available in the marine boundary layer. As expected for the combination of two radicals, the addition of O_2 with CH_3SO is nearly barrierless, which along with a high exothermicity[100] suggests a potential atmospheric role for this reaction. However, the rate of the CH_3SO reaction with O_2 is thought to be negligibly low.[69] Tyndall and Ravishankara note that the rate of this O_2 reaction must be fairly slow compared to the reaction of the methylsulfinyl radical with NO_2.[101] Atmospheric methylsulfinyl radical is therefore thought to be oxidized primarily by NO_2 and by ozone. Reaction with NO_2 predominates in regions with high levels of anthropogenic emissions, but ozone is the more important oxidant in the remote marine atmosphere.[67]

Only a single theoretical study has been performed on the title reaction. In that 2007 attempt, Li, Meng, and Zheng[102] mapped the MP2/6-311++G(2df,p) potential energy surface for the addition reaction of CH_3SO with O_3 (Figure 3.1). In the resulting view of the reaction, CH_3SO directly abstracts an oxygen

atom from O_3 via a saddle point 66 kcal mol^{-1} above the reactants. The resulting CH_3SO_2 radical and O_2 lie 67 kcal mol^{-1} below the reactants CH_3SO and O_3. This CH_3SO_2 radical would then further decompose to CH_3 and SO or would isomerize to CH_3SOO. Their prediction of a high reaction exothermicity agrees with the results of Ratliff *et al.*, as the 14 kcal mol^{-1} barrier to CH_3SO_2 dissociation would be easily surmounted with the 135 kcal mol^{-1} (!) released from reactions to products. As observed by Kukui *et al.*,[103] SO_2 would indeed be the primary sulfur-containing product in this case. However, the 66 kcal mol^{-1} reaction barrier predicted by Li and coworkers clearly contradicts experimental conclusions that the reaction occurs at atmospheric temperatures. Further, these results run counter to chemical intuition that the CH_3SO and open-shell singlet O_3 should combine in a radical-radical addition to give an adduct. This discrepancy between experiment and theory warranted further investigation and motivated the current study. Based on the multireference nature of ozone, we doubted the suitability of the single-reference MP2 methodology used by Li, Meng, and Zheng to treat the title reaction, particularly since their treatment appears to have used an unrestricted Hartree-Fock reference.

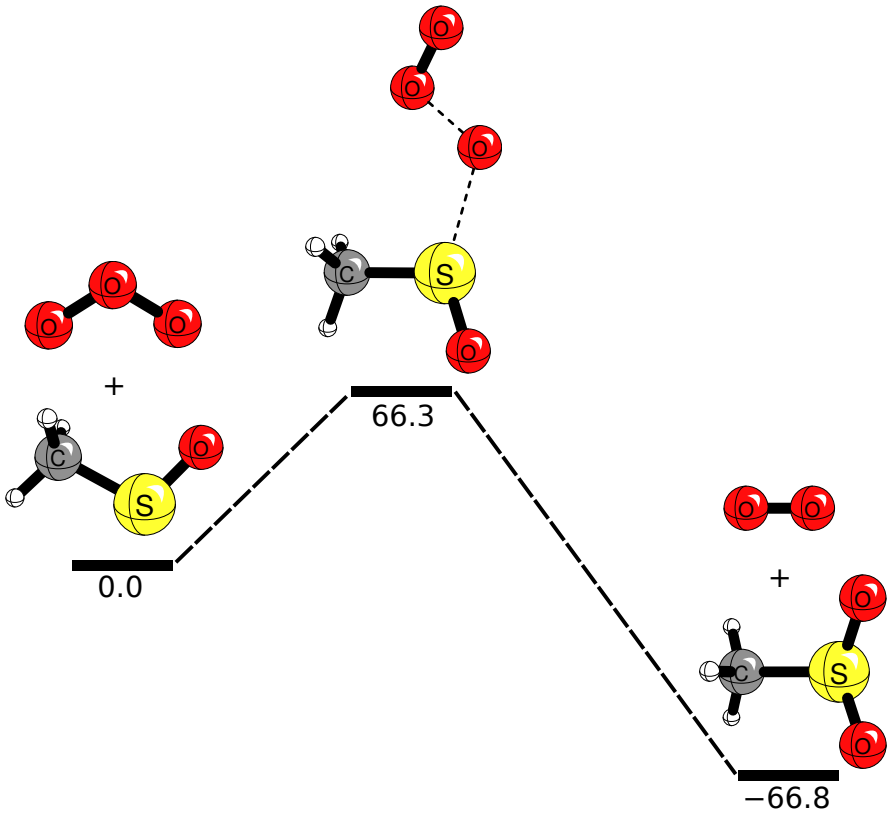

Figure 3.1: Representation of potential energy surface reported by Li, Meng, and Zheng, with energies reported in kcal mol^{-1}.

The uncertainties from the study of Li, Meng, and Zheng motivate a brief digression to the literature on similar reactions. Since CH_3SO is a sulfur congener of the methyl peroxy radical, CH_3OO, the addition of ozone to the methyl peroxy radical may appear an obvious starting point. However, the radical center in the methyl peroxy radical is situated on the terminal oxygen,[104] while the radical center in the methylsulfinyl radical is not.[70] Because of this difference, CH_3SO and CH_3OO are expected to participate in substantially different radical addition chemistry, and the ozone addition reaction of one cannot be used to guide investigations of the other.

In contrast, the $CH_3SO + NO_2$ reaction is analogous to the title reaction. We offer a brief review of the work on the $CH_3SO + NO_2$ reaction, which may shed light on a more appropriate review of the reaction of CH_3SO with ozone. The rise of NO exhibited two components in a 1989 laser-induced fluorescence flash photolysis study, leading Tyndall and Ravishankara to infer the reaction of CH_3SO with NO_2.[101] Dominé and coworkers observed both a mass 63 peak that they assigned to CH_3SO^+ and a similar rise in NO in their 1990 flow tube photoionization mass spectrometry study.[105] They determined a rate constant of 1.2×10^{-11} for the reaction of NO_2 with CH_3SO. Unfortunately, the CH_3SS also under study in the reaction mixture precluded mass spectrometric detection of the methylsulfonyl radical, CH_3SO_2, that Dominé and coworkers inferred to be the other product of the reaction. Building on these studies, in 2000 Kukui et al. reported an experimental and computational study on the mechanism of the CH_3SO addition reaction with NO_2.[103] Their results with the G2 computational method implicated an addition adduct $CH_3S(O)ONO$ that is 27 kcal mol^{-1} lower in energy than the separated reactants. The products are 10 kcal mol^{-1} higher in energy than the adduct, with no barrier reported for dissociation of the adduct to $SO + CH_3SO_2$. The excess energy in the system resulting from addition of the reactants is therefore thought to cause the adduct to promptly decompose to NO and CH_3SO_2, with the latter chemically activated. This activated CH_3SO_2 radical was not directly observed. However, Kukui and coworkers modeled the decomposition mechanism of CH_3SO_2 using RRKM with G2 and B3LYP energies under the assumption that chemically activated CH_3SO_2 is formed, and obtained rate constants that agreed with experimental rate data. They anticipated that the ozone reaction, with a higher enthalpy than the NO_2 reaction, would entail even more complete conversion of activated CH_3SO_2 to SO_2.

A subsequent study from the same group investigated the reaction of the methylsulfinyl radical with ozone simultaneously with its reaction with NO_2.[67] By comparing these two reactions, they concluded that ozone reacts with the methylsulfinyl radical to almost exclusively produce SO_2 at presssures relevant to atmospheric conditions. This requires that the CH_3SO addition reaction with O_3 release a significantly greater quantity of energy than is required to surmount the barrier to CH_3SO_2 dissociation. Ratliff and coworkers report the CH_3SO_2 dissociation barrier to 14 ± 2 kcal mol^{-1} in a 2009 velocity map imaging study.[106] This implies that

the title reaction must have an exothermicity significantly greater than 14±2 kcal mol^{-1}. The only other experimental study on the CH_3SO reaction with O_3 was published by Dominé and coworkers in 1992.[107] As with their study on the reaction of NO_2 with CH_3SO, they could not comment on whether CH_3SO_2 is formed in the title reaction, as other species obscured its mass spectrometry signal.

With this background, we computationally investigated the reaction of the methylsulfinyl radical with ozone to propose a mechanism in line with the available experimental findings, thereby correcting inconsistencies in the available literature on the topic.

Methods

We first attempted to replicate the MP2/6-311++G(2df,p) treatment of Li and coworkers.[102] As detailed in the Results and Discussion, preliminary RI-MP2 computations with 6-311++G(2df,2p), cc-pV(T+d)Z, and Def2-TZVPP[39,40] basis sets indicated that the system is severely spin-contaminated, rendering the literature results suspect. Significant spin contamination can reflect deeper issues with the ability of a single-determinant electronic wavefunction to properly reflect the character of the system. To rule out the possibility of significant multireference character along this reaction path, we turned to multireference computations.

To determine how significant multireference effects may be for this system, we systematically increased the active space for CASSCF/cc-pV(D+d)Z transition state optimizations from a (4o,5e) to a (12o, 13e) active space. Since these preliminary CASSCF/CASPT2 investigations revealed a mild degree of static correlation, we continued on this method of investigation. In further CASSCF and CASPT2 computations, we continued using the cc-pV(D+d)Z basis set. Along with geometry optimization routines, we performed scans of the S–OOO and SO–OO bond lengths in an attempt to identify a reaction transition state.

Standard formulations of Kohn-Sham density functional theory are essentially single-reference methods, but they can in principle be used to treat multireference systems exactly. Spin contamination has little meaning for Kohn-Sham DFT; we used the unrestricted open-shell formulation of DFT, which more accurately reflects the nature of the theory.[46] Were the exact functional known, it would provide an exact correspondence between the electron density and the wavefunction. In practice, even inexact functionals can fortuitously account for some multireference effects and provide a reasonable treatment of multireference systems.[108] We identified stationary points on the reaction pathway with the ωB97X-D3[109] and M06-2X[110] density functionals using a 6-31+G(d) basis sets; with the M06-2X density functional, we also identified these states with a cc-pVTZ basis set[32] that employed the $+d$ tight d correction[34] needed to properly treat sulfur.[33] To identify any additional features on the potential energy surface, we also performed scans of the

S–OOO and SO–OO bonds.

DFT computations were performed in ORCA 4.0,[111,112] CASSCF and CASPT2 computations were performed in Molpro 2010,[113] and coupled cluster computations were performed in CFOUR 1.0 and 1.2,[88] with higher-order coupled cluster computations performed in MRCC[114] using the interface to CFOUR.

Results and Discussion

Our attempts to verify the MP2/6-311++G(2df,p) reaction pathway of Li, Meng, and Zhang with a UHF reference shed doubt on their published transition state energetics. The published transition state does not contain enough information to reproduce the geometry, thwarting efforts to directly compare energetics. We optimized a transition state using resolution of the identity (RI)-MP2/6-311++G(2df,2p). However, our barrier of around 1 kcal mol^{-1} for a transition state that is visually similar to the image published by Li and coworkers stands opposed to their 66 kcal mol^{-1} reported barrier. Our CFOUR Hartree–Fock stability analysis on a similar MP2/cc-pV(T+d)Z structure changed an $\langle S^2 \rangle$ of 0.768 to an $\langle S^2 \rangle$ of 3.42 upon orbital rotation. ORCA MP2/cc-pV(T+d)Z and MP2/Def2-TZVPP transition state computations exhibited $\langle S^2 \rangle$ values of 1.35 and 1.36, similarly unreasonable for a doublet system. These results indicate that UHF is a poor reference for the molecular wavefunction of the system. The unsalvageably severe spin contamination rendered these results unusable and raised concerns about possible multireference character.

Combined with the $\langle S^2 \rangle$ values obtained in UHF-MP2 computations, CASSCF CI coefficients justified our foray into multireference computations for this system. To address concerns about the suitability of a single-reference wavefunction for this system, we employed CASSCF and CASPT2. Molpro CASSCF/cc-pV(T+d)Z computations with a 4-orbital, 5-electron active space yielded a leading CI coefficient of 0.99, which appeared sufficient justification for using a single-reference method. However, employing a larger 8-orbital, 9-electron active space resulted in coefficients of 0.955, 0.219, and 0.102, among other contributions. We searched for a transition state, but none was identified. Optimizing a transition state with increasing active spaces yielded smaller and smaller imaginary modes, indicating that a transition state may not exist at all. Extensive scans corroborate this, revealing a featureless, smooth descent to products (Figure 3.2).

Mildly multireference systems may be amenable to density functional theory treatments.[115] We identified a reaction adduct and transition state with the M06-2X and ωB97X-D3 density functionals (Figure 3.3). Less than 1 kcal mol^{-1} higher in energy than the adduct without zero-point vibrational energy, the transition state becomes lower in energy than the adduct when these are included. Two-dimensional scans of S–O and O–O bond lengths corroborate these results (Figure 3.4).

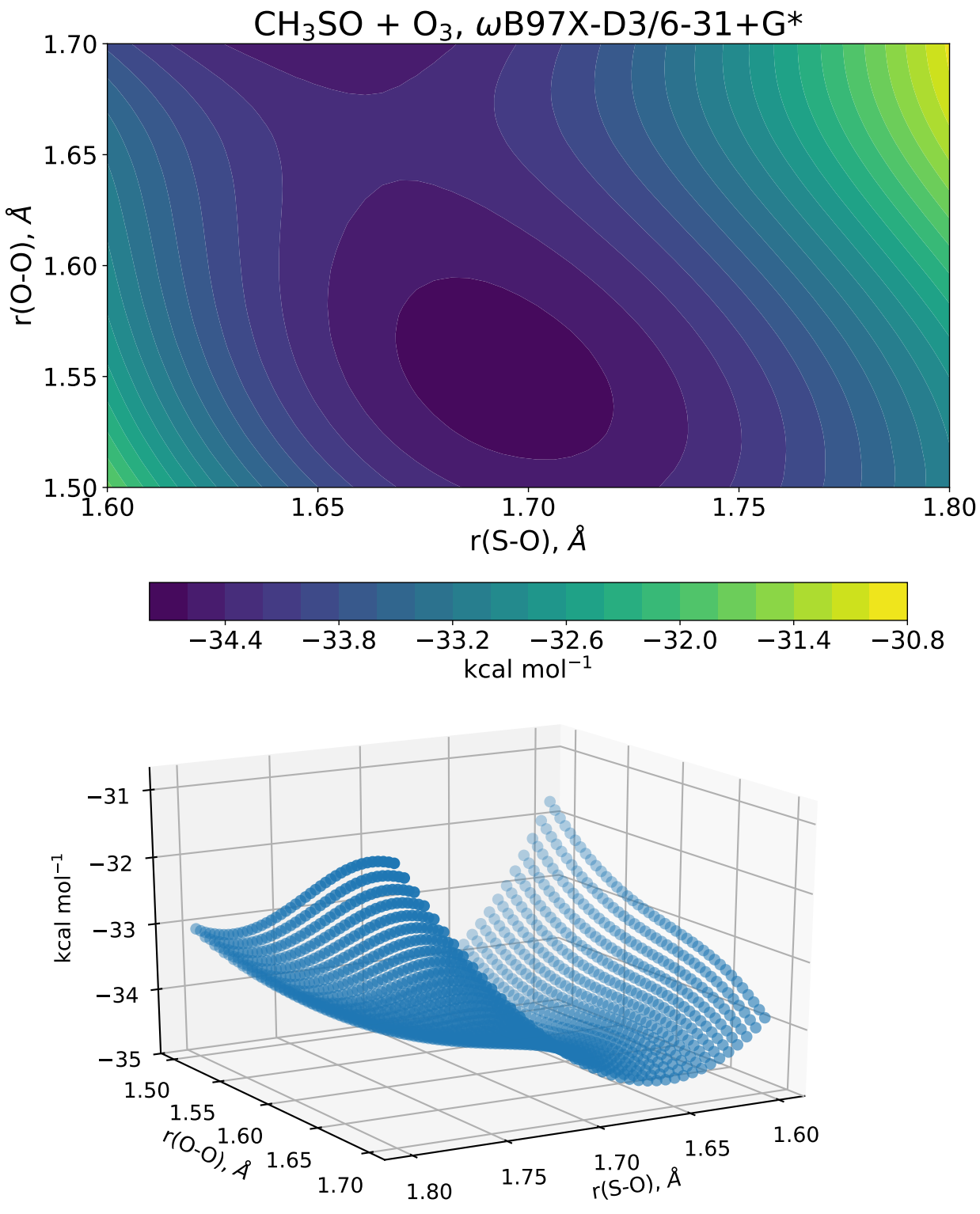

Figure 3.4: ωB97X-D3/6-31+G* single point scan exhibiting a saddle point and relative minimum corresponding to the transition state and adduct.

Although it cannot be conclusively shown that a barrier does not exist for the title reaction, these results indicate that any such barrier would be too small to significantly impede reaction progress in the event of a collision at typical temperatures in the marine boundary layer. Finally, since the intermediate products methylsulfonyl radical and molecular oxygen are around sixty kcal mol^{-1} lower in energy than the reactants, this provides sufficient internal energy to easily surmount the 14 kcal mol^{-1} barrier to methylsulfonyl radical dissociation.[106] Therefore, this intermediate product is expected to immediately dissociate to the final products of sulfur dioxide and methyl radical, as is observed experimentally.

Conclusions

This investigation indicates that the reaction of ozone with the methylsulfinyl radical is highly exothermic and proceeds directly from products with no barrier, being limited only by the collision rate.

The previous MP2 computations described in the literature provide a qualitatively different picture than the one described here, likely due to the use of a poor reference wavefunction. Using multireference methods and density functional theory, our thorough computational investigation shows that the reaction proceeds through either a small barrier or no barrier at all. On this basis, we expect the reaction of the methylsulfinyl radical and ozone to proceed rapidly to the products CH_3, SO_2, and O_2, in accord with the published experimental studies.

Acknowledgements

This research was supported by National Science Foundation Grant CHE-1661604. M. L. E. gratefully acknowledges helpful conversations with Jonathon Misiewiczand Stephen Wheeler.

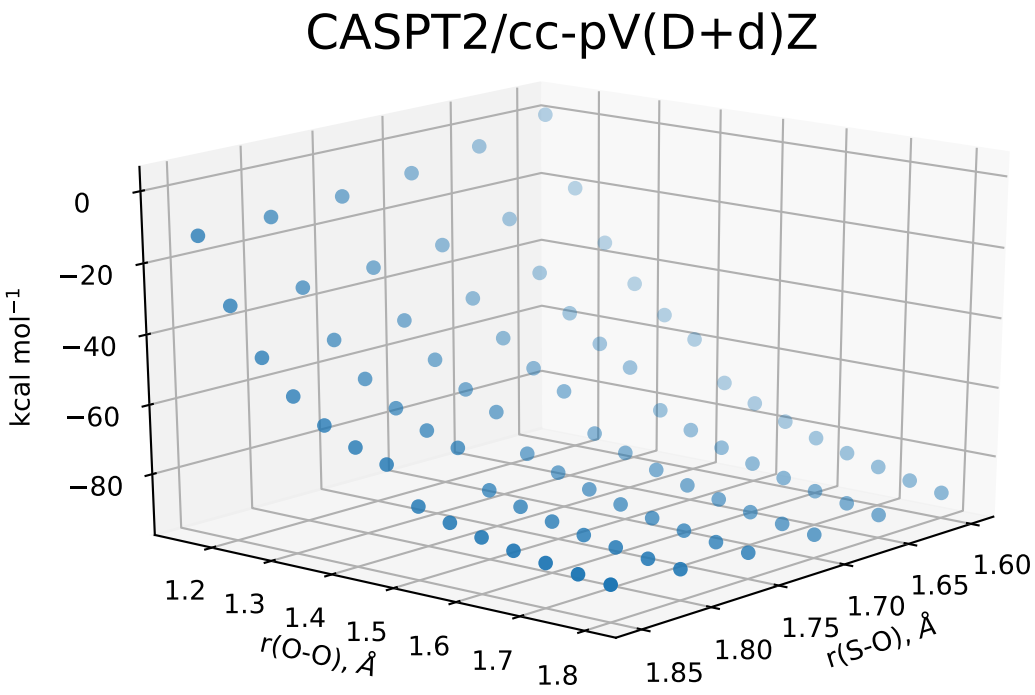

Figure 3.2: CASPT2/cc-pV(D+d)Z single point scan exhibiting smooth curvature in the vicinity of the S–O and O–O bond lengths corresponding to the DFT adduct and transition state.

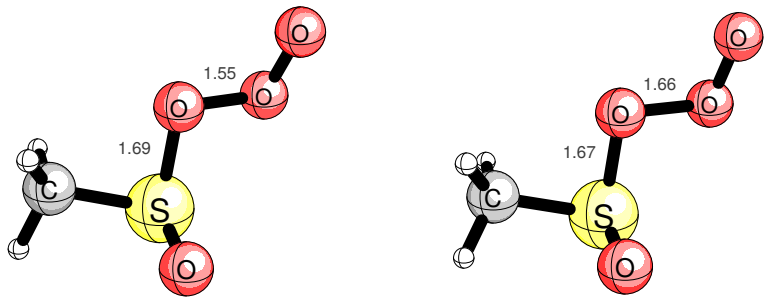

Figure 3.3: Reaction adduct (left) and transition state (right) identified using ωB97X-D3/6-31+G*. Bond parameters are in Å. The transition state exhibits an imaginary mode of $-454i$ cm^{-1} and an electronic energy 0.4 kcal mol^{-1} higher in energy than that of the adduct, well within the typical uncertainty associated with density functional theory. With zero-point vibrational energy included, the transition state is 0.2 kcal mol^{-1} lower in energy than the adduct.

CHAPTER 4

RADICALS DERIVED FROM ACETALDEHYDE AND VINYL ALCOHOL[3]

[3]Accepted by *Physical Chemistry Chemical Physics*. Reprinted here with permission of publisher. M. L. Estep, W. James Morgan, Alexander T. Winkles, Adam S. Abbott, Nery Villegas-Escobar, J. Wayne Mullinax, Walter E. Turner, Xiao Wang, Justin M. Turney and Henry F. Schaefer III. *Phys. Chem. Chem. Phys.*, 2017, **19**, 27275–27287.

Abstract

Vinyl alcohol and acetaldehyde are isoelectronic products of incomplete butanol combustion. Along with the radicals resulting from removal of atomic hydrogen or the hydroxyl radical, these species are studied here using *ab initio* methods as complete as coupled cluster theory with singles, doubles, triples, and perturbative quadruple excitations [CCSDT(Q)], with basis sets as large as cc-pV5Z. Relative energies provided herein are further refined by including corrections for relativistic effects, the frozen core approximation, and the Born–Oppenheimer approximation. The effects of anharmonic zero-point vibrational energies are also treated. The *syn* conformer of vinyl alcohol is predicted to be lower in energy than the *anti* conformer by 1.1 kcal mol^{-1}. The alcoholic hydrogen of *syn*-vinyl alcohol is found to be the easiest to remove, requiring 84.4 kcal mol^{-1}. Five other radicals are also carefully considered, with four conformers investigated for the 1-hydroxyvinyl radical. Beyond energetics, we have conducted an overhaul of the spectroscopic literature for these species. Our results also provide predictions for fundamental modes yet to be reported experimentally. To our knowledge, the ν_3 (3076 cm^{-1}) and ν_4 (2999 cm^{-1}) C–H stretches for *syn*-vinyl alcohol and all but one of the vibrational modes for *anti*-vinyl alcohol (ν_1–ν_{14}) have yet to be observed experimentally. For the acetyl radical, ν_6 (1035 cm^{-1}), ν_{11} (944 cm^{-1}), ν_{12} (97 cm^{-1}), and accounting for our changes to the assignment of a 1419.9 cm^{-1} experimental mode, ν_{10} (1441 cm^{-1}) are yet to be observed. We have predicted these unobserved fundamentals and reassigned the experimental 1419.9 cm^{-1} frequency in acetyl radical to ν_4 rather than to ν_{10}. Our work also strongly supports reassignment of the ν_{10} and ν_{11} fundamentals of the vinoxy radical. We suggest that the bands assigned to overtones of these fundamentals were in fact combination bands. Our findings may be useful in constructing improved combustion models of butanol and in spectroscopically characterizing these molecules further.

Introduction

To combat rising greenhouse gas emissions and limited fossil fuel supplies, sustainable new fuel sources bear increasing importance. One potential candidate is 1-butanol, an emerging renewable biofuel.[116] Studies by Wu *et al.*[117] have shown that butanol has 30% more usable energy per volume than the current fuel additive ethanol. With multiple carbon sites to stabilize radicals, the carbon chain of butanol supports an abundance of combustion pathways. Due to the similarity of its caloric value and stoichiometric air-fuel ratio to those of gasoline, current combustion engines are more nearly compatible with butanol than with ethanol.[118,119] This compatibility, along with potential reduction of total greenhouse gas emissions by 32–48% using biofuels,[117] makes 1-butanol an attractive alternative fuel source. However, butanol combustion must be studied further

before it can be considered a replacement for current fuels.[120]

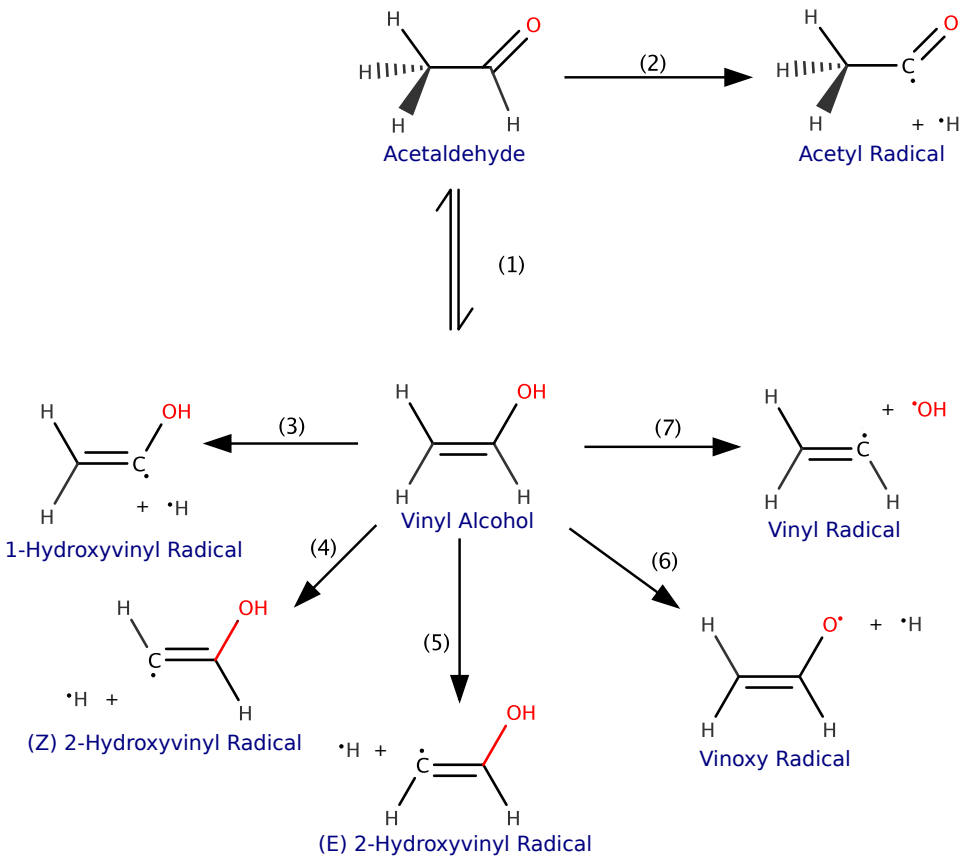

Figure 4.1: Reaction pathways under study in this research.

In 2010, Black *et al.*[121] studied autoignition delay times of 1-butanol in high and low pressure shock tubes. They discovered that acetaldehyde and vinyl alcohol are the primary products of this incomplete combustion. One year later, Green and coworkers[122] used molecular beam time-of-flight mass spectrometry to confirm this in flame-sampling experiments. Prior to the 2006 work of Taatjes *et al.*,[123,124] enols such as vinyl alcohol had not been considered in combustion models. Taatjes and coworkers rectified this omission. The four studies noted above sparked further research confirming the integral role of enols in combustion, but new research is needed.[122,125,126] This is particularly true for vinyl alcohol, a direct product of the incomplete combustion of 1-butanol.[127] Vinyl alcohol (CH_2=CHOH), also called ethenol, is the enol form of acetaldehyde. Besides its role in combustion, vinyl alcohol has been implicated in astrochemistry.[128]

The radicals derived from acetaldehyde and vinyl alcohol are of critical importance to combustion chemistry, and these radicals are carefully explored in the present paper. There have been many experimental studies of acetaldehyde, vinyl alcohol, and the radicals derived from these by removal of a hydrogen atom or

an OH radical.[128–137,137–156] A particularly important 2011 study is that of Hansen, Harper, and Green,[122] who considered the kinetics of vinyl alcohol, acetaldehyde, and several radicals thereof.

To make the connections between theory and experiment clear, experiments are discussed in the context of our theoretical predictions. The seven fragmentations considered here are shown in Figure 1.

Theoretical Methods

The NASA Ames atomic natural orbital (ANO) basis sets of Almlöf and Taylor[35] were used in the geometry optimizations and vibrational frequency computations. ANO1 refers to the truncated (H:(8s6p4d), C,O:(13s8p6d4f), contracted to (H:[4s2p1d], C,O:[4s3p2d1f]) NASA Ames ANO basis set. ANO2 refers to the full (H:(8s6p4d3f), C,O:(13s8p6d4f2g), contracted to H:[4s3p2d1f], C,O:[5s4p3d2f1g]) NASA Ames ANO basis sets. The ANO1 basis set has been shown to sometimes provide more reliable vibrational frequencies for combustion systems than do similarly sized Dunning basis sets.[36] The ANO1 and ANO2 basis sets are comparable in size to cc-pVTZ and cc-pVQZ, respectively. Dunning's correlation-consistent polarized-valence basis sets [cc-pVnZ, (n = D,T,Q,5)] were used in extrapolating the relative energies to the complete basis set limit.[32] The frozen-core approximation was employed in all but the final computations.

Molecular geometries were optimized via coupled-cluster theory with single, double, and perturbative triple excitations [CCSD(T)][84–87,157] using the large ANO2 basis set. The identity of each structure as a local minimum was confirmed by vibrational analysis. The closed-shell species acetaldehyde and vinyl alcohol were treated with restricted Hartree–Fock (RHF) reference wavefunctions. Due to significant spin contamination of the vinoxy radical ($\dot{C}H_2CHO$), the open-shell species were also treated with restricted open-shell Hartree–Fock (ROHF) reference wavefunctions; all of the radical computations were on doublet spin electronic states.

The focal point approach (FPA) of Allen and coworkers was employed to determine the relative electronic energies (E_e) of reaction extrema to high reliability.[23–26] Systematic improvements of the correlation treatment and basis set allowed extrapolation to the complete basis set (CBS) limit of coupled-cluster theory with single, double, triple, and perturbative quadruple excitations [CCSDT(Q)].[27–29] The frozen core (FC) approximation and the cc-pVnZ (n=D,T,Q,5) basis sets of Dunning and co-workers were employed.[32] For each of the species considered, we computed Hartree-Fock, second-order Møller-Plesset perturbation theory (MP2), CCSD, and CCSD(T) single-point energies using each of the four Dunning basis sets up to n=5. We then computed CCSDT and CCSDT(Q) single-point energies with the cc-pVDZ and cc-pVTZ basis sets for each of the species considered, with the exception of the 1-hydroxyvinyl radical ($H_2C{=}\dot{C}OH$), for which we did not compute a CCSDT(Q)/cc-pVTZ single point energy. Thus, all focal point analyses involving this

radical omit CCSDT(Q)/cc-pVTZ single point energies. Additionally, core correlation corrections to the valence focal point approach were computed using cc-pCVTZ,[158] the Dunning triple-zeta basis set with the energetic effects of core correlating basis functions included via

$$\Delta E_{\text{core}} = E^{\text{cc-pCVTZ}}_{\text{AE}-\text{CCSD(T)}} - E^{\text{cc-pCVTZ}}_{\text{FC}-\text{CCSD(T)}}. \tag{4.1}$$

In Eq. (4.1), AE indicates correlation of all electrons, whereas FC denotes use of the frozen-core approximation. Scalar relativistic effects at first order were accounted for by including mass-velocity contributions along with the one- and two-electron Darwin terms (MVD2).[159,160] These were obtained using the AE-CCSD/cc-pVTZ method.[161,162] The diagonal Born–Oppenheimer correction (DBOC)[163,164] values were calculated using the HF/cc-pVTZ method, following the HEAT protocol.[165] Finally, CCSD(T)/ANO2 harmonic and CCSD(T)/ANO1 anharmonic zero-point vibrational energy corrections (Δ_{ZPVE}) were determined for each stationary point and appended to the corrected CCSDT(Q)/CBS values to obtain relative enthalpies at 0 K ($\Delta H_{0\text{ K}}$). The anharmonic correction to the ZPVE was computed as the difference between the ANO2 harmonic ZPVE and the ANO1 anharmonic ZPVE using the resonance-free equations provided by Schuurmann, Allen, and Schaefer.[166]

Fundamental vibrational frequencies for each species were computed using CFOUR 1.0, and Fermi resonance analysis was performed using harmonic derivatives as implemented in the GUINEA module of CFOUR 2.0.[167] Semidiagonal CCSD(T)/ANO1 quartic force fields were generated from the corresponding ANO1 equilibrium geometry to determine anharmonic corrections using finite difference of analytic gradients. These corrections ($d\nu$) were appended to CCSD(T)/ANO2 harmonic vibrational frequencies (ω) to provide the reported fundamentals ($\omega+d\nu$) for each species. Analytic hessians were used to determine the CCSD(T)/ANO2 harmonic frequencies for closed shell species. We use the notation v: stretch, δ: bend, τ: torsion, d: deformation, t: terminal, i: internal, ρ: rock, w: wag, a: asymmetric, s: symmetric to describe the internal coordinate motion of the normal modes of vibration.

For the majority of computations described above we used the CFOUR package, version 1.0,[88,168] with our harmonic derivative analyses making use of the GUINEA module of CFOUR 2.0[88] as noted above. We employed the MRCC package of Kállay[114] for the CCSDT[27–29] and CCSDT(Q)[93] computations.

Results and Discussion

Predicted molecular structures are reported in Figures 4.2-4.9.

Acetaldehyde

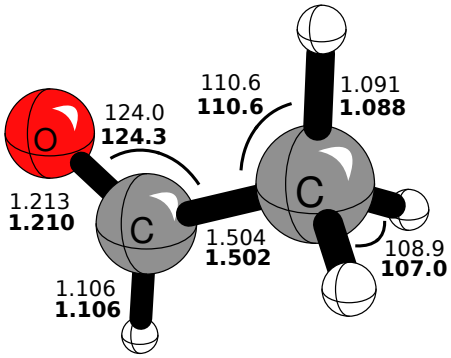

Figure 4.2: Ground state C_s equilibrium geometry of acetaldehyde computed using the CCSD(T)/ANO2 method (**bold**), with the experimental geometrical parameters of Ramsay and coworkers[129] for comparison (normal font). Bond distances in Å and angles in degrees.

A 1957 microwave spectroscopy study of Kilb, Lin, and E. B. Wilson[169] reported the microwave spectrum of acetaldehyde and included a detailed structural analysis. These results were employed by Iijima and Kimura[170] in 1969 along with the results of an electron diffraction study of the same year to obtain a zero-point averaged (r_z) structure. Ramsay and coworkers[129] made use of data from both the Kilb study and the Iijima study in reporting their effective and average gas-phase equilibrium geometries for acetaldehyde. We have included their effective geometry for comparison with our CCSD(T)/ANO2 geometry in Figure 4.2; our geometry shows excellent agreement with theirs.

We report our vibrational frequency predictions for acetaldehyde in Table 4.1, with experimental results[130,171,173] for comparison. We note that in 1999 Herman *et al.*[173] performed new Fourier transform interferometry and opto-acoustic laser spectroscopy experiments; however, the recommendations they made take into account their own results along with the 1971 results of Hollenstein and Günthard[171] and the 1986 results of Findsen *et al.*[172] Our computational modes for acetaldehyde display generally good agreement with the experimental fundamentals. However, the theoretical carbonyl C-H stretch (ν_3) does not agree well with experiment, with a discrepancy of 89.4 cm^{-1} from the value reported by Herman *et al.* A very strong $\nu_4/2\nu_9$ resonance was evident from the perturbed VPT2 results which provided an unphysical value for ν_4. The eigenvalue with dominant ν_4 character from the effective Hamiltonian treatment of 1757 cm^{-1}

Table 4.1: Comparison of acetaldehyde (CH_3CHO) experimental vibrational frequencies to fundamentals predicted in this research (cm^{-1}), with harmonic CCSD(T)/ANO2 infrared intensities in parentheses (km mol^{-1}).

Mode	Present Work		Expt[a]	Expt[b]	Description
$\mathbf{a}'$					
ν_1	3005	(7)	2967	3014	a CH_3 vCH
ν_2	2922	(2)	2920	2923	s CH_3 vCH
ν_3	2805	(92)	2876	2715.77	HCO vCH
ν_4	1757*	(140)	–	1747	vCO
ν_5	1428	(20)	1422	1429.91	vCC
ν_6	1396	(10)	1390	1395.2	a δCH_3
ν_7	1350	(16)	1349	1352.6	s δCH_3
ν_8	1110	(22)	1120	1114.04	i wCH
ν_9	855	(7)	888	866.9629	i ρCH_3
ν_{10}	502	(14)	517	–	δCCO
$\mathbf{a}''$					
ν_{11}	2961	(6)	3007	2964.44	*oop* CH_3 vCH
ν_{12}	1436	(9)	1422	1436.64	d CH_3
ν_{13}	1104	(0.0_3)	–	1107.30	*oop* ρCH_3
ν_{14}	758	(1)	772	767.150	*oop* wCH
ν_{15}	113	(2)	–	143.7434	τ
ZPVE	34.33 kcal mol^{-1}				

* Resonance treated: $\nu_4/2\nu_9$

[a] Solid phase - Evans and Bernstein,[130] 1956.

[b] Updates to frequencies from previous literature[171,172] suggested by Herman *et al.*[173] on the basis of Fourier transform interferometry and opto-acoustic laser spectroscopy experiments performed by the latter, 1999.

agrees well with the only reported experimental assignment of this mode, 1747 cm^{-1}, provided by Evans and Bernstein's work in the solid phase.

Vinyl Alcohol

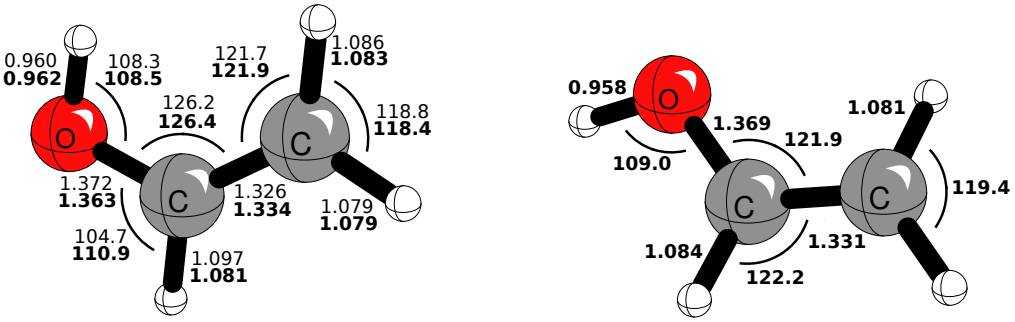

Figure 4.3: Ground state C_s equilibrium geometries of (left) *syn*- and (right) *anti*-vinyl alcohol predicted using the CCSD(T)/ANO2 method. Bond distances in Å and angles in degrees. **Bold** features represent our computational results; the experimental structure of Rodler and Bauder is given (normal font) for the *syn* conformer.[132]

The orientation of the hydroxyl hydrogen in vinyl alcohol distinguishes the *syn* and *anti* conformers of the planar molecule (Figure 4.3). The *syn* conformer is lower in energy, an effect that Bond and Schleyer[174] explained in terms of intramolecular electrostatic interactions. As a result of its lower energy, more spectroscopic results are available for the *syn* conformer[132] than for the *anti* conformer,[134] although both have received attention.[131,175,176] Rodler and Bauder[132] deduced a microwave spectroscopy substitution structure of the lower-energy *syn* conformer. Our computational CCSD(T)/ANO2 geometries for both conformers are shown in Figure 4.3 along with the experimental *syn* conformer geometry of Rodler and Bauder.[132] The theoretical O–H lengths of *syn*- and *anti*-vinyl alcohol are the same to within 0.004 Å. The *anti* conformer has a slightly shorter (0.003 Å) C–C bond length than does the *syn*.

Rodler, Blom, and Bauder[133] employed infrared spectroscopy to investigate Ar matrix-isolated *syn*-vinyl alcohol in 1984. Koga *et al.*[177] studied the gas-phase infrared spectrum of *syn*-vinyl alcohol in 1991. Our results for *syn*-vinyl alcohol (Table 4.2) agree well with both sets of experimental fundamentals. The agreement with the most recent (2017) and precise experiments of Raston and coworkers[178] is outstanding.

We note that two of the C–H stretches for *syn*-vinyl alcohol (ν_3, 3076 cm^{-1} and ν_4, 2999 cm^{-1}) have yet to be observed experimentally.

Our predictions for *anti*-vinyl alcohol are reported in Table 4.3 alongside the experimental ν_{15} value of 261.77 cm^{-1} reported by Bunn *et al.* in 2017.[178] We note fair agreement between our ν_{15} (248.6 cm^{-1}) and that of Bunn (261.55 cm^{-1}). To our knowledge, no experimental observations of the other fourteen modes of

Table 4.2: Comparison of *syn*-vinyl alcohol (CH_2=CHOH) experimental vibrational frequencies to the theoretical fundamentals of this research (cm^{-1}). We report harmonic CCSD(T)/ANO2 infrared intensities (km mol^{-1}) in parentheses.

Mode	Present Work		Expt[a]	Expt[b]	Expt[c]	Description
$\mathbf{a}'$						
ν_1	3638	(40)	3634	3620	–	vOH
ν_2	3117	(5)	3122	–	–	vCH
ν_3	3076	(4)	–	–	–	vCH
ν_4	2999*	(4)	–	–	–	vCH
ν_5	1658	(143)	1645	1648	–	vCC
ν_6	1418	(16)	1412	–	–	vCO
ν_7	1325	(3)	1300	1326	–	δCH_2
ν_8	1300	(5)	1260	1300	–	ρCH_2
ν_9	1082	(174)	1098	1090	–	δCCO
ν_{10}	943	(13)	948	943	–	i δCCH
ν_{11}	484	(13)	–	486	–	δCOH
$\mathbf{a}''$						
ν_{12}	960	(32)	–	971	–	τHCCO
ν_{13}	812	(54)	817	814	–	$w CH_2$
ν_{14}	696	(1)	699	698	–	o δCCH
ν_{15}	406	(95)	–	413	407.17	τOH
ZPVE	34.98 kcal mol^{-1}					

* Resonance treated: $\nu_4/(\nu_5 + \nu_6)$

[a] Gas Phase - Koga *et al.*,[177] 1991.

[b] Argon, 4 K - Rodler, Blom, and Bauder,[133] 1984.

[c] Gas Phase - Bunn,[178] 2017.

Table 4.3: *anti*-vinyl alcohol (CH_2=CHOH) vibrational frequencies (cm^{-1}) compared to the *anti*-vinyl alcohol ν_{15} experimental frequency which has been reported in the literature. We report harmonic CCSD(T)/ANO2 infrared intensities (km mol^{-1}) in parentheses.

Mode	Present Work		Expt[a]	Description
a′				
ν_1	3693	(85)	–	vOH
ν_2	3129	(3)	–	vCH
ν_3	3048	(4)	–	vCH
ν_4	3007*	(8)	–	vCH
ν_5	1683	(89)	–	vCC
ν_6	1408	(0.1)	–	vCO
ν_7	1318	(11)	–	δCH_2
ν_8	1261	(187)	–	ρCH_2
ν_9	1125	(15)	–	δCCO
ν_{10}	938	(49)	–	i δCCH
ν_{11}	470	(4)	–	δCOH
a″				
ν_{12}	943	(23)	–	τHCCO
ν_{13}	837	(48)	–	$w CH_2$
ν_{14}	697	(18)	–	o δCCH
ν_{15}	249	(96)	261.55	τOH
ZPVE	34.80 kcal mol^{-1}			

* Resonance treated: $\nu_4/(\nu_5+\nu_6)$
[a] Gas Phase - Bunn,[178] 2017.

anti-vinyl alcohol are available to date. We treated a resonance between the ν_4 fundamental and the $\nu_5+\nu_6$ combination band for both conformers. This treatment changed the anharmonic correction for ν_4 from -55 cm^{-1} to -157 cm^{-1} in the *syn* conformer, and from 290 cm^{-1} to -158 cm^{-1} in the *anti* conformer. When the resulting CCSD(T)/ANO1 anharmonic corrections were combined with our CCSD(T)/ANO2 harmonic frequencies, this yielded final fundamental values of 2999 cm^{-1} and 3007 cm^{-1} for the *syn* and *anti* conformers, respectively.

Acetyl Radical

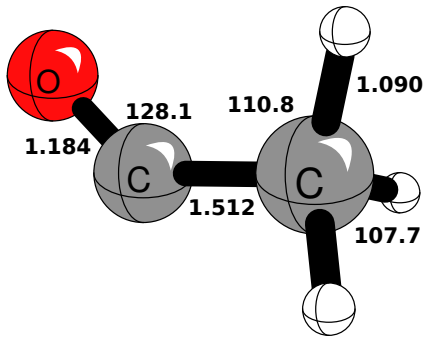

Figure 4.4: Ground state C_s $^2A''$ equilibrium geometry of the acetyl radical computed using the CCSD(T)/ANO2 method. Bond distances in Å and angles in degrees.

Compared to the C–C bond of 1.502 Å in acetaldehyde, the acetyl radical has a slightly longer (by 0.010 Å) C–C bond distance of 1.512 Å but a significantly shorter C–O bond of 1.184 Å compared to the 1.210 Å C–O bond in acetaldehyde.

Table 4.4: Acetyl radical ($CH_3C\dot{O}$) $\tilde{X}$ $^2A''$ computational fundamental modes (this research) and harmonic CCSD(T)/ANO2 infrared intensities (km mol^{-1}) in parentheses compared to experimental frequencies (cm^{-1}) with relative intensities in parentheses.

Mode	Present Work		Expt	Expt[c]		Description
a′						
ν_1	2993	(6)	–	2989.1	(1.9)	a vCH$_3$
ν_2	2925	(4)	–	2915.6	(2.9)	s vCH$_3$
ν_3	1886*	(113)	1844[a]	1880.5	(100)	vCO
ν_4	1427	(20)	–	1419.9	(8.0)	dCH$_3$
ν_5	1328	(9)	–	1323.2	(10.9)	uCH$_3$
ν_6	1035*	(16)	–	–		dCCH
ν_7	829	(4)	–	836.6	(4.5)	vCC
ν_8	468	(6)	490 ± 30 cm^{-1}[b]	468.1	(2.8)	vCCO
a″						
ν_9	2983	(1)	–	2990.3	(4.2)	a vCH$_2$
ν_{10}	1441*	(11)	–	–		a dCH$_3$
ν_{11}	944*	(0.1)	–	–		o d
ν_{12}	97	(1)	–	–		τ
ZPVE	26.70 kcal mol^{-1}					

* Resonances treated: $\nu_3/(\nu_6+\nu_7)/2\nu_{11}$, $\nu_6/(\nu_8+\nu_{11})$, $\nu_{10}/(\nu_5+\nu_{12})$, and $\nu_{11}/(\nu_7+\nu_{12})$

[a] Shirk and Pimentel,[136] 1968.

[b] Photoelectron spectroscopy - Nimlos, Soderquist, and Ellison,[138] 1989.

[c] Solid *para*-H_2 matrix - Das and Y.-P. Lee,[142] 2014.

Our theoretical acetyl radical fundamental modes are reported in Table 4.4, with available experimental frequencies for comparison. Acetyl radical has been studied using electron spin resonance.[179,180] In 1968,

Shirk and Pimental[136] noted an acetyl radical C–O stretching frequency of 1844 cm^{-1} (earlier reported by Shirk in his 1966 doctoral dissertation); while this frequency does not agree with our computed C–O stretching frequency ν_3 of 1886 cm^{-1}, the 1880.5 cm^{-1} mode later reported by Das and Y. P. Lee[142] does agree well. In her 1982 Ar matrix work (cited in her 1994 compendium[181]), Jacox[137] identified one of the species under study as the acetyl radical (Species A). Among the bands observed, she assigned the bands at 1875 cm^{-1} and at 1842 cm^{-1} to the C=O stretch, with the splitting attributed to an unidentified Fermi resonance with an overtone or a combination band. We identified this interaction to have contributions from both the combination band $\nu_6 + \nu_7$ and from the overtone $2\nu_{11}$. This treatment changed the anharmonic correction for ν_3 from -52 cm^{-1} to -14 cm^{-1}, giving a final value of 1886 cm^{-1} for our fundamental, in as good agreement as possible with the band Jacox observed at 1875 cm^{-1} via matrix isolation.

Jacox further assigned a band at 1420 cm^{-1} to a CH_3 deformation, in good agreement with our computed 1427 cm^{-1} CH_3 deformation mode, and a band at 1329 cm^{-1} to a CH_3 deformation mode, in excellent agreement with our value of 1328 cm^{-1}. Nimlos, Soderquist, and Ellison[138] reported the ν_8 δCCO bending frequency ($490 \pm 30 cm^{-1}$) of the acetyl radical in 1989. Considering the experimental error bars, this value agrees with our 468 cm^{-1} mode. Das and Y.P. Lee[142] in 2014 reported the infrared spectrum of acetyl radical in solid *para*-H_2. Our computed fundamental modes agree well with those determined by Das and Lee. Das and Lee suggested that the band they observed at 1419.9 cm^{-1} be assigned to either ν_{10} or ν_4. On the basis of IR intensities, they believed that the band most likely corresponds to ν_{10}. However, our computational results, including normal mode analysis, suggest that the experimentally observed band at 1419.9 cm^{-1} corresponds to the methyl deformation mode ν_4. Das and Lee indicated uncertainty in their assignment of the observed band at 468.1 cm^{-1} to the ν_8 fundamental of acetyl radical; however, this observation agrees beautifully with our computational result. The fundamentals ν_6 (CCH deformation, 1035 cm^{-1}), ν_{11} (out-of-plane deformation, 944 cm^{-1}), and ν_{12} (methyl torsion, 97 cm^{-1}) are yet to be observed in the laboratory. Furthermore, if our assignment of the experimental 1419.9 cm^{-1} band of Das and Y.-P. Lee[142] to the fundamental ν_4 is correct, the antisymmetric methyl deformation ν_{10} (1331.0 cm^{-1}) has also been unobserved to date.

Vinyl Radical

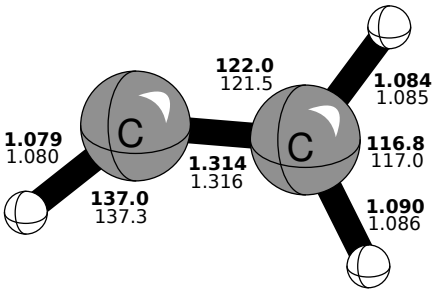

Figure 4.5: Ground state C_s $^2A'$ equilibrium geometry of the vinyl radical predicted using the CCSD(T)/ANO2 method (**bold**), with the semi-experimental geometrical parameters of Hirota and coworkers[145] for comparison (normal font). Bond distances in Å and angles in degrees.

The vinyl radical (CH_2=$\dot{C}$H) has been studied extensively.[143,145–148,182–187] With a C_s minimum energy structure, the vinyl radical has one α hydrogen on the radical carbon and two β hydrogens on the adjacent carbon. A fully experimental structure has not to our knowledge been reported, although Kanamori, Endo, and Hirota[145] reported geometrical parameters for vinyl radical in a 1990 paper. Some of their values were fixed to allow calculation of the remaining parameters from experimental rotational constants. Our CCSD(T)/ANO2 geometry is reported in Figure 4.5 along with the experimental geometrical parameters of Kanamori, Hirota, and Endo;[145] we find that our results agree with their geometrical parameters to within 0.5° for angles and to within 0.004 Å for bond lengths. The departure of the hydroxyl radical moves the two carbon atoms closer (1.326 Å in *syn*-vinyl alcohol to 1.314 Å in the radical.) Several studies have reported electron spin resonance investigations of vinyl radical.[188–191] In particular, Fessenden and Schuler[188] obtained electron spin resonance results indicating that the two β hydrogens are rapidly exchanged, interconverting the vinyl radical between the two equivalent forms. Cochran, Adrian, and Bowers[189] proved the three protons of vinyl to be nonequivalent, with different hyperfine splittings. An important 1983 electronic spectroscopy paper by Hunziker *et al.*[143] established the $^2A'$ ground state of the vinyl radical, with a $^2A''$ lowest excited state.

A number of excellent theoretical and experimental studies have considered the vinyl radical vibrational modes, several of which are noted in Table 4.5 along with our computational results. A 1988 Fourier transform infrared (FTIR) study by Shepherd, Doyle, and Graham[144] detected a mode at 900 cm^{-1}, in line with previous computational work of Dupuis and Wendoloski.[193] Kanamori, Endo, and Hirota[145] used infrared laser diode spectroscopy in 1990 to investigate the vibrational spectrum of vinyl radical generated by photolysis of vinyl halides, and like Shepherd, Doyle, and Graham, they observed a mode around 900 cm^{-1}.

Table 4.5: Comparison of vinyl radical (CH_2=$\dot{C}$H) experimental vibrational frequencies to computational fundamentals of this work (cm^{-1}).

Mode	Present Work		Expt[a]		Expt[b]		Expt[c]		Expt[d]		Description
$\mathbf{a}'$											
ν_1	3132	(1)	3235 ± 12	(7)	–		3117.6	(0.67)	3141.0	(2.0)	α vCH
ν_2	3021	(3)	3164 ± 20	(11)	–		3018.2	(0.9)	2953.6	(3.0)	a $v$$CH_2$
ν_3	2931	(3)	3103 ± 11	(0.5)	–		2902.0	(1)	2911.5	(2.6)	s $v$$CH_2$
ν_4	1582	(2)	1700 ± 35	(0.1)	1595 ± 10	(3.3)	–		–		vCC
ν_5	1359	(7)	1277 ± 20	(100)	1401 ± 5	(4.2)	–		1357.4	(24)	s $\delta$$CH_2$
ν_6	1022	(8)	1099 ± 16	(43)	1074 ± 8	(6.9)	–		–		a $\delta$$CH_2$ + α δCH
ν_7	693	(19)	758 ± 5	(32)	–		–		677.1	(32)	CH_2 + α CH a δ
$\mathbf{a}''$											
ν_8	897	(71)	955 ± 7	(11)	944 ± 6	(100)	–		895.3	(100)	CH_2 + α-CH s o δ
ν_9	796	(8)	895 ± 9	(93)	897 ± 6	(65)	–		857.0	(9.6)	CH_2 + α-CH a o δ
ZPVE	22.59 kcal mol^{-1}										

[a] Time-resolved Fourier transform emission spectroscopy - Letendre *et al.*,[146] 2000.
[b] Infrared emission spectroscopy - Nikow, Wilhelm, and Dai,[147] 2009.
[c] Helium nanodroplet spectroscopy - Raston, Liang, and Douberly,[148] 2013.
[d] Ne matrix VUV photolysis - Wu, Lin, Cheng, Chen, Y.-P. Lee,[192] 2008.

Specifically, Hirota's group found a feature around 895 cm^{-1} and assigned it to a CH_2 wagging motion. Until 2000, only the 895 cm^{-1} mode had been observed for vinyl; at this point, Dai and coworkers[146] reported all nine vibrational fundamental modes of the vinyl radical using time-resolved Fourier transform emission spectroscopy. A 2002 computational study by Sattelmeyer and Schaefer[183] computed EOMIP-CCSD/cc-pVQZ harmonic frequencies for the vinyl radical. Based on the 1419 cm^{-1} value Sattelmeyer and Schaefer obtained for ν_5, they concluded that the experimental $1277 \pm 20(100)$ cm^{-1} feature of Dai and coworkers had been misassigned.

The latter prediction was confirmed in a 2005 isotopic noble gas matrix FTIR and EPR study by Tanskanen and coworkers,[194] in which the value of ν_5 was found to be 1348.9 cm^{-1}, 1353.2 cm^{-1}, and 1356.7 cm^{-1} in Xe, Kr, and Ar matrices, respectively. Following the Sattelmeyer and Tanskanen studies, Y.-P. Lee's Ne matrix vacuum ultraviolet study supplied new recommendations for several modes of the vinyl radical.[192] Dai's group performed further experiments, resulting in a set of recommendations with the value of ν_5 compatible with that predicted by Sattelmeyer.[147] For those modes reported in the Ne matrix work from Y.-P. Lee's group, we find good or excellent agreement for all modes reported except for ν_2 and ν_9. For the remaining two modes not reported by Y. P. Lee's group, ν_4 and ν_6, our results agree well with the values of Dai and coworkers.[146] Building on the body of experimental vibrational frequencies available for vinyl radical, Nikow, Wilhelm, and Dai[147] recorded complete infrared emission spectra for vinyl radical. Agreement of the Nikow study with our results is not as close as that between our results and those from Y.-P. Lee's group.

Although our value for ν_2 does not agree well with the Ne matrix results of Y.-P. Lee's group, it does agree very well with the 2013 high-resolution study by Raston, Liang, and Douberly.[148] These latter results were obtained for the three highest-frequency vibrational frequencies of vinyl radical using helium nanodroplet

spectroscopy. The three modes reported show good agreement with our predictions. Our most concerning discrepancy with experiment is for the ν_9 fundamental; here our value of 796 cm^{-1} differs from Y. P. Lee's work[192] by 61 cm^{-1} and from Dai's more recent study[147] by 101 cm^{-1}. We note, however, that our value agrees well with the 805.9 cm^{-1} frequency that Bowman and coworkers[186] computed using a semiglobal potential energy surface (PES/S).

Vinoxy Radical

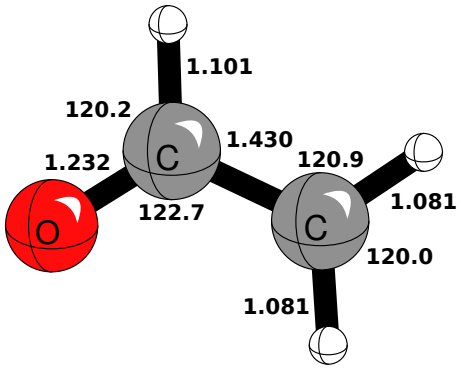

Figure 4.6: Ground state C_s $^2A''$ equilibrium geometry of the vinoxy radical computed using the CCSD(T)/ANO2 method. Bond distances in Å and angles in degrees.

The vinoxy radical ($\dot{C}H_2CH{=}O$) is isoelectronic to the allyl radical[149] and has received substantial attention.[137,149–156,195–197] Two possible structures have been discussed for this radical, distinguished by their bonding. We may draw a distinction between the formyl methyl structure, with substantial C=O double bond character, and the ethenyloxy structure, with greater C=C double bond character, as denoted in Figure 4.7.[149,195]

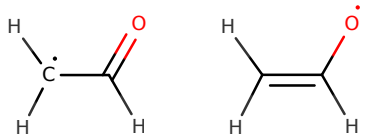

Formyl methyl Ethenyloxy

Figure 4.7: Two vinoxy radical bonding situations proposed in the literature.

The electron spin resonance spectrum of vinoxy radical has been reported in the literature.[198]

Inoue and Akimoto[149] observed the vinoxy radical using laser-induced fluorescence. Their results support a greater C=O double bond character than C=C double bond character; Inoue reported an estimated C=O

bond order of 1.74 and a C–C bond order of 1.21, along with estimated C=O (1.27 Å) and C–C (1.48 Å) bond lengths. Dupuis, Wendoloski, and Lester[195] found two distinct minima on the $^2A''$ ground state potential energy surface of the vinoxy radical using spin-restricted Hartree-Fock and multiconfiguration Hartree-Fock methods. One of these minima corresponds to the formyl methyl structure, the other to the ethenyloxy structure, but Dupuis and coworkers found the formyl methyl structure to be the lower in energy of the two. On the basis of isotopic shifts, Jacox also suggested that the ground state be identified with the formyl methyl structure.[137]

The 1985 microwave spectroscopy results of Endo, Saito, and Hirota support a planar structure and provide additional support for the formyl methyl ground state structure.[199] Endo and coworkers[199] further include geometrical parameters derived under the assumption that Dupuis and coworkers correctly computed the bond lengths and angles involving hydrogen.[195] Nearly twenty years after Endo studied the microwave spectrum of the vinoxy radical with Saito and Hirota in 1985, he returned to this pursuit with Nakajima[200] in 2014 using Fourier-transform microwave spectroscopy. However, Endo was still unable to determine a centrifugal distortion constant, and did not report an updated geometry. Removal of the vinyl alcohol OH hydrogen to produce the vinoxy radical causes the C–C bond to increase from 1.334 Å (a normal C=C double bond distance) to 1.430 Å, nearly 0.1 Å longer. In contrast, the C–O bond decreases from 1.363 Å, a conventional single bond distance, to 1.232 Å, ~ 0.15 Å shorter.

We report our vinoxy radical computational fundamental modes in Table 4.6 along with the results of several experimental studies. We obtain excellent agreement to within 15 cm^{-1} with experiment for the a' modes ν_4, ν_6, ν_7, ν_8, and ν_9, as well as for the a'' mode ν_{12}. Three of the a' modes, ν_4, ν_7, and ν_9, have been reported several times in the literature, and our results agree beautifully with these observations. Inoue and Akimoto[149] investigated the vinoxy radical using laser-induced fluorescence in 1981. Their experimentally-motivated inference that vinoxy radical should have a greater double bond character in the C–O bond than in the C–C bond adds credence to the assignment of the observed 1560 cm^{-1} mode to the C–O stretch ν_4 and the observed 1150 cm^{-1} mode to the C–C stretch. In 1990, on the basis of a Franck-Condon factor treatment of the Duschinsky effect (a mixing of ground and excited state vibrational modes), Yamaguchi, Momose, and Shida[201] argued for reassignment of the 1981 Inoue frequencies. Yamaguchi and coworkers suggest that allylic radicals must be treated for the Duschinsky effect. Their 1993 study invokes anharmonicity and Fermi resonance to explain spectral deviations from anticipated behavior. The hole-burning spectra obtained in 1993 by Gejo and coworkers show disagreement with the Franck-Condon factors calculated by Yamaguchi and coworkers; the Gejo paper posits that the Duschinsky effect may be even more pronounced than Yamaguchi suggested.

Brock and Rohlfing[154] recorded the vibrational spectrum of the vinoxy radical in 1997. For the a' in-

Table 4.6: Vinoxy radical ($\dot{C}H_2CH{=}O$) anharmonic frequencies (cm^{-1}) with gas-phase experimental results for comparison.

Mode	Present Work		Expt[a]	Expt[b]	Expt[c]	Description
$\mathbf{a'}$						
ν_1	3132	(1)	–	–	–	a vCH$_2$
ν_2	3032	(2)	–	–	–	s vCH$_2$
ν_3	2808*	(65)	–	–	–	CHO vCH
ν_4	1548	(41)	1560	1540	1543	vCO
ν_5	1511*	(11)	–	–	1486	δCH$_2$
ν_6	1366	(9)	–	–	1366	δOCH
ν_7	1143*	(27)	1150	1143	1143	ρCH$_2$
ν_8	952	(2)	–	–	957	vCC
ν_9	499	(13)	530	496	500	δCCO
$\mathbf{a''}$						
ν_{10}	958	(0.2)	–	–	703	wHCO
ν_{11}	720	(38)	–	–	557	wCH$_2$
ν_{12}	417	(0.2)	–	–	404	τ
ZPVE	26.30 kcal mol^{-1}					

* Resonances treated: $\nu_3/(\nu_4+\nu_6)$, $\nu_5/2\nu_{11}$, and $\nu_7/(\nu_{11}+\nu_{12})$
[a] Laser induced fluorescence - Inoue and Akimoto,[149] 1981.
[b] Laser induced fluorescence - DiMauro, Heaven, and Miller,[151] 1984.
[c] Dispersed fluorescence spectroscopy - Brock and Rohlfing,[154] 1997.

plane modes, their results agree well with theory, both with previously published work and with the research performed here. However, the a'' out-of-plane modes they report exhibit poor agreement with theoretical results, a phenomenon Brock and Rohlfing attributed to vibronic coupling. Our current results suggest an alternative explanation. We first note that Brock and Rohlfing obtained the frequencies of the a'' out-of-plane modes by taking half of what appeared to be $2\nu_{10}$, $2\nu_{11}$, and $2\nu_{12}$, the first overtones of ν_{10}, ν_{11}, and ν_{12}, respectively. However, those overtones are of a' symmetry, as were a number of other bands observed in their experiments.

Our value of 958 cm^{-1} for ν_{10} is 255 cm^{-1} off from the 703 cm^{-1} frequency suggested by Brock and Rohlfing as half of the $2\nu_{10}$ overtone, which they observed at 1405 cm^{-1}. Our results instead direct assignment of this band to the combination band $\nu_8+\nu_9$, which has a' symmetry. Unlike the other assignments made by Brock and Rohlfing, this level showed a small inertial defect, further suggesting this has little to no contribution from the a'' modes. Accounting for anharmonicity, the CCSD(T)/ANO1 value of this combination band is 1400 cm^{-1}, a good match for the 1405 cm^{-1} band observed by Brock and Rohlfing. Furthermore, our value of 720 cm^{-1} for ν_{11} is 163 cm^{-1} off from the 519 cm^{-1} frequency assigned by Brock and Rohlfing. Their observed band appeared at 1113 cm^{-1}, which is in reasonably good agreement with

our computational value of 1135 cm^{-1} for the combination band $\nu_{10} + \nu_{12}$. While agreement is not as close for this reassignment, two factors bolster our confidence in it. First, errors are anticipated to be larger for VPT2 predictions containing multiple quanta. Second and most importantly, Brock and Rohlfing's argument regarding the large positive inertial defect observed in this band is consistent with this assignment, as the two modes involved in the combination level are both of a'' symmetry. In contrast to the situation with the other two a'' modes, our ν_{12} value of 417 cm^{-1} agrees well with the experimentally reported value of 404 cm^{-1}. Our results support Brock and Rohlfing's assignment of their 808 cm^{-1} band to $2\nu_{12}$.

Based on page 213 of the excellent 1998 compilation of vinoxy radical experimental frequencies by Jacox,[155] we note that our theoretical ν_1 (3132 cm^{-1}) and ν_2 (3032 cm^{-1}), two of the high-frequency C–H stretches, are unobserved to date. However, a 2003 study by Utkin *et al.*[202] reports the band origin of ν_3, the third of these stretches, to be 2827.9125(3) cm^{-1}, which is similar to our theoretical prediction, namely 2808 cm^{-1}.

1-Hydroxyvinyl Radical

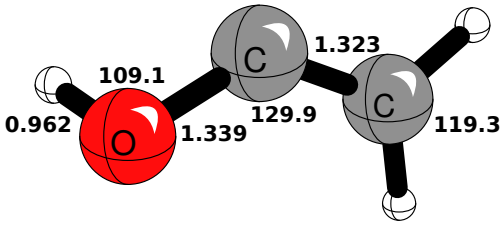

Figure 4.8: Ground state C_1 equilibrium geometry of the 1-hydroxyvinyl radical predicted using the CCSD(T)/ANO2 method. Bond distances in Å and angles in degrees.

We expect the 1-hydroxyvinyl radical ($H_2C{=}\dot{C}OH$) to exhibit double bonding between the two carbons. It likely tautomerizes to the lower-energy vinoxy radical in combustion scenarios. We report our CCSD(T)/ANO2 computational structure of the 1-hydroxyvinyl radical in Figure 4.8.

In 2006, da Silva, Kim, and Bozzelli[203] predicted a B3LYP/6-31G(d,p) geometry of the 1-hydroxyvinyl radical in a study aimed at computing enthalpies and other thermodynamic properties. In contrast to the acetyl radical, the vinyl radical, and the vinoxy radical, which have been studied extensively, the 1-hydroxyvinyl radical has received little attention in the literature.[122,135,204,205] While this could be an indicator that this radical is produced only fleetingly, we decided to investigate this potential combustion

intermediate. Neither experimental vibrational frequencies nor computational anharmonic frequencies are currently available for this radical. Compared to its parent *syn*-vinyl alcohol, abstraction of hydrogen to 1-hydroxyvinyl radical shortens the C–C bond length from 1.334 Å to 1.323 Å and, to a larger degree, the C–O bond length from 1.363 to 1.339 Å.

Most likely, the 1-hydroxyvinyl radical is formed only transiently. We report our theoretical frequencies and assignments for 1-hydroxyvinyl radical in Table 4.7. From the IR intensities, it appears that the O–H stretch (ν_1, 3640 cm^{-1}), the C–C stretch (ν_4, 1664 cm^{-1}), the COH deformation (ν_6, 1206 cm^{-1}), and the CCOH torsion (ν_{12}, 259 cm^{-1}) fundamentals will be the easiest to observe spectroscopically.

Table 4.7: 1-hydroxyvinyl radical ($H_2C{=}\dot{C}OH$) harmonic vibrational frequencies (cm^{-1}), anharmonic frequencies (cm^{-1}), and harmonic CCSD(T)/ANO2 infrared intensities (km mol^{-1}).

Mode	Fundamental		Description
ν_1	3640	(125)	νOH
ν_2	3105	(0.3)	a νCH_2
ν_3	3065*	(1)	νCH
ν_4	1664	(117)	νCC
ν_5	1376	(3)	δCH_2
ν_6	1206	(184)	δCOH
ν_7	1105	(8)	s νCCO
ν_8	945	(41)	$\nu CO/\rho CH_2$
ν_9	795	(52)	wCH_2
ν_{10}	607*	(10)	τHCCO
ν_{11}	436	(10)	δCCO
ν_{12}	259	(141)	τCCOH
ZPVE	26.53 kcal mol^{-1}		

* Resonances treated: $\nu_3/(\nu_4 + \nu_5)$, $\nu_{10}/2\nu_{12}$

2-Hydroxyvinyl Radical

In their 2006 study that predicted a B3LYP/6-31G(d,p) geometry of the 1-hydroxyvinyl radical, Bozzelli and coworkers[203] report computations at the same level on the 2-hydroxyvinyl radical ($H\dot{C}{=}CHOH$). Like the 1-hydroxyvinyl radical, the 2-hydroxyvinyl radical has been only briefly mentioned in the literature.[122,204,205] Experimental vibrational frequencies and computational anharmonic frequencies are currently unavailable for this radical. Like the 1-hydroxyvinyl radical, the $H\dot{C}{=}CHOH$ radical lends minimal favorability to the unpaired electron, and is likely to tautomerize or react promptly. Our CCSD(T)/ANO2 geometries for the four conformers of the 2-hydroxyvinyl radical we considered are reported in Figure 4.9; the (E) and the (Z)

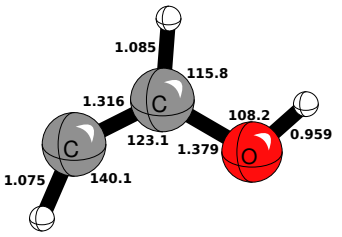

(*Z*) *anti*-2-hydroxyvinyl radical

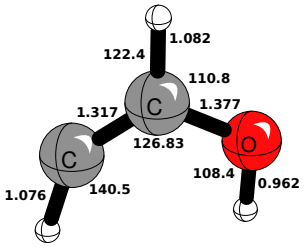

(*Z*) *syn*-2-hydroxyvinyl radical

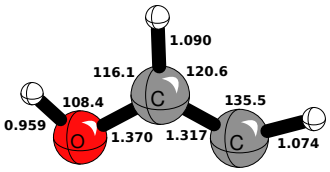

(*E*) *anti*-2-hydroxyvinyl radical

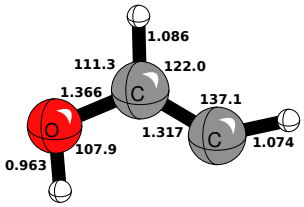

(*E*) *syn*-2-hydroxyvinyl radical

Figure 4.9: Ground state C_s equilibrium conformer geometries of the 2-hydroxyvinyl radical predicted using the CCSD(T)/ANO2 method. Bond distances in Å and angles in degrees.

forms of the 2-hydroxyvinyl radical are also depicted in the reaction pathway scheme of Figure 1, but in the latter figure without the distinction between the *syn* and *anti* positions of the alcoholic hydrogen. Compared to the bond lengths in *syn*-vinyl alcohol, removal of either β hydrogen decreases the C–C bond by ~ 0.02 Å and decreases the C–O bond from 1.363 Å in *syn*-vinyl alcohol to 1.317 Å in the (E) *syn* conformer. However, in the (Z) *syn* conformer, this H atom removal increases the C–O bond from 1.362 Å to 1.377 Å.

As with the 1-hydroxyvinyl radical, experimental vibrational frequencies, to our knowledge, are not available for the 2-hydroxyvinyl radical (H$\dot{\text{C}}$=CHOH), which is most likely formed only transiently. We report our theoretical frequencies and assignments for 2-hydroxyvinyl radical in Table 8. Among the fundamentals predicted for the four conformers, the lowest fundamental is 206 cm^{-1}, for ν_{12} of the (Z) *anti* structure. Based on the harmonic intensities, we expect modes ν_6, ν_7, and ν_{12} of the (Z) *anti* conformer; modes ν_4, ν_7, and ν_{12} of the (Z) *syn* conformer; modes ν_1 and ν_6 of the (E) *anti* conformer, and modes ν_4, ν_7, and ν_{12} of the (E) *syn* conformer to be the easiest to observe spectroscopically. We defer the relative energies of the

four structures to Table 4.9.

Table 4.8: Fundamental modes (cm^{-1}) of the four 2-hydroxyvinyl radical structures.

Mode	(Z) *anti*		Description	(Z) *syn*		Description
$\mathbf{a}'$						
ν_1	3669	(72)	vOH	3636	(43)	vOH
ν_2	3164	(7)	t vCH	3155[b]	(5)	t vCH
ν_3	3012	(7)	i vCH	3049	(3)	i vCH
ν_4	1632[a]	(63)	vCC	1599[b]	(109)	vCC
ν_5	1296	(23)	vCC/δCOH	1328	(2)	vCC/δCOH
ν_6	1208	(142)	δCOH/ρCH	1219[b]	(10)	ρCH
ν_7	1046[a]	(99)	vCO	1031	(179)	vCO
ν_8	771	(4)	δCCH	726	(38)	δCCH
ν_9	446[a]	(18)	δCCO	429	(8)	δCCO
$\mathbf{a}''$						
ν_{10}	845	(49)	d	874	(48)	d
ν_{11}	600	(46)	τHCCO	571	(49)	τHCCO
ν_{12}	206	(93)	τCCOH	375	(89)	τCCOH
ZPVE	27.26 kcal mol^{-1}			26.44 kcal mol^{-1}		

Mode	(E) *anti*		Description	(E) *syn*		Description
$\mathbf{a}'$						
ν_1	3685	(81)	vOH	3629	(46)	vOH
ν_2	3168	(7)	t vCH	3171[d]	(8)	t vCH
ν_3	2955	(11)	i vCH	2993	(5)	i vCH
ν_4	1656	(72)	vCC	1623[d]	(117)	vCC
ν_5	1284	(66)	vCC/δCOH	1330	(3)	vCC/δCOH
ν_6	1243[c]	(109)	δCOH/ρCH	1236[d]	(12)	δCOH
ν_7	1091	(42)	vCO	1072	(160)	vCO
ν_8	776	(60)	δCCH	743	(30)	δCCH
ν_9	472[c]	(4)	δCCO	466	(22)	δCCO
$\mathbf{a}''$						
ν_{10}	746	(9)	d	809	(14)	d
ν_{11}	613	(71)	t wCH	578	(14)	τHCCO
ν_{12}	248	(67)	τHCCO	414	(147)	τCCOH
ZPVE	26.23 kcal mol^{-1}			26.45 kcal mol^{-1}		

[a] Resonances treated: $\nu_4/2\nu_8$, $\nu_7/(\nu_{10}+\nu_{12})$, and $\nu_9/2\nu_{12}$
[b] Resonances treated: $\nu_2/2\nu_4$, $\nu_4/2\nu_8$, $\nu_6/(\nu_8+\nu_9)$
[c] Resonances treated: $\nu_6/(\nu_8+\nu_9)$, $\nu_9/2\nu_{12}$
[d] Resonances treated: $\nu_2/2\nu_4$, $\nu_4/2\nu_{10}$, and $\nu_6/(\nu_8+\nu_9)/(\nu_{10}+\nu_{12})$

Energetics

Prior to discussing the radical species under consideration, we examine the conversion from *syn*- to *anti*-vinyl alcohol. With a final exothermicity of 1.08 kcal mol^{-1}, the *syn* conformer is the lower in energy of the two conformers, as Saito[131] observed in microwave spectroscopy experiments. We include only the lower-energy *syn* conformer in the focal point analyses of Reactions 3-7. In Table 4.9, we relate the relative FPA energies of the radicals considered in this work. We note that the *syn* conformers of both the (E) and (Z)

2-hydroxyvinyl radicals are lower in energy than the corresponding *anti* conformers, and further focal point analysis has considered only the *syn* conformers.

Table 4.9: Relative energies in kcal mol^{-1} of the radicals considered in this research (excluding vinyl) with respect to acetyl radical ($CH_3\dot{C}$=O). Energies were computed at the CCSDT(Q)/CBS level of theory. Corrections for the diagonal Born-Oppenheimer approximation, relativistic effects, and core correlation effects were applied to the energies, along with zero-point vibrational energies. The value marked with an asterisk (*) was computed without CCSDT(Q)/cc-pVTZ single point energies.

Radical	ΔH_{0K}
1-hydroxyvinyl (CH_2=$\dot{C}$OH)	29.93*
(Z) *anti*-2-hydroxyvinyl ($\dot{C}$H=CHOH)	37.68
(Z) *syn*-2-hydroxyvinyl ($\dot{C}$H=CHOH)	35.11
(E) *anti*-2-hydroxyvinyl ($\dot{C}$H=CHOH)	35.95
(E) *syn*-2-hydroxyvinyl ($\dot{C}$H=CHOH)	33.71
Vinoxy ($\dot{C}H_2$CH=O)	6.44
Acetyl ($CH_3\dot{C}$=O)	0.00

As noted above, the seven fragmentations considered are shown in Figure 1. Table 4.10 summarizes the final energies of the various reactions determined using the focal point approach. Although vibrational modes are considered for both the *syn* and the *anti* conformers of vinyl alcohol, the *anti* conformer is examined here only in the context of its relative energy with respect to the lower-energy *syn* conformer. We include only the *syn* conformer in the focal point analysis of Reactions 3-7. These results are relative reaction enthalpies.

At the CCSDT(Q) CBS limit, the tautomerization of acetaldehyde to *syn*-vinyl alcohol (Reaction 1) is endothermic by 9.7 kcal mol^{-1}. This energetically unfavorable tautomerization agrees with the observation that keto isomers are generally more stable than enols.[206] The loss of the hydrogen on the aldehyde group

Table 4.10: Final exothermicities (kcal mol^{-1}) determined from the energetics of the focal point approach along with corrections. Discussion of the methods and corrections may be found in the Methods section. Reaction indices given in parentheses correspond to the reactions shown in Figure 1. The value marked with an asterisk (*) was computed without CCSDT(Q)/cc-pVTZ single point energies.

Reaction	ΔE_e	$+\Delta_{ZPVE}$	$+\Delta_{Core}$	$+\Delta_{DBOC}$	$+\Delta_{Rel}$	$= \Delta H_{0K}$
syn → *anti* conversion	1.26	−0.17	−0.01	0.00	0.00	1.08
CH_3CHO → *syn*-CH_2CHOH (1)	9.14	0.65	−0.03	−0.06	0.00	9.70
CH_3CHO → $CH_3\dot{C}$=$\dot{O}$ + $\dot{H}$ (2)	95.35	−7.63	0.00	−0.15	−0.07	87.50
CH_2CHOH → H_2C=$\dot{C}$OH + $\dot{H}$ (3)	116.30 *	−8.68	0.17	−0.14	−0.03	107.63
CH_2CHOH → (Z) $H\dot{C}$=CHOH + $\dot{H}$ (4)	121.53	−8.54	0.21	−0.14	−0.03	113.03
CH_2CHOH → (E) $H\dot{C}$=CHOH + $\dot{H}$ (5)	120.14	−8.53	0.19	−0.13	−0.03	111.64
CH_2CHOH → $\dot{C}H_2$CH=O + $\dot{H}$ (6)	92.98	−8.68	0.24	−0.06	−0.10	84.38
CH_2CHOH → CH_2=$\dot{C}$H + $\dot{O}$H (7)	115.04	−7.10	0.38	0.09	−0.23	108.18

from acetaldehyde produces the acetyl radical (Reaction 2). As a result, the loss only requires 87.5 kcal mol^{-1} of energy, less than that required by most other hydrogen atom loss reactions we consider. The removal of the hydrogen attached to the α carbon of vinyl alcohol to produce 1-hydroxyvinyl radical (CH_2=$\dot{C}$OH) (Reaction 3) requires 107.6 kcal mol^{-1}, the second lowest relative enthalpy of the vinyl alcohol hydrogen dissociations. Removal of a β hydrogen for vinyl alcohol can happen in two ways, the first of which leads to the (Z) 2-hydroxyvinyl (H$\dot{C}$=CHOH) radical (Reaction 4). Breaking this C–H bond to result in the lower-energy *syn* conformer requires 113.0 kcal mol^{-1}. Removal of the other β hydrogen from vinyl alcohol leads to the (E) 2-hydroxyvinyl radical and requires 111.6 kcal mol^{-1} to yield the lower-energy *syn* conformer (Reaction 5 of Figure 4.1).

The removal of the alcoholic hydrogen from vinyl alcohol to create the vinoxy radical (Reaction 6 in Figure 4.1) is the most energetically favorable (+84.4 kcal mol^{-1}) of all the dissociation processes studied. This result is not entirely surprising, since removal of the hydrogen atom may be viewed as the first step in the energetically favored tautomerization into acetaldehyde. Since acetaldehyde is the lower energy tautomer, this dissociation might be expected to require less energy to initiate the tautomerization. Reaction 7 in Figure 4.1, which results in the vinyl radical, is the only hydroxyl radical removal studied. With an enthalpy of 108.2 kcal mol^{-1}, it is much less energetically favorable than the analogous reaction leading to the vinoxy radical. Chemically, this can be explained in terms of the loss of the C–O bond in the reaction leading to the vinyl radical.

In a 2005 study of the reaction between acetylene and the hydroxy radical, Senosiain, Klippenstein and Miller[204] found the RQCISD(T) energy barrier for conversion of H$\dot{C}$=CHOH to H_2C=$\dot{C}$OH to be 38.4 kcal mol^{-1}. This would suggest that at high temperatures, the 2-hydroxyvinyl radical (H$\dot{C}$=CHOH) may be observed, although it may not be long-lived at temperatures relevant to combustion. The 2011 study by Hansen, Harper, and Green[122] considered the kinetics of the H$\dot{C}$=CHOH and H_2C=$\dot{C}$OH radicals (as well as the kinetics of vinyl alcohol and acetyl radical) using parameters estimated with group and bond additivity schemes; our computational parameters provide an alternative source for these values.

Conclusions

In this study, high-level coupled-cluster theory was applied to acetaldehyde and vinyl alcohol and the radicals related thereto through removal of a hydrogen atom or the hydroxyl radical. Reaction enthalpies were determined at the CCSDT(Q)/CBS limit. These predictions should prove useful in future examinations of butanol combustion models. In addition, the fundamental frequencies predicted for the 1-hydroxyvinyl and 2-hydroxyvinyl radicals are the first to appear in the literature, providing the first look at their vibrational

structure. Although both *syn*- and *anti*-vinyl alcohol have been considered in spectroscopic research reported in the literature, our fundamental mode predictions of ν_3 (3076 cm^{-1}) and ν_4 (2999 cm^{-1}) for *syn*-vinyl alcohol and of $\nu_1 - \nu_{14}$ for *anti*-vinyl alcohol supply values that have not been experimentally reported. No observations have been reported of the modes ν_6 (1035 cm^{-1}), ν_{11} (944 cm^{-1}), and ν_{12} (97 cm^{-1}), of acetyl radical. Furthermore, we propose revised assignments for modes ν_4 and ν_{10} of acetyl radical. The experimental value of 1419.9 cm^{-1} tentatively assigned to the ν_{10} fundamental of acetyl radical should instead be assigned to ν_4 (1427 cm^{-1}), which means that ν_{10} (1441 cm^{-1}) also has yet to be observed experimentally. Reassignment of two vinoxy radical modes, ν_{10} (958 cm^{-1}) and ν_{11} (720 cm^{-1}) is presented in light of the present research.

Acknowledgements

The authors would like to acknowledge helpful discussions with Jay Agarwal, Preston R. Hoobler, and Kevin B. Moore III. This research was supported by the Department of Energy, Basic Energy Sciences, Computational and Theoretical Chemistry (CTC) Program, Grant DE-SC0015512.

Focal Point Tables

Table 4.11: *syn*→ *anti* Conversion

Method	HF	δMP2	δCCSD	δCCSD(T)	δCCSDT	δCCSDT(Q)	[Net]
cc-PVDZ	+2.11	+0.20	−0.26	+0.05	−0.01	+0.01	[+2.09]
cc-PVTZ	+1.60	+0.08	−0.18	+0.04	−0.01	+0.01	[+1.54]
cc-PVQZ	+1.44	+0.05	−0.14	+0.03	[−0.01]	[+0.01]	[+1.38]
cc-PV5Z	+1.37	+0.03	−0.13	+0.03	[−0.01]	[+0.01]	[+1.31]
CBS	[+1.34]	[+0.00]	[−0.11]	[+0.02]	[−0.01]	[+0.01]	[+1.26]
$\Delta E_{\rm final} = \Delta$E[CCSDT(Q)/CBS] + $\Delta_{\rm ZPVE} + \Delta_{\rm core} + \Delta_{\rm DBOC} + \Delta E_{\rm rel}$							
$\Delta E_{\rm final} = 1.26 - 0.17 - 0.01 + 0.00 + 0.00 =$**1.08 kcal mol**$^{-1}$							

Table 4.12: acetaldehyde → *syn*-vinyl alcohol (Reaction 1)

Method	HF	δMP2	δCCSD	δCCSD(T)	δCCSDT	δCCSDT(Q)	[Net]
cc-PVDZ	+12.99	+0.25	−0.34	+0.10	+0.01	−0.03	[+12.98]
cc-PVTZ	+11.81	−1.49	−0.16	−0.19	+0.03	−0.05	[+9.96]
cc-PVQZ	+11.77	−1.89	−0.10	−0.24	[+0.03]	[−0.05]	[+9.52]
cc-PV5Z	+11.66	−2.02	−0.05	−0.26	[+0.03]	[−0.05]	[+9.32]
CBS	[+11.58]	[−2.16]	[+0.00]	[−0.27]	[+0.03]	[−0.05]	[+9.14]
$\Delta E_{\rm final} = \Delta$E[CCSDT(Q)/CBS] + $\Delta_{\rm ZPVE} + \Delta_{\rm core} + \Delta_{\rm DBOC} + \Delta E_{\rm rel}$							
$\Delta E_{\rm final} = 9.14 + 0.65 - 0.03 - 0.06 + 0.00 =$**9.70 kcal mol**$^{-1}$							

Table 4.13: $CH_3CHO \rightarrow CH_3\dot{C}O + H$ (Reaction 2)

Basis Set	HF	δMP2	δCCSD	δCCSD(T)	δCCSDT	δCCSDT(Q)	[Net]
cc-pVDZ	+77.03	+11.02	+2.95	−0.40	−0.10	−0.00	[+90.51]
cc-pVTZ	+77.75	+14.62	+2.40	−0.33	−0.07	−0.02	[+94.35]
cc-pVQZ	+77.68	+15.57	+2.17	−0.31	[−0.07]	[−0.02]	[+95.01]
cc-pV5Z	+77.68	+15.85	+2.05	−0.32	[−0.07]	[−0.02]	[+95.17]
CBS LIMIT	[+77.69]	[+16.15]	[+1.93]	[−0.33]	[−0.07]	[−0.02]	[+95.35]
$\Delta E_{\text{final}} = \Delta\text{E[CCSDT(Q)/CBS]} + \Delta_{\text{ZPVE}} + \Delta_{\text{core}} + \Delta_{\text{DBOC}} + \Delta E_{\text{rel}}$							
$\Delta E_{\text{final}} = 95.35 - 7.63 - 0.00 - 0.15 - 0.07 =$**87.50 kcal mol^{-1}**							

Table 4.14: *syn*-$CH_2CHOH \rightarrow CH_2{=}\dot{C}OH + H$ (Reaction 3)

Method	HF	δMP2	δCCSD	δCCSD(T)	δCCSDT	δCCSDT(Q)	[Net]
cc-PVDZ	+94.40	+16.90	−0.06	+0.17	−0.16	+0.03	[+111.29]
cc-PVTZ	+94.95	+20.43	−0.52	+0.35	−0.18	[+0.03]	[+115.06]
cc-PVQZ	+94.94	+21.45	−0.77	+0.38	[−0.18]	[+0.03]	[+115.85]
cc-PV5Z	+94.97	+21.78	−0.91	+0.38	[−0.18]	[+0.03]	[+116.07]
CBS	[+95.00]	[+22.13]	[−1.05]	[+0.38]	[−0.18]	[+0.03]	[+116.30]
$\Delta E_{\text{final}} = \Delta E\text{[CCSDT(Q)/CBS]} + \Delta_{\text{ZPVE}} + \Delta_{\text{core}} + \Delta_{\text{DBOC}} + \Delta E_{\text{rel}}$							
$\Delta E_{\text{final}} = 116.30 - 8.68 + 0.17 - 0.14 - 0.03 =$**107.63 kcal mol^{-1}**							

Cartesian CCSD(T)/ANO2 Geometries (in Bohr)

Table 4.25: *syn*-Vinyl Alcohol (CH_2=CHOH)

	X	Y	Z
C	−2.363 208 57	0.398 946 93	0.000 000 00
C	−0.157 867 69	−0.821 084 50	0.000 000 00
O	2.181 834 28	0.254 882 79	0.000 000 00
H	−0.023 918 44	−2.860 191 79	0.000 000 00
H	−2.469 043 64	2.443 118 27	0.000 000 00
H	−4.103 294 47	−0.663 666 12	0.000 000 00
H	1.986 986 34	2.061 884 46	0.000 000 00

Table 4.15: *syn*-CH_2=CHOH → (Z) *syn*-$H\dot{C}$=CHOH + $\dot{H}$ (Reaction 4)

basis set	HF	δMP2	δCCSD	δCCSD(T)	δCCSDT	δCCSDT(Q)	NET
cc-pVDZ	+98.28	+18.63	−0.61	+0.36	−0.17	+0.01	[+116.51]
cc-pVTZ	+99.18	+21.74	−1.00	+0.58	−0.20	+0.01	[+120.31]
cc-pVQZ	+99.23	+22.65	−1.21	+0.62	[−0.20]	[+0.01]	[+121.10]
cc-pV5Z	+99.27	+22.95	−1.33	+0.62	[−0.20]	[+0.01]	[+121.32]
CBS	[+99.29]	[+23.27]	[−1.46]	[+0.63]	[−0.20]	[+0.01]	[**+121.53**]
$\Delta E_{\text{final}} = \Delta E$[CCSDT(Q)/CBS] + Δ_{ZPVE} + Δ_{core} + Δ_{DBOC} + ΔE_{rel}							
$\Delta E_{\text{final}} = 121.53 - 8.54 + 0.21 - 0.14 - 0.03 =$**113.03 kcal mol^{-1}**							

Table 4.16: *syn*-CH_2=CHOH → (E) *syn*-$H\dot{C}$=CHOH + $\dot{H}$ (Reaction 5)

Method	HF	δMP2	δCCSD	δCCSD(T)	δCCSDT	δCCSDT(Q)	NET
cc-pVDZ	+96.76	+18.76	−0.54	+0.42	−0.16	+0.01	[+115.26]
cc-pVTZ	+97.59	+21.92	−0.99	+0.66	−0.19	+0.01	[+119.00]
cc-pVQZ	+97.62	+22.83	−1.22	+0.69	[−0.19]	[+0.01]	[+119.74]
cc-pV5Z	+97.63	+23.13	−1.34	+0.70	[−0.19]	[+0.01]	[+119.94]
CBS	[+97.65]	[+23.45]	[−1.48]	[+0.70]	[−0.19]	[+0.01]	[+120.14]
$\Delta E_{\text{final}} = \Delta E$[CCSDT(Q)/CBS] + Δ_{ZPVE} + Δ_{core} + Δ_{DBOC} + ΔE_{rel}							
$\Delta E_{\text{final}} = 120.14 - 8.53 + 0.19 - 0.13 - 0.03 =$**111.64 kcal mol^{-1}**							

Table 4.26: *anti*-Vinyl Alcohol (CH_2=CHOH)

	X	Y	Z
C	−2.36627421	0.38472674	−0.00000000
C	−0.15950180	−0.82344652	0.00000000
O	2.09290336	0.44816573	0.00000000
H	−0.03561830	−2.86855272	0.00000000
H	−2.45727742	2.42520811	−0.00000000
H	−4.09664825	−0.69333181	0.00000000
H	3.44763115	−0.75227774	−0.00000000

Table 4.17: *syn*-CH_2=CHOH → $\dot{C}H_2$CH=O (Reaction 6)

Method	HF	δMP2	δCCSD	δCCSD(T)	δCCSDT	δCCSDT(Q)	NET
cc-pVDZ	+69.35	+15.31	+0.51	+0.09	−0.17	−0.02	[+85.05]
cc-pVTZ	+71.12	+19.69	+0.04	+0.53	−0.20	−0.02	[+91.16]
cc-pVQZ	+71.20	+20.88	−0.13	+0.59	[−0.20]	[−0.02]	[+92.31]
cc-pV5Z	+71.28	+21.26	−0.26	+0.60	[−0.20]	[−0.02]	[+92.65]
CBS	[+71.33]	[+21.66]	[−0.40]	[+0.60]	[−0.20]	[−0.02]	[**+92.98**]
$\Delta E_{\text{final}} = \Delta E$[CCSDT(Q)/CBS] + Δ_{ZPVE} + Δ_{core} + Δ_{DBOC} + ΔE_{rel}							
$\Delta E_{\text{final}} = 92.98 - 8.68 + 0.24 - 0.06 - 0.10$ =**84.38 kcal mol**$^{-1}$							

Table 4.18: *syn*-CH_2CHOH → CH_2=$\dot{C}$H + $\dot{O}$H (Reaction 7)

Method	HF	δMP2	δCCSD	δCCSD(T)	δCCSDT	δCCSDT(Q)	[Net]
cc-PVDZ	+80.13	+36.79	−10.28	+2.31	−0.25	+0.26	[+108.96]
cc-PVTZ	+81.18	+40.13	−11.60	+3.25	−0.45	+0.24	[+112.74]
cc-PV5Z	+81.15	+41.62	−11.83	+3.37	[−0.45]	[+0.24]	[+114.10]
cc-PVQZ	+81.11	+42.19	−11.93	+3.40	[−0.45]	[+0.24]	[+114.56]
CBS	[+81.08]	[+42.79]	[−12.04]	[+3.43]	[−0.45]	[+0.24]	[+115.04]
$\Delta E_{\text{final}} = \Delta E$[CCSDT(Q)/CBS] + Δ_{ZPVE} + Δ_{core} + Δ_{DBOC} + ΔE_{rel}							
$\Delta E_{\text{final}} = 115.04 - 7.10 + 0.38 + 0.09 - 0.23$ =**108.18 kcal mol**$^{-1}$							

Table 4.27: 1-Hydroxyvinyl Radical (CH_2=$\dot{C}$OH)

	X	Y	Z
C	2.41650197	0.27274813	−0.02296243
C	0.14443152	−0.76795343	0.01341273
H	4.08131749	−0.88717384	0.17332040
H	2.62867163	2.29709790	−0.28414435
O	−2.13882366	0.31934158	0.07931463
H	−3.25790176	−0.58178204	−1.03425026

Table 4.19: Focal point analysis of 1-hydroxyvinyl radical (H_2C=$\dot{C}$OH) energy compared to that of acetyl radical (CH_3C=$\dot{O}$).

Method	HF	δMP2	δCCSD	δCCSD(T)	δCCSDT	δCCSDT(Q)	[Net]
cc-PVDZ	+30.36	+6.13	−3.35	+0.67	−0.06	+0.00	[+33.76]
cc-PVTZ	+29.02	+4.32	−3.08	+0.49	−0.08	[+0.00]	[+30.67]
cc-PVQZ	+29.03	+3.99	−3.03	+0.45	[−0.08]	[+0.00]	[+30.37]
cc-PV5Z	+28.96	+3.91	−3.01	+0.44	[−0.08]	[+0.00]	[+30.23]
CBS	[+28.90]	[+3.82]	[−2.98]	[+0.43]	[−0.08]	[+0.00]	[+30.10]
$\Delta E_{\text{final}} = \Delta E$[CCSDT(Q)/CBS] + Δ_{ZPVE} + Δ_{core} + Δ_{DBOC} + ΔE_{rel}							
$\Delta E_{\text{final}} = 30.10 - 0.17 - 0.08 - 0.04 + 0.12$= **29.93 kcal mol**$^{-1}$							

Table 4.20: Focal point analysis of (Z) *anti*-2-hydroxyvinyl radical ($\dot{\text{H}}\text{C}$=CHOH) energy compared to that of acetyl radical ($CH_3C{=}\dot{O}$).

Method	HF	δMP2	δCCSD	δCCSD(T)	δCCSDT	δCCSDT(Q)	[Net]
cc-PVDZ	+36.25	+8.50	−4.16	+0.99	−0.07	−0.01	[+41.49]
cc-PVTZ	+34.73	+6.18	−3.76	+0.86	−0.10	−0.01	[+37.90]
cc-PVQZ	+34.67	+5.74	−3.65	+0.82	[−0.10]	[−0.01]	[+37.47]
cc-PV5Z	+34.54	+5.61	−3.59	+0.82	[−0.10]	[−0.01]	[+37.26]
CBS	[+34.44]	[+5.47]	[−3.53]	[+0.81]	[−0.10]	[−0.01]	[+37.08]
$\Delta E_{\text{final}} = \Delta E$[CCSDT(Q)/CBS] + Δ_{ZPVE} + Δ_{core} + Δ_{DBOC} + ΔE_{rel}							
$\Delta E_{\text{final}} = 37.08 + 0.56 - 0.05 - 0.04 + 0.13$= **37.68 kcal mol^{-1}**							

Table 4.21: Focal point analysis of (Z) *syn*-2-hydroxyvinyl radical ($\dot{\text{H}}\text{C}$=CHOH) energy compared to that of acetyl radical ($CH_3C{=}\dot{O}$).

Method	HF	δMP2	δCCSD	δCCSD(T)	δCCSDT	δCCSDT(Q)	[Net]
cc-PVDZ	+34.24	+7.87	−3.90	+0.86	−0.07	−0.02	[+38.99]
cc-PVTZ	+33.24	+5.63	−3.56	+0.73	−0.09	−0.03	[+35.92]
cc-PVQZ	+33.33	+5.19	−3.48	+0.69	[−0.09]	[−0.03]	[+35.61]
cc-PV5Z	+33.25	+5.08	−3.43	+0.69	[−0.09]	[−0.03]	[+35.47]
CBS	[+33.19]	[+4.96]	[−3.38]	[+0.68]	[−0.09]	[−0.03]	[+35.33]
$\Delta E_{\text{final}} = \Delta E$[CCSDT(Q)/CBS] + Δ_{ZPVE} + Δ_{core} + Δ_{DBOC} + ΔE_{rel}							
$\Delta E_{\text{final}} = 35.33 - 0.26 - 0.04 - 0.04 + 0.12$= **35.11 kcal mol^{-1}**							

Table 4.22: Focal point analysis of (E) *anti*-2-hydroxyvinyl radical ($\dot{\text{H}}\text{C}$=CHOH) energy compared to that of acetyl radical ($CH_3C{=}\dot{O}$).

Method	HF	δMP2	δCCSD	δCCSD(T)	δCCSDT	δCCSDT(Q)	[Net]
cc-PVDZ	+36.02	+8.45	−4.23	+0.97	−0.07	−0.01	[+41.13]
cc-PVTZ	+34.34	+6.16	−3.84	+0.84	−0.10	−0.01	[+37.37]
cc-PVQZ	+34.18	+5.69	−3.74	+0.80	[−0.10]	[−0.01]	[+36.82]
cc-PV5Z	+34.01	+5.56	−3.68	+0.80	[−0.10]	[−0.01]	[+36.57]
CBS	[+33.90]	[+5.42]	[−3.62]	[+0.79]	[−0.10]	[−0.01]	[+36.37]
$\Delta E_{\text{final}} = \Delta E$[CCSDT(Q)/CBS] + Δ_{ZPVE} + Δ_{core} + Δ_{DBOC} + ΔE_{rel}							
$\Delta E_{\text{final}} = 36.37 - 0.47 - 0.05 - 0.03 + 0.13$= **35.95 kcal mol^{-1}**							

Table 4.23: Focal point analysis of (E) *syn*-2-hydroxyvinyl radical ($\dot{\text{H}}\text{C}$=CHOH) energy compared to that of acetyl radical ($CH_3C{=}\dot{O}$).

Method	HF	δMP2	δCCSD	δCCSD(T)	δCCSDT	δCCSDT(Q)	[Net]
cc-PVDZ	+32.72	+8.00	−3.83	+0.92	−0.06	−0.02	[+37.73]
cc-PVTZ	+31.66	+5.81	−3.55	+0.80	−0.09	−0.02	[+34.61]
cc-PVQZ	+31.71	+5.37	−3.48	+0.77	[−0.09]	[−0.02]	[+34.26]
cc-PV5Z	+31.62	+5.26	−3.44	+0.76	[−0.09]	[−0.02]	[+34.09]
CBS	[+31.55]	[+5.14]	[−3.40]	[+0.76]	[−0.09]	[−0.02]	[+33.93]
$\Delta E_{\text{final}} = \Delta E$[CCSDT(Q)/CBS] + Δ_{ZPVE} + Δ_{core} + Δ_{DBOC} + ΔE_{rel}							
$\Delta E_{\text{final}} = 33.93 - 0.25 - 0.06 - 0.04 + 0.13$= **33.71 kcal mol^{-1}**							

Table 4.24: Focal point analysis of vinoxy radical ($\dot{C}H_2CH{=}O$) energy compared to that of acetyl radical ($CH_3C{=}\dot{O}$).

Method	HF	δMP2	δCCSD	δCCSD(T)	δCCSDT	δCCSDT(Q)	[Net]
cc-PVDZ	+5.30	+4.54	−2.79	+0.59	−0.07	−0.05	[+7.52]
cc-PVTZ	+5.19	+3.58	−2.52	+0.67	−0.09	−0.05	[+6.77]
cc-PVQZ	+5.29	+3.42	−2.40	+0.66	[−0.09]	[−0.05]	[+6.83]
cc-PV5Z	+5.26	+3.39	−2.36	+0.66	[−0.09]	[−0.05]	[+6.80]
CBS	[+5.23]	[+3.35]	[−2.32]	[+0.66]	[−0.09]	[−0.05]	[+6.77]
$\Delta E_{\text{final}} = \Delta E[\text{CCSDT(Q)/CBS}] + \Delta_{\text{ZPVE}} + \Delta_{\text{core}} + \Delta_{\text{DBOC}} + \Delta E_{\text{rel}}$							
$\Delta E_{\text{final}} = 6.77 - 0.40 - 0.01 + 0.03 + 0.05$= **6.44 kcal mol**$^{-1}$							

Table 4.28: (Z) *anti*-2-Hydroxyvinyl Radical ($\dot{C}H{=}CHOH$)

	X	Y	Z
O	−2.01790884	0.48603575	0.00000000
C	0.23541970	−0.82336093	0.00000000
C	2.45668825	0.29526910	0.00000000
H	−3.37315932	−0.71746202	−0.00000000
H	0.08076780	−2.86798477	−0.00000000
H	3.26360102	2.15960570	0.00000000

Table 4.29: (Z) *syn*-2-Hydroxyvinyl Radical ($\dot{C}H{=}CHOH$)

	X	Y	Z
C	−2.44727795	0.31824363	−0.00000000
C	−0.23951871	−0.83142728	0.00000000
H	−3.24077965	2.19052593	−0.00000000
O	2.10592398	0.29549434	−0.00000000
H	−0.06597642	−2.86846460	0.00000000
H	1.87544178	2.09861891	−0.00000000

Table 4.30: (E) *anti*-2-Hydroxyvinyl Radical ($\dot{C}$H=CHOH)

	X	Y	Z
C	2.40451874	0.48850537	0.00000000
C	0.24460052	−0.74581534	−0.00000000
H	4.36779322	−0.02879450	−0.00000000
O	−2.06500244	0.42508011	0.00000000
H	−3.35233815	−0.84901044	−0.00000000
H	0.21502306	−2.80477920	−0.00000000

Table 4.31: (E) *syn*-2-Hydroxyvinyl Radical ($\dot{C}$H=CHOH)

	X	Y	Z
C	2.38644718	0.50793212	−0.00000000
C	0.24515655	−0.76203461	−0.00000000
H	4.37051102	0.07829181	−0.00000000
O	−2.13709182	0.23409161	0.00000000
H	0.19612655	−2.81431632	−0.00000000
H	−1.98349433	2.04637562	0.00000000

Table 4.32: Acetaldehyde (CH_3CHO)

	X	Y	Z
O	−2.15910280	0.43922255	0.00000000
C	−0.23561810	−0.79580918	−0.00000000
C	2.37678464	0.31347786	0.00000000
H	−0.32930757	−2.88392840	−0.00000000
H	2.28889276	2.36673962	0.00000000
H	3.40621991	−0.35527773	1.65989715
H	3.40621991	−0.35527773	−1.65989715

Table 4.33: Acetyl Radical ($CH_3C\dot{O}$)

	X	Y	Z
O	−2.18483227	0.33515626	0.00000000
C	−0.25825721	−0.80117117	0.00000000
C	2.40215001	0.24121760	0.00000000
H	2.38232507	2.30068452	0.00000000
H	3.38279208	−0.47629315	1.66292407
H	3.38279208	−0.47629315	−1.66292407

Table 4.34: Vinyl Radical ($CH_2{=}\dot{C}H$)

	X	Y	Z
C	1.17056527	0.04344375	0.00000000
C	−1.30355350	−0.16017932	0.00000000
H	2.39499755	−1.59940034	0.00000000
H	2.09110324	1.88553562	−0.00000000
H	−2.90263271	1.10381515	0.00000000

Table 4.35: Vinoxy Radical ($\dot{C}H_2CH{=}O$)

	X	Y	Z
C	2.33952604	0.35058494	−0.00000000
C	−0.10201988	−0.80716171	0.00000000
H	4.03882359	−0.78354085	0.00000000
H	2.47172569	2.38919910	−0.00000000
O	−2.07853640	0.42323079	−0.00000000
H	−0.16427074	−2.88625656	0.00000000

CHAPTER 5

INTERACTIONS OF URACIL WITH NEUTRAL ALKALI METALS[2]

[4]To be submitted to *Physical Chemistry Chemical Physics*.

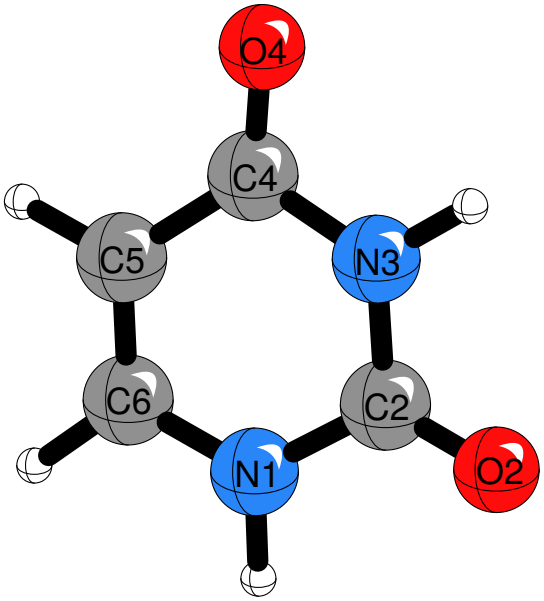

Figure 5.1: Geometry of uracil base, with atoms numbered according to the scheme used for the remainder of this paper.

Abstract

Introduction

Nucleic acids serve as the basis for the storage and transfer of genetic information in all known living organisms. However, organisms are regularly exposed to conditions that can damage the nucleic acids used for information storage. If not promptly corrected by endogenous repair machinery, the resulting mutations can accumulate to the point of cell death or unchecked proliferation. As has been extensively covered in a 2012 review by Gu, Leszczynski, and Schaefer,[207] low-energy electrons can attach to nucleobases, resulting in DNA damage. For instance, electrons with energies close to zero eV that attach to pyrimidine bases can induce strand breaks.[208]

The canonical nucleobases adenine (A), thymine (T), cytosine (C), and guanine (G) are found in DNA, and are directly involved in information storage and thus mutagenesis of multicellular organisms. The nucleic acid used in a number of capacities for information transfer and use, RNA, similarly contains A, C, and G, but contains uracil (U) instead of T.

Considerable controversy has plagued determination of the adiabatic electron affinities (AEAs) of the canonical nucleobases. However, uracil (Figure 5.1) appears to have the most positive electron affinity of these nucleobases.[209]

In 1990, Chen and coworkers used substitution rules and the electron affinity of unsubstituted pyrimidine to estimate an electron affinity of around 0.75 eV for uracil. Desfrançois and coworkers observed both valence and dipole-bound radical anions of uracil in Rydberg electron transfer experiments,[210,211] indicating in agreement with the earlier work of Chen and coworkers that the valence radical anion has a positive AEA. Hendricks and coworkers[212,213] studied the dipole-bound uracil radical anion using photodetachment-photoelectron spectroscopy (PD-PES), and later found that solvating the anion to more closely resemble *in vivo* conditions results primarily in observation of the valence radical anion rather than its dipole-bound counterpart. Schiedt *et al.* also performed PD-PES on pyrimidine nucleobases, including uracil, and estimated the electron affinity of uracil to be positive, between 0 and 200 meV.

The 2012 review by Gu and coworkers[207] discusses the different signs given for the AEA of uracil by theoretical investigations. Some theoretical studies, such as that by Dediková and coworkers,[214] predict a negative electron affinity for uracil. However, both experiment and some density functional theory methods predict a positive electron affinity.[207]

Schaefer and coworkers[209] addressed the controversy about the AEAs corresponding to the covalent radical anions using density functional theory (DFT). They found that uracil and thymine have the most positive AEAs, while those of cytosine and guanine may be either positive or negative, and that of adenine is most likely negative. Several different DFT functionals indicated that uracil had the most positive AEA of the canonical nucleobases; it is energetically more favorable to add an electron to uracil than to add an electron to one of the other nucleobases. When the DNA nucleobases are treated in the context of nucleosides with glycosidic linkages connecting them to deoxyribose units, the AEAs are larger than for the isolated bases.[215] Kim and Schaefer found that microsolvation of uracil makes the electron affinity even more positive upon addition of each water molecule.[216]

In 2014, Gu and coworkers[217] reported a benchmark study to establish methods that can be used to correctly describe the positive AEA of uracil. As a reference method, they selected W1BD,[218] which employs Brueckner doubles corrections on a base method W1 that allows an accuracy of 0.3 kcal/mol.[219] The M06-2X functional[110] performed favorably, yielding a value for the AEA close to that obtained using the reference method.

Despite all of the previous work on the electron affinities of the canonical nucleobases, some controversy still exists; for instance, Pal and coworkers[220] reported negative electron affinities for all of the canonical nucleobases in 2015.

Hobza, Leszczynski, and coworkers have used theoretical methods to extensively study the interactions of alkali metal cations with nucleobases and other components of nucleic acids.[221–224]

Cerda and Wesdemiotis[225] found that uracil has the lowest alkali metal cation affinities of the canonical

nucleobases, with Li^+, Na^+, and K^+ binding with similar geometries, and affinity decreasing with atomic number. Rodgers and Armentrout[226] studied the interactions of adenine, thymine, and uracil with alkali metal cations using threshold collision-induced dissocation, along with computations of the structures and energetics of the complexes involved. Their experimental dissociation energies matched well with those they computed, validating their computational finding that the complexes are all very close to planarity. Gillis and coworkers[227] used mid-infrared mutiple-photon dissociation (IRMPD) spectroscopy to investigate the structure of hydrated complexes of Li^+ with uracil; they found that the water molecules preferentially bind to the Li^+, which in turn preferentially binds to O4 of uracil, consistent with other studies.

In contrast to the plethora of theoretical and experimental studies that have been performed on the positively charged complexes of alkali metals and nucleobases, very little has been done on the neutral versions of such complexes.[228–231]

A 2007 study by Krasnokutski and coworkers[231] indicated that the O4 oxygen of uracil is the preferred binding site for neutral aluminum atoms. For instance, uracil, the nucleobase with the best-studied AEA, has been the subject of a small number of joint experimental and theoretical studies on its neutral complexes with metals.[229,232] In 2005, Martínez computed several possible structures for a neutral complex between uracil and copper atoms as part of a study of copper-nucleobase complexes. The most energetically favorable of these neutral complex structures, with the metal atom interacting with the O4 oxygen of uracil, exhibited a small negative Mulliken charge on the copper atom. The first study to cover neutral complexes of uracil with alkali metals in particular was performed in 2010, when Krasnokutski and coworkers[233] investigated both neutral and cationic complexes of lithium with adenine and uracil using zero-electron-kinetic-energy (ZEKE) spectroscopy. To help interpret their experimental results, they also performed B3LYP/6-311+G(d,p) computations. Based on the similarity of the C4–O4 bond length in the Li-uracil O4 complex to the C–O bond lengths in organic acids, the Krasnokutski study deduced a largely electrostatic Li–O interaction.

In light of the controversy that long surrounded the AEAs of nucleobases and in light of the excellent work that has been done on noncovalent interactions of nucleobases with metal cations, we sought to characterize the bonding between the canonical nucleobases and the first five neutral alkali metal atoms.

In contrast to the tenuous AEA values for nucleobases, the ionization energies of the alkali metals are well-established to be quite small. Neutral alkali metal atoms readily donate the unpaired *s* electron to other molecules. Of note, in THF solution, alkali metals are largely present as cations in complexes with unbound electrons,[234,235] which indicates that some heterocycles, perhaps including nucleobases, can accept the *s* electron from an alkali metal. Therefore, it seemed that further insight related to the electron affinities could be obtained by studying the bonding in complexes composed of uracil, with its postive electron affinity, and neutral alkali metals.

Following the finding of Gu and coworkers[217] that M06-2X performs well in computing the AEA of uracil, we report our investigations of the structures, frequencies, energetics, and electron localization of complexes between the neutral alkali metals and the nucleobase uracil using M06-2X. We additionally employed the ωB97X-D3 method, which performs well for treating weak interactions.[109] With a primary focus on the strength of the interaction as described by dissociation to the neutral base and neutral alkali metal, we additionally computed the energetics of dissociation to the ionic limit. We used NBO[236] to study the nature of the interaction and determine where the unpaired electron of the alkali metal localizes: on the metal, or on the base. This, in turn, will provide a more complete picture of how nucleobases, with their small electron affinities, behave in environments with electrons that could potentially attach to them.

Methods

We employed augmented Dunning basis sets for most of our computations. For H, C, N, O[237] and for Li and Na,[238] we used aug-cc-pVTZ. The three heaviest alkal metals we treated all require the use of pseudopotentials; for K, Rb, and Cs, we used the aug-cc-pVTZ-DK basis[239,240] with the SDD(10,MWB) pseudopotential for K and with the Rb(ecp-28) and Cs(ecp-46) Def2-ECPs pseudopotentials for Rb and Cs, respectively.[241]

In addition to the Dunning basis sets, we employed the Ahlrichs Def2 basis sets,[39,40] which are commonly used in density functional theory computations but may require added augmentation to properly treat anions and electron affinities.[41]

We optimized the structures, computed the energies, and predicted the harmonic vibrational frequencies of our structures of interest using density functional theory (DFT). We employed both the M06-2X[110] and the ωB97X-D3[109] exchange-correlation functionals in our computations, both of which are included in ORCA from the XCFun DFT library.[242] The M06-2X functional, so named because it is a Minnesota function constructed using twice as much local exchange as M06,[110] handles dispersion reasonably well. We expected dispersion to be a significant component of any interaction between a neutral alkali metal and a neutral nucleobase, and accordingly chose two functionals that treat dispersion using two different mechanisms. Similar answers are therefore less likely due to systematic errors introduced by the form of the functional.

Optimizations and energy and frequency computations were performed using the ORCA 4.0 program package.[111,112] We employed the AutoAux auxiliary basis set generation procedure[243] alongside the RIJCosx and DLPNO approximations. Geometry optimizations employed the TightOpt and TightSCF keywords. The Minnesota functionals exhibit a particularly sensitive dependence on grid size,[244] and we therefore used the largest predefined grid in ORCA, Grid 7, which corresponds to a Lebedev770 angular grid and a radial grid

Table 5.1: Bond lengths (Å) for M–O bonds in the O2 and O4 complexes compared to experimental bond lengths of the ground states for the corresponding diatomics, MO, where M = Li, Na, K, Rb, Cs. The literature on KO has documented substantial uncertainty about which of its states is the ground state; however, recent studies[246,247] indicate that it is likely the $^2\Sigma^+$ state, which we have used here.

	Li	Na	K	Rb	Cs
O4	1.622	1.994	2.268	2.482	2.474
O2	1.808	2.290	2.618	2.800	2.957
MO	1.68822159(2)[a]	2.051548(1)[b]	2.1675[c]	2.2541931(15)[d]	2.300745(16)[e]

[a] Microwave spectroscopy $^2\Pi$ state r_e value[248]
[b] Microwave spectroscopy $^2\Pi$ state r_e value[249]
[c] $^2\Sigma^+$, Ref.[250] and unpublished rotational spectroscopy work cited therein.
[d] Microwave spectroscopy $^2\Sigma^+$, Ref.[251]
[e] Microwave spectroscopy $^2\Sigma^+$, Ref.[252]

Table 5.2: Bond lengths in uracil (U), uracil radical anion (U^{-1}), and the complexes of alkali metals with uracil oxygen atom O2.

Bond	U	U^-	Li	Na	K	Rb	Cs
C5-C6	1.339	1.407	1.338	1.338	1.335	1.338	1.338
N1-C6	1.368	1.417	1.374	1.372	1.364	1.371	1.369
N3-C4	1.399	1.445	1.408	1.404	1.401	1.404	1.403
C2-O2	1.206	1.234	1.224	1.217	1.205	1.216	1.219
C4-O4	1.207	1.249	1.202	1.204	1.193	1.205	1.206
N1-C2	1.382	1.357	1.363	1.371	1.366	1.373	1.372
N3-C2	1.374	1.364	1.354	1.362	1.360	1.366	1.365
C4-C5	1.394	1.456	1.456	1.456	1.453	1.456	1.454
M-O2			1.808	2.290	2.618	2.800	2.957

parameter of 5.67, with the predefined GridX5 for the RIJCOSX approximation for all of our computations.

NBO analyses[236] were performed using the ORCA interface to NBO 6.0.[245]

Results

Structures found for the O2, and O4, and π complexes are depicted in Figure 5.2, with further details in following figures and tables.

The bond lengths of the O2 and O4 complexes (Table 5.3 and Figure 5.3) indicate that the metal is more closely bound to uracil in the O4 complexes than in the O2 complexes. Additionally, the bond distances of the base in the O4 complexes are closer to the bond distances of uracil radical anion than to those of neutral uracil. In contrast, the bond distances of the base in the O2 complexes are in general closer to the bond distances of neutral uracil than to those of the uracil radical anion.

With the decently tight grids used in this study, the M06-2X/cc-pVTZ AEA of uracil that includes

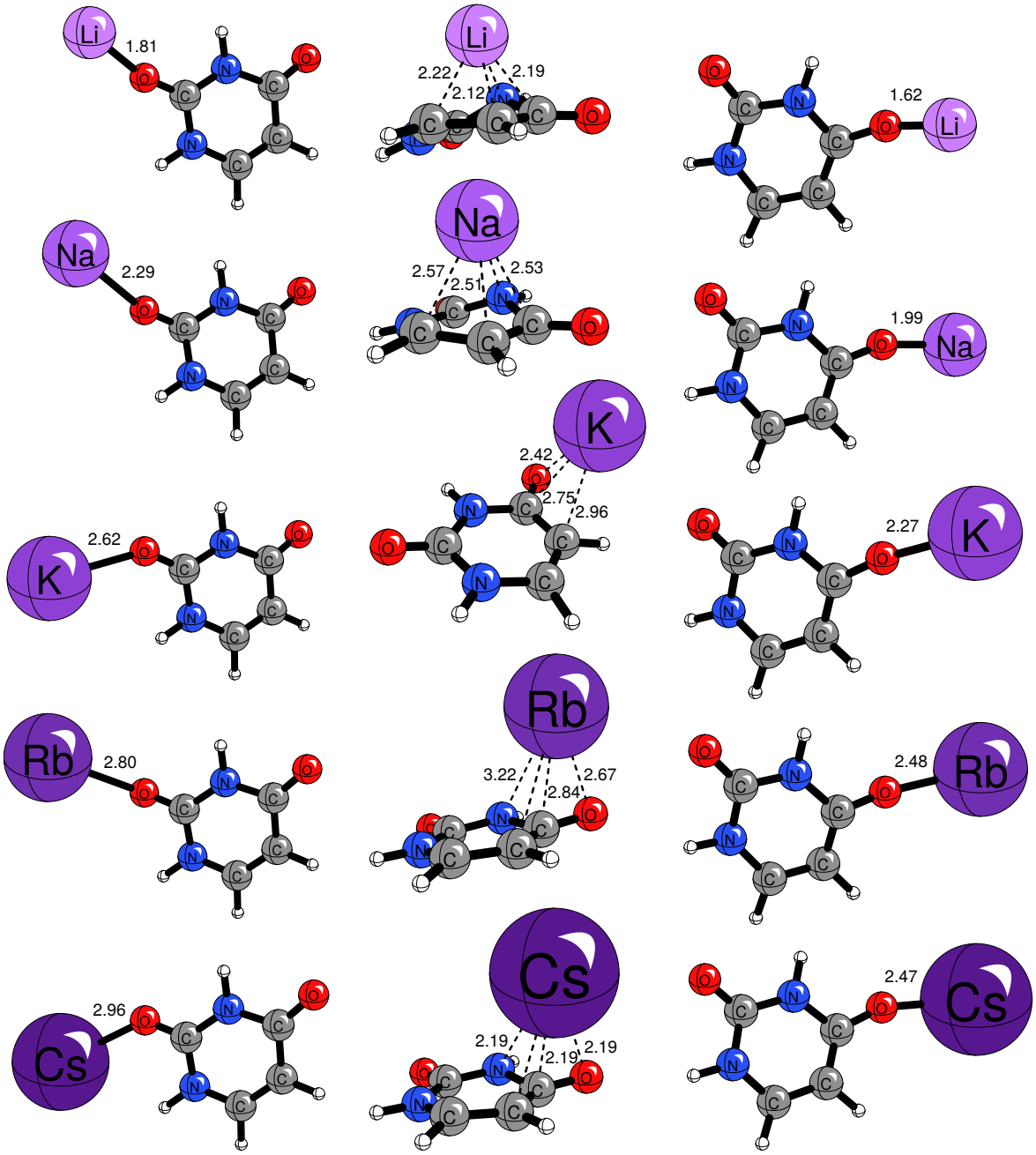

Figure 5.2: From left to right, structures for the O2, π, and O4 complexes considered in this paper; bond distances shown are in Å.

Table 5.3: Bond lengths in uracil (U), uracil radical anion (U^{-1}), and the complexes of alkali metals with uracil oxygen atom O4.

					O4		
Bond	U	U^-	Li	Na	K	Rb	Cs
C5-C6	1.339	1.407	1.395	1.399	1.398	1.400	1.398
N1-C6	1.368	1.417	1.405	1.407	1.408	1.408	1.408
N3-C4	1.399	1.445	1.408	1.414	1.416	1.421	1.412
C2-O2	1.206	1.234	1.216	1.219	1.220	1.221	1.219
C4-O4	1.207	1.249	1.300	1.292	1.289	1.289	1.288
N1-C2	1.382	1.357	1.365	1.363	1.362	1.362	1.364
N3-C2	1.374	1.364	1.375	1.374	1.373	1.374	1.372
C4-C5	1.394	1.456	1.374	1.376	1.377	1.379	1.375
M-O4			1.622	1.994	2.269	2.482	2.474

Table 5.4: Energies of cationic complexes in kcal mol^{-1} (eV) relative to dissociation to neutral base and metal cation. Although pi structures were found for the neutral complexes, they were not found for the cationic complexes.

	O4	O2
Li	−50.5(−2.180)	−46.5(−2.005)
Na	−35.4(−1.525)	−31.8(−1.370)
K	−27.5(−1.185)	−24.0(−1.036)
Rb	−24.0(−1.033)	−20.8(−0.896)
Cs	−21.8(−0.942)	−19.1(−0.822)

Table 5.5: Complex energies with the M06-2X functional and the cc-pVTZ (cc-pVTZ-PP for K, Rb, and Cs) basis set in kcal mol^{-1} (eV) relative to neutral dissociation limit

	O4	O2	Pi
Li	−24.0(−1.036)	−11.7(−0.506)	−15.2(−0.657)
Na	−3.9(−0.170)	−4.8(−0.207)	−0.7(−0.031)
K	−11.9(−0.512)	−7.1(−0.305)	−14.5(−0.626)
Rb	−8.5(−0.368)	−5.1(−0.220)	−11.5(−0.494)
Cs	−6.8(−0.295)	−13.3(−0.573)	−16.7(−0.719)

Table 5.6: Complex energies with the M06-2X functional and the Def2-TZVP basis set in kcal mol^{-1} (eV) relative to neutral dissociation limit

	O4	O2	Pi
Li	−21.8(−0.941)	−11.3(−0.486)	−13.2(−0.571)
Na	−3.9(−0.169)	− − −	−0.6(−0.024)
K	−9.0(−0.388)	−6.3(−0.271)	−11.2(−0.484)
Rb	−7.0(−0.302)	−5.1(−0.219)	− − −
Cs	−10.9(−0.470)	−6.2(−0.269)	−14.5(−0.626)

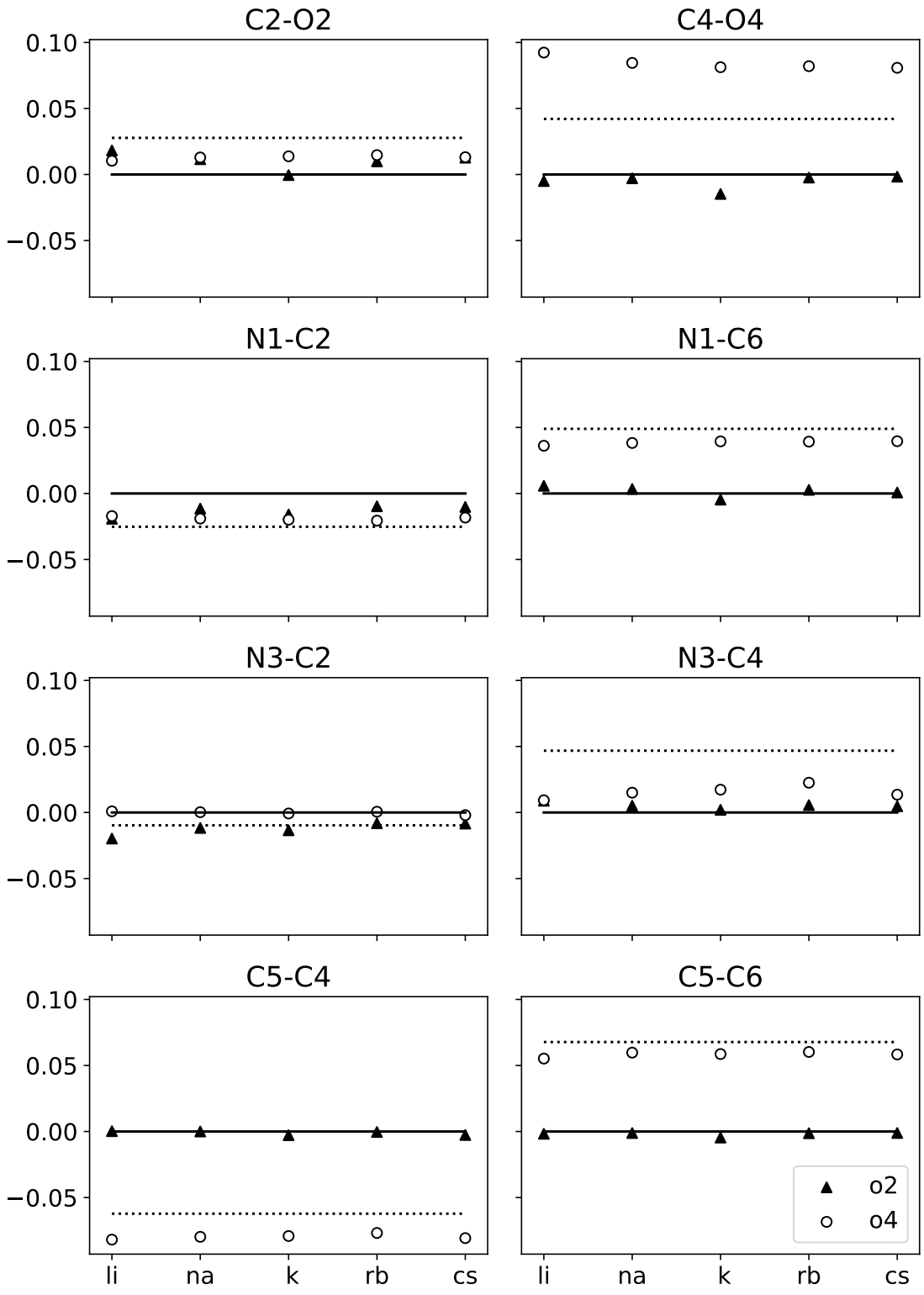

Figure 5.3: Relative bond lengths (Å) of the complexes with respect to those of uracil. The solid line at 0 Å represents the value of each parameter in uracil, while the dotted line represents its value in the uracil radical anion. Triangles represent the value in the O2 complexes and circles represent the O4 complex value. For many of the bonds considered, the complex with the metal bound to the O4 atom yields a parameter closer to the corresponding value in the radical anion, while the geometric parameters of the O2 complexes remain closer to those in the neutral uracil base.

Table 5.7: Complex energies with the ωB97X-D3 functional in kcal mol^{-1} (eV) relative to neutral dissociation limit

	O4	O2	Pi
Li	−20.1(−0.869)	−10.8(−0.468)	−8.8(−0.381)
Na	−4.9(−0.212)	−5.1(−0.220)	0.7(0.029)
K	−13.3(−0.573)	− − −	−15.0(−0.648)
Rb	−10.7(−0.463)	−4.8(−0.205)	−12.6(−0.543)
Cs	−16.8(−0.726)	−3.2(−0.139)	−19.0(−0.818)

Table 5.8: Complex energies in kcal mol^{-1} (eV) relative to ionic dissociation limit

	O4	O2	Pi
Li	−145.8(−6.287)	−133.5(−5.757)	−137.0(−5.909)
Na	−119.6(−5.157)	−120.4(−5.194)	−116.4(−5.019)
K	−107.4(−4.634)	−102.7(−4.428)	−110.1(−4.749)
Rb	−100.8(−4.347)	−97.3(−4.199)	−103.7(−4.473)
Cs	−98.9(−4.268)	−92.5(−3.990)	−102.3(−4.414)

zero-point vibrational energy is 0.125 eV (2.9 kcal mol^{-1}), in agreement with the value of 0.11 eV found by Gu and coworkers[217] using M06-2X. This indicates that our convergence parameters and grid size are likely comparable. Of note, the M06-2X/Def2-TZVP AEA of uracil computed here is -0.016 eV (-0.4 kcal mol-1), a negative value. However, the dissociation energies of the complexes are similar, indicating thate these energies are less sensitive to basis set choice than is the AEA of uracil.

We computed natural population analysis (NPA) charges on the atoms to determine where the unpaired electron was localized. The resulting charges indicate that in many cases, the electron is localized entirely on the base rather than on the metal.

Both the geometries and bonding analysis results indicate that the alkali metal atoms have donated their unpaired electrons to uracil, resulting in an ionic complex primarily bound by electrostatic interactions. This finding is in agreement with the 2010 deduction of Krasnokutski, Lee, and Yang that the O4 Li-uracil complex is bound by electrostatic interactions.

Table 5.9: NPA charges on metal atoms in the complexes indicate that in many cases, the electron has been transferred almost completely to uracil.

	Li	Na	K	Rb	Cs
O4	0.97	0.98	0.98	0.99	0.97
O2	-0.47	0.01	0.49	0.01	0.08
Pi	0.91	0.92	0.49	0.97	0.49

Conclusion

In summary, some of the complexes under study may be bound strongly enough to be observed experimentally. Along with further experimental studies of these complexes, we recommend further computational work on these systems that includes treatments of solvent effects, as microhydration has been found to increase the electron affinity of uracil.[216]

CHAPTER 6

CONCLUSION

This dissertation has detailed investigations of the electronic structure of the methylsulfinyl radical, of the reaction of the methylsulfinyl radical with ozone, of several radicals derived from acetaldehyde and vinyl alcohol, and finally of the nature of the interactions between neutral alkali metals and uracil.

High-level characterization of the ground and first excited electronic states of the methylsulfinyl radical yielded an accurate transition origin for the excitation between these two electronic states, as well as population analysis for the radical and a barrier to rotation about the C–S bond.

Study of the reaction between the methylsulfinyl radical and ozone indicates a highly exothermic reaction that proceeds directly to products with no barrier. This conclusion is consistent with the available experimental results, which indicate that the reaction proceeds rapidly and has no observable dependence on pressure.

The application of high-level coupled-cluster theory to acetaldehyde and vinyl alcohol and to related radicals yielded CCSDT(Q)/CBS reaction enthalpies that can be used in models of butanol combustion, as well as hitherto unreported fundamental frequencies. Some of the vinyl alcohol frequencies reported here for vinyl alcohol have not been experimentally observed. Additionally, we proposed revised assignments of experimental modes for several radicals. Density functional theory investigations of the interactions between uracil and neutral alkali metals indicate that the two form complexes bound by several kcal mol^{-1}. Despite the small and disputed electron affinity of uracil, the unpaired electron appears in many of these complexes to be localized almost entirely on the nucleobase.

Bibliography

[1] Krylov, A. I. In *Reviews in Computational Chemistry*; Parrill, A. L., Lipkowitz, K. B., Eds.; John Wiley & Sons, Inc., 2017; Vol. 30; pp 151–224.

[2] Dirac, P. A. M. *Proc. Royal Soc. Lond. A* **1929**, *123*, 714–733.

[3] Schrödinger, E. *Ann. der Phys.* **1926**, *384*, 361.

[4] Schrödinger, E. *Ann. der Phys.* **1926**, *384*, 32.

[5] Schrödinger, E. *Phys. Rev.* **1926**, *28*, 1049–1070.

[6] Dirac, P. A. M. *Proc. Royal Soc. Lond. A* **1928**, *117*, 610–624.

[7] Hartree, D. R. *Rep. Prog. Phys.* **1960**, *32*, 179–185.

[8] Roothaan, C. C. J. *Rev. Mod. Phys.* **1951**, *23*, 69–89.

[9] Pople, J. A.; Nesbet, R. K. *J. Chem. Phys.* **1954**, *22*, 571–572.

[10] Roothaan, C. C. J. *Rev. Mod. Phys.* **1960**, *32*, 179–185.

[11] Segal, G. A. *J. Chem. Phys.* **1970**, *52*, 3530–3533.

[12] Brueckner, K.; Lockett, A.; Rotenberg, M. *Phys. Rev.* **1961**, *121*, 255–269.

[13] Stanton, J. F.; Gauss, J.; Bartlett, R. J. *J. Chem. Phys.* **1992**, *97*, 5554–5559.

[14] Crawford, T. D.; Stanton, J. F. *J. Chem. Phys.* **2000**, *112*, 7873–7879.

[15] Møller, C.; Plesset, M. S. *Phys. Rev.* **1934**, *46*, 618–622.

[16] Wheeler, S. E.; Allen, W. D.; Schaefer, H. F. *J. Chem. Phys.* **2008**, *128*, 074107.

[17] Leininger, M. L.; Allen, W. D.; Schaefer, H. F.; Sherrill, C. D. *J. Chem. Phys.* **2000**, *112*, 9213–9222.

[18] Čížek, J. *J. Chem. Phys.* **1966**, *45*, 4256–4266.

[19] Crawford, T. D.; Schaefer, H. F. In *Reviews in Computational Chemistry*; Lipkowitz, K. B., Boyd, D. B., Eds.; Wiley-VCH, John Wiley and Sons, Inc., New York, 2000; Vol. 14; pp 33–136.

[20] Nooijen, M.; Shamasundar, K. R.; Mukherjee, D. *Mol. Phys.* **2005**, *103*, 2277–2298.

[21] Stanton, J. F. *Chem. Phys. Lett.* **1997**, *281*, 130–134.

[22] Riplinger, C.; Pinski, P.; Becker, U.; Valeev, E. F.; Neese, F. *J. Chem. Phys.* **2016**, *144*, 024109.

[23] East, A. L. L.; Allen, W. D. *J. Chem. Phys.* **1993**, *99*, 4638–4650.

[24] Császár, A. G.; Allen, W. D.; Schaefer, H. F. *J. Chem. Phys.* **1998**, *108*, 9751–9764.

[25] Gonzales, J. M.; Pak, C.; Cox, R. S.; Allen, W. D.; Schaefer, H. F.; Császár, A. G.; Tarczay, G. *Chem. Eur. J.* **2003**, *9*, 2173–2192.

[26] Schuurman, M. S.; Muir, S. R.; Allen, W. D.; Schaefer, III, H. F. *J. Chem. Phys.* **2004**, *120*, 11586–11599.

[27] Bomble, Y. J.; Stanton, J. F.; Kállay, M.; Gauss, J. *J. Chem. Phys.* **2005**, *123*, 054101.

[28] Kállay, M.; Gauss, J. *J. Chem. Phys.* **2005**, *123*, 214105.

[29] Kállay, M.; Gauss, J. *J. Chem. Phys.* **2008**, *129*, 144101.

[30] Stanton, J. F. *J. Chem. Phys.* **1994**, *101*, 371–374.

[31] Ditchfield, R.; Hehre, W. J.; Pople, J. A. *J. Chem. Phys.* **1971**, *54*, 724–728.

[32] Dunning, T. H. *J. Chem. Phys.* **1989**, *90*, 1007–1023.

[33] Yockel, S.; Wilson, A. K. *Theor. Chem. Acc.* **2008**, *120*, 119–131.

[34] Dunning, T. H.; Peterson, K. A.; Wilson, A. K. *J. Chem. Phys.* **2001**, *114*, 9244–9253.

[35] Almlöf, J.; Taylor, P. R. *J. Chem. Phys.* **1987**, *86*, 4070–4077.

[36] McCaslin, L.; Stanton, J. *Mol. Phys.* **2013**, *111*, 1492–1496.

[37] Lee, T. J.; Schaefer, H. F. *J. Chem. Phys.* **1985**, *83*, 1784–1794.

[38] Rienstra-Kiracofe, J. C.; Tschumper, G. S.; Schaefer, H. F. *Chem. Rev.* **2002**, *102*, 231–282.

[39] Weigend, F.; Furche, F.; Ahlrichs, R. *J. Chem. Phys.* **2003**, *119*, 12753.

[40] Weigend, F.; ; Ahlrichs, R. *Phys. Chem. Chem. Phys.* **2005**, *7*, 3297–3305.

[41] Zheng, J.; Xu, X.; Truhlar, D. G. *Theor. Chem. Acc.* **2011**, *128*, 295–305.

[42] Papajak, E.; Zheng, J.; Xu, X.; Leverentz, H. R.; Truhlar, D. G. *J. Chem. Theory Comput.* **2011**, *7*, 3027–3034.

[43] Kohn, W.; Sham, L. J. *Phys. Rev.* **1965**, *140*, A1133–A1138.

[44] Hohenberg, P.; Kohn, W. *Phys. Rev.* **1964**, *136*, B864–B871.

[45] Perdew, J. P.; Schmidt, K. *AIP Conf. Proc.* **2001**, *577*, 1–20.

[46] Pople, J. A.; Gill, P. M. W.; Handy, N. C. *Int. J. Quant. Chem.* **1995**, *56*, 303–305.

[47] Veryazov, V.; Malmqvist, P.; Roos, B. O. *Int. J. Quant. Chem.* **2011**, *111*, 3329–3338.

[48] Andersson, K.; Malmqvist, P.-Å.; Roos, B.; Sadlej, A. J.; Wolinski, K. *J. Phys. Chem.* **1990**, *94*, 5483–5488.

[49] Andersson, K.; Malmqvist, P.-Å.; Roos, B. *J. Chem. Phys.* **1992**, *96*, 1218–1226.

[50] Werner, H.-J.; Knowles, P. J. *J. Chem. Phys.* **1988**, *89*, 5803–5814.

[51] Lee, T. J.; Taylor, P. R. *Int. J. Quant. Chem. Symp.* **1989**, *S23*, 199–207.

[52] Lee, T. J. *Chem. Phys. Lett.* **2003**, *372*, 362–367.

[53] Bartlett, R. J. *Int. J. Mol. Sci.* **2002**, *3*, 579–603.

[54] Krylov, A. I. *Annu. Rev. Phys. Chem.* **2008**, *59*, 433–462.

[55] Stanton, J. F.; Bartlett, R. J. *J. Chem. Phys.* **1993**, *98*, 7029–7039.

[56] Charlson, R. J.; Lovelock, J. E.; Andreae, M. O.; Warren, S. G. *Nature* **1987**, *326*, 655–661.

[57] Yoch, D. C. *Appl. Environ. Microbiol.* **2002**, *68*, 5804–5815.

[58] Andreae, M. O.; Raemdonck, H. *Science* **1983**, *221*, 744–747.

[59] Andreae, M. O.; Ferek, R. J.; Bermond, F.; Byrd, K. P.; Engstrom, R. T.; Hardin, S.; Houmere, P. D.; LeMarrec, F.; Raemdonck, H.; Chatfield, R. B. *J. Geophys. Res.* **1985**, *90*, 12891–12900.

[60] Li, C.-Y.; Wei, T.-D.; Zhang, S.-H.; Chen, X.-L.; Gao, X.; Wang, P.; Xie, B.-B.; Su, H.-N.; Qin, Q.-L.; Zhang, X.-Y.; Yu, J.; Zhang, H.-H.; Zhou, B.-C.; Yang, G.-P.; Zhang, Y.-Z. *Proc. Nat. Acad. Sci. USA.* **2014**, *111*, 1026–31.

[61] Stefels, J. *J. Sea Res.* **2000**, *43*, 183–197.

[62] Sunda, W.; Kieber, D. J.; Kiene, R. P.; Huntsman, S. *Nature* **2002**, *418*, 317–320.

[63] Simó, R. *Trends Ecol. Evol.* **2001**, *16*, 287–294.

[64] Kiene, R. P.; Linn, L. J.; Bruton, J. A. *J. Sea Res.* **2000**, *43*, 209–224.

[65] Barone, S. B.; Turnipseed, A. A.; Ravishankara, A. R. *Faraday Discuss.* **1995**, *100*, 39–54.

[66] Cvetanovic, R. J.; Singleton, D. L.; Irwin, R. S. *J. Am. Chem. Soc.* **1981**, *103*, 6672–6677.

[67] Borissenko, D.; Kukui, A.; Laverdet, G.; Le Bras, G. *J. Phys. Chem. A* **2003**, *107*, 1155–1161.

[68] Lucas, D. D. *J. Geophys. Res.* **2002**, *107*, 1–26.

[69] Barnes, I.; Hjorth, J.; Mihalopoulos, N. *Chem. Rev.* **2006**, *106*, 940–975.

[70] Sevilla, M. D.; Becker, D.; Swarts, S.; Herrington, J. *Biochem. Biophys. Res. Commun.* **1987**, *144*, 1037–1042.

[71] Davis, D.; Chen, G.; Bandy, A.; Thornton, D.; Eisele, F.; Mauldin, L.; Tanner, D.; Lenschow, D.; Fuelberg, H.; Hueberg, B.; Heath, J.; Clarke, A.; Blake, D. *J. Geophys. Res.* **1999**, *104*, 5765–5784.

[72] Turnipseed, A. A.; Barone, S. B.; Ravishankara, A. R. *J. Phys. Chem.* **1993**, *97*, 5926–5934.

[73] Reisenauer, H. P.; Romański, J.; Mlostoń, G.; Schreiner, P. R. *Chem. Comm.* **2013**, *49*, 9467–9469.

[74] Copan, A. V.; Schaefer, H. F.; Agarwal, J. *Mol. Phys.* **2015**, *113*, 2992–2998.

[75] Morrison, A. M.; Agarwal, J.; Schaefer, H. F.; Douberly, G. E. *J. Phys. Chem. A* **2012**, *116*, 5299–5304.

[76] Lesar, A.; Tusar, S. *J. Phys. Chem. A* **2014**, *118*, 7855–7862.

[77] Reisenauer, H. P.; Schreiner, P. R.; Romański, J.; Mlostoń, G. *J. Phys. Chem. A* **2015**, *119*, 2211–2216.

[78] Curtiss, L. A.; Redfern, P. C.; Raghavachari, K. *J. Chem. Phys.* **2007**, *126*, 1–12.

[79] Chu, L. K.; Lee, Y. P. *J. Chem. Phys.* **2010**, *133*, 184303, 1–11.

[80] Kawamura, T.; Krusic, P. J.; Kochi, J. K. *Tetrahedron Lett.* **1972**, *13*, 4075–4078.

[81] Nishikida, K.; Williams, F. *J. Am. Chem. Soc.* **1974**, *233*, 4781–4784.

[82] Hinchliffe, A. *J. Mol. Struct.* **1982**, *88*, 213–216.

[83] Swarts, S. G.; Becker, D.; Debolt, S.; Sevilla, M. D. *J. Phys. Chem.* **1989**, *93*, 155–161.

[84] Bartlett, R. J.; Musiał, M. *Rev. Mod. Phys.* **2007**, *79*, 291–352.

[85] Raghavachari, K.; Trucks, G. W.; Pople, J. A.; Head-Gordon, M. *Chem. Phys. Lett.* **1989**, *157*, 479–483.

[86] Bartlett, R. J.; Watts, J. D.; Kucharski, S. A.; Noga, J. *Chem. Phys. Lett.* **1990**, *164*, 513–522.

[87] Deegan, M. J. O.; Knowles, P. J. *Chem. Phys. Lett.* **1994**, *227*, 321–326.

[88] Stanton, J. F.; Gauss, J.; Harding, M. E.; Szalay, P. G. CFOUR, Coupled-Cluster techniques for Computational Chemistry, a quantum-chemical program package written by Stanton, J.F.; Gauss, J.; Hardng, M.E.; and Szalay, P.G. with contributions from Auer, A.A.; Bartlett, R.J.; Benedikt, U.; Berger, C.; Bernholdt, D.E.; Bomble, Y. J.; Cheng, L.; Christiansen, O.; Heckert, M.; Heun, O.; Huber, C.; Jagau, T.-C.; Jonsson, D.; Jusélius, J.; Klein, K.; Lauderdale, W.J.; Lipparini, F.; Matthews, D.A.; Metzroth, T.; Mück, L.A.; O'Neill, D.P.; Price, D.R.; Prochnow, E.; Puzzarini, C.; Ruud, K.; Schiffmann, F.; Schwalbach, W.; Simmons, C.; Stopkowicz, S.; Tajti, A.; Vázquez, J.; Wang, F.; Watts, J.D.; and the integral packages MOLECULE (Almlöf, J. and Taylor, P.R.), PROPS (Taylor, P.R.), ABACUS (Helgaker, T.; Jensen, H.J. Aa.; Jørgensen, P.; and Olsen, J.), and ECP routines by Mitin, A. V. and van Wüllen, C. For the current version, see http://www.cfour.de.

[89] Stanton, J. F.; Gauss, J. *Adv. Chem. Phys.* **2003**, *125*, 101–146.

[90] Mills, I. M. In *Molecular Spectroscopy: Modern Research*; Rao, K. N., Matthews, C. W., Eds.; Academic Press, New York, NY, 1972; pp 115–140.

[91] PyVPT2 is a vibrational anharmonicity program written in Python by J. Agarwal. Center for Computational Quantum Chemistry, University of Georgia, Athens, GA.

[92] Copan, A. V.; Wiens, A. E.; Nowara, E. M.; Schaefer, H. F.; Agarwal, J. *J. Chem. Phys.* **2015**, *142*, 054303.

[93] Kállay, M.; Surján, P. *J. Chem. Phys.* **2001**, *115*, 2945.

[94] Turney, J. M. et al. *WIREs: Comput. Mol. Sci.* **2012**, *2*, 556–565.

[95] Harding, M. E.; Metzroth, T.; Gauss, J.; Auer, A. a. *J. Chem. Theory Comput.* **2008**, *4*, 64–74.

[96] Clark, W. W.; De Lucia, F. C. *J. Mol. Spec.* **1976**, *60*, 332–342.

[97] Jin, S.; Schaefer, H. F. *J. Chem. Phys.* **1990**, *93*, 1799–1804.

[98] Tiemann, E. *J. Mol. Spec.* **1974**, *51*, 316–320.

[99] Hoffmann, E. H.; Tilgner, A.; Schröder, R.; Bräuer, P.; Wolke, R.; Herrmann, H. *Proc. Nat. Acad. Sci. USA.* **2016**, *113*, 11776–11781.

[100] Reisenauer, H. P.; Romański, J.; Mlostoń, G.; Schreiner, P. R. *Chem. Comm.* **2015**, *51*, 10022–10025.

[101] Tyndall, G. S.; Ravishankara, A. R. *J. Phys. Chem.* **1989**, *93*, 2426–2435.

[102] Li, X.; Meng, L.; Zheng, S. *J. Mol. Struct.* **2007**, *847*, 52–58.

[103] Kukui, A.; Bossoutrot, V.; Laverdet, G.; Le Bras, G. *J. Phys. Chem. A* **2000**, *104*, 935–946.

[104] Besler, B. H.; Sevilla, M. D.; MacNeille, P. *J. Phys. Chem.* **1986**, *90*, 6446–6451.

[105] Dominé, F.; Murrells, T. P.; Howard, C. J. *J. Phys. Chem.* **1990**, *94*, 5839–5847.

[106] Ratliff, B. J.; Tang, X.; Butler, L.; Szpunar, D. E.; Lau, K.-C. *J. Chem. Phys.* **2009**, *131*, 044304–15.

[107] Dominé, F.; Ravishankara, A. R.; Howard, C. J. *J. Phys. Chem.* **1992**, *96*, 2171–2178.

[108] Cremer, D.; Filatov, M.; Polo, V.; Kraka, E.; Shaik, S. *Int. J. Mol. Sci.* **2002**, *3*, 604–638.

[109] Lin, Y.-S.; Li, G.-D.; Mao, S.-P.; Chai, J.-D. *J. Chem. Theory Comput.* **2013**, *9*, 263–272.

[110] Zhao, Y.; Truhlar, D. G. *Theor. Chem. Acc.* **2008**, *120*, 215–241.

[111] Neese, F. *WIREs: Comput. Mol. Sci.* **2012**, *2*, 73–78.

[112] Neese, F. *WIREs: Comput. Mol. Sci.* **2018**, *8*, 4–9.

[113] MOLPRO is a package of *ab initio* programs written by H.-J. Werner, P. J. Knowles, G. Knizia, F. R. Manby, M. Schütz, P. Celani, W. Györffy, D. Kats, T. Korona, R. Lindh, A. Mitrushenkov, G. Rauhut, K. R. Shamasundar, T. B. Adler, R. D. Amos, A. Bernhardsson, A. Berning, D. L. Cooper, M. J. O. Deegan, A. J. Dobbyn, F. Eckert, E. Goll, C. Hampel, A. Hesselmann, G. Hetzer, T. Hrenar, G. Jansen, C. Köppl, Y. Liu, A. W. Lloyd, R. A. Mata, A. J. May, S. J. McNicholas, W. Meyer, M. E. Mura, A. Nicklaß, D. P. O'Neill, P. Palmieri, D. Peng, K. Pflüger, R. Pitzer, M. Reiher, T. Shiozaki, H. Stoll, A. J. Stone, R. Tarroni, T. Thorsteinsson, M. Wang .

[114] Mrcc, a quantum chemical program suite written by M. Kállay, Z. Rolik, J. Csontos, I. Ladjánszki, L. Szegedy, B. Ladóczki, and G. Samu. See also Z. Rolik, L. Szegedy, I. Ladjánszki, B. Ladóczki, and M. Kállay, J. Chem. Phys. **139**, 094105 (2013), as well as: www.mrcc.hu.

[115] Cremer, D. *Mol. Phys.* **2009**, *99*, 1899–1940.

[116] Lee, J. Y.; Jang, Y.-S.; Lee, J.; Papoutsakis, E. T.; Lee, S. Y. *Biotech.* **2009**, *4*, 1432–1440.

[117] Wu, M.; Wang, M.; Liu, J.; Huo, H. *Biotech. Prog.* **2008**, *24*, 1204–1214.

[118] Venugopal, T.; Ramesh, A. *Fuel* **2014**, *115*, 295–305.

[119] Dernotte, J.; Mounaim-Rousselle, C.; Halter, F.; Seers, P. *Oil & Gas Science and Technology Revue de lInstitut Français du Pétrole* **2010**, *65*, 345–351.

[120] Sarathy, S. M.; Vranckx, S.; Yasunaga, K.; Mehl, M.; Oßwald, P.; Metcalfe, W. K.; Westbrook, C. K.; Pitz, W. J.; Kohse-Höinghaus, K.; Fernandes, R. X.; Curran, H. J. *Combust. Flame* **2012**, *159*, 2028–2055.

[121] Black, G.; Curran, H. J.; Pichon, S.; Simmie, J. M.; Zhukov, V. *Combust. Flame* **2010**, *157*, 363–373.

[122] Hansen, N.; Harper, M. R.; Green, W. H. *Phys. Chem. Chem. Phys.* **2011**, *13*, 20262–20274.

[123] Taatjes, C. A.; Hansen, N.; McIlroy, A.; Miller, J. A.; Senosiain, J. P.; Klippenstein, S. J.; Qi, F.; Sheng, L.; Zhang, Y.; Cool, T. A.; Wang, J.; Westmoreland, P. R.; Law, M. E.; Kasper, T.; Kohse-Höinghaus, K. *Science* **2005**, *308*, 1887–1889.

[124] Taatjes, C. A.; Hansen, N.; Miller, J. A.; Cool, T. A.; Wang, J.; Westmoreland, P. R.; Law, M. E.; Kasper, T.; Kohse-Höinghaus, K. *J. Phys. Chem. A* **2006**, *110*, 3254–3260.

[125] Harper, M. R.; Van Geem, K. M.; Pyl, S. P.; Marin, G. B.; Green, W. H. *Combust. Flame* **2011**, *158*, 16–41.

[126] Van Geem, K. M.; Pyl, S. P.; Marin, G. B.; Harper, M. R.; Green, W. H. *Ind. Eng. Chem. Res.* **2010**, *49*, 10399–10420.

[127] Oßwald, P.; Güldenberg, H.; Kohse-Höinghaus, K.; Yang, B.; Yuan, T.; Qi, F. *Combust. Flame* **2011**, *158*, 2–15.

[128] Turner, B. E.; Apponi, A. J. *Astrophys. J.* **2001**, *561*, L207–L210.

[129] Harmony, M. D.; Laurie, V. W.; Kuczkowski, R. L.; Schwendeman, R. H.; Ramsay, D. A.; Lovas, F. J.; Lafferty, W. J.; Maki, A. G. *J. Phys. Chem. Ref. Data* **1979**, *8*, 619–721.

[130] Evans, J. C.; Bernstein, H. J. *Can. J. Chem.* **1956**, *34*, 1083–1092.

[131] Saito, S. *Chem. Phys. Lett.* **1976**, *42*, 399–402.

[132] Rodler, M.; Bauder, A. *J. Am. Chem. Soc.* **1984**, *106*, 4025–4028.

[133] Rodler, M.; Blom, C. E.; Bauder, A. *J. Am. Chem. Soc.* **1984**, *106*, 4029–4035.

[134] Rodler, M. *J. Mol. Spec.* **1985**, *114*, 23–30.

[135] Ruscic, B.; Boggs, J. E.; Burcat, A.; Császár, A. G.; Demaison, J.; Janoschek, R.; Martin, J. M. L.; Morton, M. L.; Rossi, M. J.; Stanton, J. F.; Szalay, P. G.; Westmoreland, P. R.; Zabel, F.; Bérces, T. *J. Phys. Chem. Ref. Data* **2005**, *34*, 573–656.

[136] Shirk, J. S.; Pimental, G. C. *J. Am. Chem. Soc.* **1968**, *90*, 3349–3351.

[137] Jacox, M. E. *Chem. Phys.* **1982**, *69*, 407–422.

[138] Nimlos, M. R.; Soderquist, J. A.; Ellison, G. B. *J. Am. Chem. Soc.* **1989**, *111*, 7675–7681.

[139] Rowland, B.; Hess, W. P. *J. Phys. Chem. A* **1997**, *101*, 8049–8056.

[140] Hirota, E.; Mizoguchi, A.; Ohshima, Y.; Katoh, K.; Sumiyoshi, Y.; Endo, Y. *Mol. Phys.* **2007**, *105*, 455–466.

[141] Tang, X.; Ratliff, B. J. F.; FitzPatrick, B. L.; Butler, L. J. *J. Phys. Chem. B* **2008**, *112*, 16050–16058.

[142] Das, P.; Lee, Y.-P. *J. Chem. Phys.* **2014**, *140*, 244303.

[143] Hunziker, H. E.; Kneppe, H.; McLean, A. D.; Siegbahn, P.; Wendt, H. R. *Can. J. Chem.* **1983**, *61*, 993–995.

[144] Shepherd, R. A.; Doyle, T. J.; Graham, W. R. M. *J. Chem. Phys.* **1988**, *89*, 2738–2742.

[145] Kanamori, H.; Endo, Y.; Hirota, E. *J. Chem. Phys.* **1990**, *92*, 197–205.

[146] Letendre, L.; Liu, D.-K.; Pibel, C. D.; Halpern, J. B.; Dai, H.-L. *J. Chem. Phys.* **2000**, *112*, 9209–9212.

[147] Nikow, M.; Wilhelm, M. J.; Dai, H.-L. *J. Phys. Chem. A* **2009**, *113*, 8857–8870.

[148] Raston, P. L.; Liang, T.; Douberly, G. E. *J. Chem. Phys.* **2013**, *138*, 174302.

[149] Inoue, G.; Akimoto, H. *J. Chem. Phys.* **1981**, *74*, 425–433.

[150] Hunziker, H. E.; Kneppe, H.; Wendt, H. R. *J. Photochem.* **1981**, *17*, 377–387.

[151] DiMauro, L. F.; Heaven, M.; Miller, T. A. *J. Chem. Phys.* **1984**, *81*, 2339–2346.

[152] Gejo, T.; Takayanagi, M.; Kono, T.; Hanazaki, I. *Chemistry Letters* **1993**, *22*, 2065–2068.

[153] Osborn, D. L.; Choi, H.; Mordaunt, D. H.; Bise, R. T.; Neumark, D. M.; Rohlfing, C. M. *J. Chem. Phys.* **1997**, *106*, 3049–3066.

[154] Brock, L. R.; Rohlfing, E. A. *J. Chem. Phys.* **1997**, *106*, 10048–10065.

[155] Jacox, M. E. *J. Phys. Chem. Ref. Data* **1998**, *27*, 115–393.

[156] Miller, J. L.; McCunn, L. R.; Krisch, M. J.; Butler, L. J.; Shu, J. *J. Chem. Phys.* **2004**, *121*, 1830–1838.

[157] Stanton, J. F. *Chem. Phys. Lett.* **1997**, *281*, 130–134.

[158] Woon, D. E.; Dunning, T. H. *J. Chem. Phys.* **1995**, *103*, 4572.

[159] Cowan, R. D.; Griffin, D. C. *J. Opt. Soc. Am.* **1976**, *66*, 1010–1014.

[160] Kutzelnigg, W.; Ottschofski, E.; Franke, R. *J. Chem. Phys.* **1995**, *102*, 1752.

[161] Davidson, E. R.; Ishikawa, Y.; Malli, G. L. *Chem. Phys. Lett.* **1981**, *84*, 226–227.

[162] Bauschlicher, C. W.; Martin, J. M. L.; Taylor, P. R. *J. Phys. Chem. A* **1999**, *103*, 7715–7718.

[163] Sellers, H.; Pulay, P. *Chem. Phys. Lett.* **1984**, *103*, 463–465.

[164] Handy, N. C.; Yamaguchi, Y.; Schaefer, H. F. *J. Chem. Phys.* **1986**, *84*, 4481.

[165] Tajti, A.; Szalay, P. G.; Császár, A. G.; Kállay, M.; Gauss, J.; Valeev, E. F.; Flowers, B. A.; Vázquez, J.; Stanton, J. F. *J. Chem. Phys.* **2004**, *121*, 11599–11613.

[166] Schuurman, M. S.; Allen, W. D.; Schaefer, H. F. *J. Comp. Chem.* **2005**, *26*, 1106–1112.

[167] Matthews, D. A.; Stanton, J. F. *Mol. Phys.* **2009**, *107*, 213–222.

[168] Harding, M. E.; Metzroth, T.; Gauss, J.; Auer, A. A. *J. Chem. Theory Comput.* **2008**, *4*, 6474.

[169] Kilb, R. W.; Lin, C. C.; Wilson, E. B. *J. Chem. Phys.* **1957**, *26*, 1695–1703.

[170] Iijima, T.; Kimura, M. *Bull. Chem. Soc. Japan* **1969**, *42*, 2159–2164.

[171] Hollenstein, H.; Günthard, H. H. *Spectrochimica. Acta.* **1971**, *27A*, 2027–2060.

[172] Findsen, L. A.; Fang, H. L.; Swofford, R. L.; Birge, R. R. *J. Chem. Phys.* **1986**, *84*, 16–27.

[173] Herman, M.; Herregodts, F.; Georges, R.; Hepp, M.; Bachir, I. H.; Lecoutre, M.; Kleiner, I. *Chem. Phys.* **1999**, *246*, 433–443.

[174] Bond, D.; Schleyer, P. v. R. *J. Org. Chem.* **1990**, *55*, 1003–1013.

[175] Matti, G. Y.; Osman, O. I.; Upham, J. E.; Suffolk, R. J.; Kroto, H. W. *J. Electron. Spectrosc. Relat. Phenom.* **1989**, *49*, 195–201.

[176] Hays, B. M.; Wehres, N.; DePrince, B. A.; Roy, A. A. M.; Laas, J. C.; Weaver, S. L. W. *Chem. Phys. Lett.* **2015**, *630*, 18–26.

[177] Koga, Y.; Nakanaga, T.; Sugawara, K.-I.; Watanabe, A.; Sugi, M.; Takeo, H.; Konda, S.; Matsumura, C. *J. Mol. Spec.* **1991**, *145*, 315–322.

[178] Bunn, H.; Hudson, R. J.; Gentleman, A. S.; Raston, P. L. *ACS Earth Space Chem.* **2017**, *1*, 70–79.

[179] Morton, J. R.; Falconer, W. E. *Nature* **1963**, *197*, 1103.

[180] Bennett, J. E.; Mile, B.; Ward, B. *Chem. Comm.* **1969**, 13–14.

[181] Jacox, M. E. Vibrational and Electronic Energy Levels of Polyatomic Transient Molecules, 1994.

[182] Wang, J.-H.; Chang, H.-C.; Chen, Y.-T. *Chem. Phys.* **1996**, *206*, 43–56.

[183] Sattelmeyer, K. W.; Schaefer, H. F. *J. Chem. Phys.* **2002**, *117*, 7914–7916.

[184] Simmonett, A. C.; Wheeler, S. E.; Schaefer, H. F. *J. Phys. Chem. A* **2004**, *108*, 1608–1615.

[185] Nesbitt, D. J.; Dong, F. *Phys. Chem. Chem. Phys.* **2008**, *10*, 2113–2122.

[186] Sharma, A. R.; Braams, B. J.; Carter, S.; Shepler, B. C.; Bowman, J. M. *J. Chem. Phys.* **2009**, *130*, 174301.

[187] Agarwal, J.; Turney, J. M.; Schaefer, H. F. *J. Phys. Chem. Lett.* **2011**, *2*, 2587–2592.

[188] Fessenden, R. W.; Schuler, R. H. *J. Chem. Phys.* **1963**, *39*, 2147–2195.

[189] Cochran, E. L.; Adrian, F. J.; Bowers, V. A. *J. Chem. Phys.* **1964**, *40*, 213–220.

[190] Kasai, P. H.; Whipple, E. B. *J. Am. Chem. Soc.* **1967**, *89*, 1033–1034.

[191] Kasai, P. H. *J. Am. Chem. Soc.* **1972**, *94*, 5950–5956.

[192] Wu, Y.-J.; Lin, M.-Y.; Cheng, B.-M.; Chen, H.-F.; Lee, Y.-P. *J. Chem. Phys.* **2008**, *128*, 204509.

[193] Dupuis, M.; Wendoloski, J. J. *J. Chem. Phys.* **1984**, *80*, 5696–5702.

[194] Tanskanen, H.; Khriachtchev, L.; Räsänen, M.; Feldman, V. I.; Sukhov, F. F.; Orlov, A. Y.; Tyurin, D. A. *J. Chem. Phys.* **2005**, *123*, 064318.

[195] Dupuis, M.; Wendoloski, J. J.; Lester, W. A. J. *J. Chem. Phys.* **1982**, *76*, 488–492.

[196] Bacchus-Montabonel, M. C.; Piechowska, K.; Tergiman, Y. S.; Sienkiewicz, J. E. *J. Mol. Spec.* **2005**, *729*, 115–123.

[197] Piechowska-Strumik, K.; Lauvergnat, D.; Bacchus-Montabonel, M.-C.; Desouter-Lecomte, M. *Chem. Phys. Lett.* **2006**, *425*, 16–21.

[198] Buley, A. L.; Norman, R. O. C.; Pritchett, R. J. *J. Chem. Soc. B* **1966**, 849–852.

[199] Endo, Y.; Saito, S.; Hirota, E. *J. Chem. Phys.* **1985**, *83*, 2026–2034.

[200] Endo, Y.; Nakajima, M. *J. Mol. Spec.* **2014**, *301*, 15–19.

[201] Yamaguchi, M.; Momose, T.; Shida, T. *J. Chem. Phys.* **1990**, *93*, 4211–4222.

[202] Utkin, Y. G.; Han, J.-X.; Sun, F.; Chen, H.-B.; Scott, G.; Curl, R. F. *J. Chem. Phys.* **2003**, *118*, 10470.

[203] da Silva, G.; Kim, C.-H.; Bozzelli, J. W. *J. Phys. Chem. A* **2006**, *110*, 7925–7934.

[204] Senosiain, J. P.; Klippenstein, S. J.; Miller, J. A. *J. Phys. Chem. A* **2005**, *109*, 6045–6055.

[205] Altarawneh, M.; Al-Muhtaseb, A. H.; Dlugogorski, B. Z.; Kennedy, E. M.; Mackie, J. C. *J. Comp. Chem.* **2011**, *32*, 1725–1733.

[206] Holmes, J. L.; Lossing, F. P. *J. Am. Chem. Soc.* **1980**, *102*, 1591–1595.

[207] Gu, J.; Leszczynski, J.; Schaefer, H. F. *Chem. Rev.* **2012**, *112*, 5603–5640.

[208] Bao, X.; Sun, H.; Wong, N. B.; Gu, J. *J. Phys. Chem. B* **2006**, *110*, 5865–5874.

[209] Wesolowski, S. S.; Leininger, M. L.; Pentchev, P. N.; Schaefer, H. F. *J. Am. Chem. Soc.* **2001**, *123*, 4023–4028.

[210] Desfrancois, C. *J. Chem. Phys.* **1996**, *104*, 7792.

[211] Desfrançois, C.; Periquet, V.; Bouteiller, Y.; Schermann, J. P. *J. Phys. Chem. A* **1998**, *102*, 1274–1278.

[212] Hendricks, J. H.; Lyapustina, S. A.; De Clercq, H. L.; Snodgrass, J. T.; Bowen, K. H. *J. Chem. Phys.* **1996**, *104*, 7788–7791.

[213] Hendricks, J. H.; Lyapustina, S. A.; De Clercq, H. L.; Bowen, K. H. *J. Chem. Phys.* **1998**, *108*, 8–11.

[214] Dedíková, P.; Demovič, L.; Pitoňák, M.; Neogrády, P.; Urban, M. *Chem. Phys. Lett.* **2009**, *481*, 107–111.

[215] Richardson, N. A.; Gu, J.; Wang, S.; Xie, Y.; Schaefer, H. F. *J. Am. Chem. Soc.* **2004**, *126*, 4404–4411.

[216] Kim, S.; Schaefer, H. F. *The Journal of chemical physics* **2006**, *125*, 144305.

[217] Gu, J.; Xie, Y.; Schaefer, H. F. *Journal of Chemical Theory and Computation* **2014**, *10*, 609–612.

[218] Barnes, E. C.; Petersson, G. A.; Montgomery, J. A.; Frisch, M. J.; Martin, J. M. *J. Chem. Theory Comput.* **2009**, *5*, 2687–2693.

[219] Martin, J. M.; De Oliveira, G. *J. Chem. Phys.* **1999**, *111*, 1843–1856.

[220] Dutta, A. K.; Sengupta, T.; Vaval, N.; Pal, S. *Int. J. Quant. Chem.*

[221] Hobza, P.; Sandorfy, C. *Biophys. Chem.* **1984**, *19*, 201–209.

[222] Schneider, B.; Kabela, M.; Hobza, P. *J. Am. Chem. Soc.* **1996**, *118*, 12207–12217.

[223] Šponer, J.; Leszczynski, J.; Hobza, P. *Journal of Molecular Structure: ...* **2001**, *573*, 43–53.

[224] Burda, J. V.; Leszczynki, J. **2006**, 389–410.

[225] Cerda, B. A.; Wesdemiotis, C. *J. Am. Chem. Soc.* **1996**, *118*, 11884–11892.

[226] Rodgers, M. T.; Armentrout, P. B. *J. Am. Chem. Soc.* **2000**, *122*, 8548–8558.

[227] Gillis, E. A. L.; Rajabi, K.; Fridgen, T. D. **2009**, 824–832.

[228] Vázquez, M.-V.; Moussatova, A.; Martínez, A.; Dolgounitcheva, O.; Zakrzewski, V. G.; Ortiz, J. V. *J. Phys. Chem. A* **2004**, *108*, 5845–5850.

[229] Martínez, A. *J. Chem. Phys.* **2005**, *123*.

[230] Kumar, A.; Mishra, P. C. **2006**, 7719–7727.

[231] Krasnokutski, S. A.; Yang, D. S. *J. Phys. Chem. A* **2007**, *111*, 10567–10573.

[232] Gao, J.; Berden, G.; Rodgers, M. T.; Oomens, J. *Phys. Chem. Chem. Phys.* **2016**, *18*, 7269–7277.

[233] Krasnokutski, S. A.; Lee, J. S.; Yang, D. S. *J. Chem. Phys.* **2010**, *132*.

[234] Glover, W. J.; Larsen, R. E.; Schwartz, B. J. *Journal of Physical Chemistry B* **2010**, *114*, 11535–11543.

[235] Glover, W. J.; Larsen, R. E.; Schwartz, B. J. *J. Phys. Chem. A* **2011**, *115*, 5887–5894.

[236] Glendening, E. D.; Landis, C. R.; Weinhold, F. *WIREs: Comput. Mol. Sci.* **2012**, *2*, 1–42.

[237] Kendall, R. A.; Dunning, T. H.; Harrison, R. J. *J. Chem. Phys.* **1992**, *96*, 6796–6806.

[238] Prascher, B. P.; Woon, D. E.; Peterson, K. A.; Dunning, T. H.; Wilson, A. K. *Theor. Chem. Acc.* **2011**, *128*, 69–82.

[239] Hill, J. G.; Peterson, K. A. *J. Chem. Phys.* **2017**, *147*.

[240] Sun, Z.; Moore, K. B.; Hill, J. G.; Peterson, K. A.; Schaefer, H. F.; Hoffmann, R. *J. Phys. Chem. B* **2018**, *122*, 3339–3353.

[241] Leininger, T.; Nicklass, A.; Küchle, W.; Stoll, H.; Dolg, M.; Bergner, A. *Chem. Phys. Lett.* **1996**, *255*, 274–280.

[242] Ekström, U.; Visscher, L.; Bast, R.; Thorvaldsen, A. J.; Ruud, K. *J. Chem. Theory Comput.* **2010**, *6*, 1971–1980.

[243] Stoychev, G. L.; Auer, A. A.; Neese, F. *J. Chem. Theory Comput.* **2017**, *13*, 554–562.

[244] Wheeler, S. E.; Houk, K. N. *J. Chem. Theory Comput.* **2010**, *6*, 395–404.

[245] NBO 6.0. E. D. Glendening, J. K. Badenhoop, A. E. Reed, J. E. Carpenter, J. A. Bohmann, C. M. Morales, C. R. Landis, and F. Weinhold, Theoretical Chemistry Institute, University of Wisconsin, Madison, WI, (2013).

[246] Mintz, B.; Chan, B.; Sullivan, M. B.; Buesgen, T.; Scott, A. P.; Kass, S. R.; Radom, L.; Wilson, A. K. *J. Phys. Chem. A* **2009**, *113*, 9501–9510.

[247] Vasiliu, M.; Li, S.; Peterson, K. A.; Feller, D.; Gole, J. L.; Dixon, D. A. *J. Phys. Chem. A* **2010**, *114*, 4272–4281.

[248] Yamada, C.; Fujitake, M.; Hirota, E. *J. Chem. Phys.* **1989**, *90*, 3033–3037.

[249] Yamada, C.; Fujitake, M.; Hirota, E. *J. Chem. Phys.* **1989**, *91*, 137–141.

[250] Hirota, E. Recent Progress in High-Resolution Spectroscopic Studies on Transient Molecules. 1995.

[251] Yamada, C.; Hirota, E. *Journal of Chemical Physics* **1999**, *111*, 9587–9592.

[252] Yamada, C.; Hirota, E. *The Journal of Chemical Physics* **1999**, *110*, 2853–2857.